Landing Gear Integration in Aircraft Conceptual Design

by

Sonny T. Chai

Thesis submitted to the Faculty of the

Virginia Tech Polytechnic Institute and State University

in partial fulfillment of the requirements for the degree of

MASTERS OF SCIENCE

IN

AEROSPACE ENGINEERING

APPROVED:

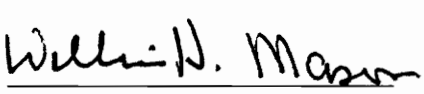

William H. Mason, Chair

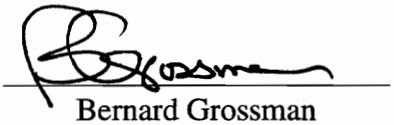

Bernard Grossman

Eric R. Johnson

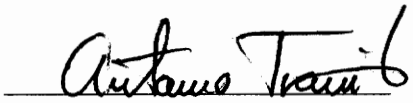

Antonio A. Trani

July 1, 1996

Blacksburg, Virginia

Key words: Center of gravity, Flotation, Kinematics, Landing gear, Weight

LANDING GEAR INTEGRATION IN AIRCRAFT CONCEPTUAL DESIGN

by

Sonny T. Chai

William H. Mason, Chairman

Aerospace and Ocean Engineering

(ABSTRACT)

The design of the landing gear is one of the more fundamental aspects of aircraft design. The design and integration process encompasses numerous engineering disciplines, *e.g.*, structure, weights, runway design, and economics, and has become extremely sophisticated in the last few decades. Although the design process is well-documented, no attempt has been made until now in the development of a design methodology that can be used within an automated environment. As a result, the process remains to be a key responsibility for the configuration designer and is largely experience-based and graphically-oriented. However, as industry and government try to incorporate multidisciplinary design optimization (MDO) methods in the conceptual design phase, the need for a more systematic procedure has become apparent.

The development of an MDO-capable design methodology as described in this work is focused on providing conceptual designer with tools to help automate the disciplinary analyses, *i.e.*, geometry, kinematics, flotation, and weight. Documented design procedures and analyses were examined to determine their applicability, and to ensure compliance with current practices and regulations. Using the latest information as obtained from industry during initial industry survey, the analyses were in terms modified and expanded to accommodate the design criteria associated with the advanced large subsonic transports. Algorithms were then developed based on the updated analysis procedures to be incorporated into existing MDO codes.

To Carol

Although separated
by ocean and continent
by light and darkness
you have always been there
for me
at times both good and bad.

Arigatoo.

Acknowledgments

This work would not have been possible without the tireless efforts of my faculty advisor, Dr. William H. Mason. I would like to thank Dr. Mason and the other committee members, Dr. Bernard Grossman, Dr. Eric R. Johnson, and Dr. Antonio A. Trani for their support and encouragement. Special thanks go to Dr. Paul Gelhausen and Mr. Shahab Hasan at NASA Ames Research Center for their support. Also, Mr. Bill Perrella and Mr. John Rice at the Federal Aviation Administration, Mr. Edward Gervais, Mr. Jerry Kileer, Mr. Bob Nielson, Mr. Dave Nielson, Mr. Scott Perkins, and Mr. John Potter at Boeing Commercial Aircraft Group, Mr. Al Kernik at McDonnell Douglas, Mr. Gene Stuczynski at Cleveland Pneumatic, Mr. Bill Luce at Menasco Aerosystems, Mr. Derek Duxbury at British Aerospace, Mr. Ron Olds, Mr. Dean Peters, and Mr. Paul Snyder at B.F. Goodrich, Mr. Joe Pacuit at the Tire and Rim Association, Inc., Mr. Richard Vandame of the SAE A-5 Committee, Mr. James Gallivan at United Airlines, and Mr. Steve Lydon at Northwest Airlines for their assistance and valuable input during the initial industry survey. Last but not least, Mr. Nathan Kirschbaum at Virginia Tech for his insight into landing gear design considerations at the aircraft conceptual design stage. This work was funded by NASA Grant NAG-2-919 and is gratefully acknowledged.

Table of Contents

List of Figures

List of Tables

Nomenclature

Symbols

A	Area
ACN	Aircraft classification number
AR	Aspect ratio
C	Clearance, moment component
C_L	Lift coefficient
CBR	California bearing ratio
D	Drag, diameter
$ESWL$	Equivalent single wheel load
E	Energy, modulus of elasticity
F	Fillet radius, force
$F.S.$	Factor of safety
H	Height
I	Moment of inertia, second area moment
KE	Kinetic energy
L	Lift, length
M	Bending moment
$MTOW$	Maximum takeoff weight
N	Landing load factor, axial force
P	Pressure, load
R	Radius of centerline curve, offset
S	Safety margin, wing area, stroke, offset
T	Thrust, torque
V	Speed, volume, shear force
W	Weight, width, offset
X	Distance

a	Acceleration
b	Wheelbase
c	Constant
cg	Center of gravity
d	Displacement
e	Deflection
f	Constant
g	Gravitational acceleration
h	Height
k	Modulus of subgrade reaction, machinability factor
l	Length, direction cosine, radius of relative stiffness
m	Direction cosine
mac	Mean aerodynamic chord
n	Direction cosine, aircraft load factor
q	Shear flow
r	Radius
s	Span
t	Wheel track, thickness
u	Deflection
v	Deflection
w	Deflection, flange width

Greek Letters

Γ	Dihedral angle
Λ	Sweep angle
Ψ	Turnover angle
α	Angle of attack, repetition factor
β	Steering angle
δ	Main assembly offset angle
ϕ	Roll angle, retraction angle

η	Efficiency factor
φ	Castor angle, rotation angle
μ	Poisson's ratio
π	Pi
θ	Pitch angle, axle inclination angle
ρ	Sea-level air density, radius of gyration
σ	Stress
τ	Stress

Acronyms

ACN-PCN	Aircraft-Pavement Classification Number
ACSYNT	AirCraft SYNThesis
FAA	Federal Aviation Administration
ICAO	International Civil Aviation Organization
LCN	Load Classification Number
MDO	Multidisciplinary Design Optimization
NASA	National Aeronautic and Space Administration
PCA	Portland Cement Association
FLOPS	Flight Optimization System
DIS	Dynamic Integration System

Chapter 1 Introduction

1.1. Introduction

The design of the landing gear, which is considered "the essential intermediary between the aeroplane and catastrophe" [1], is one of the more fundamental aspects of aircraft design. The design and integration process encompasses numerous engineering disciplines, *e.g.*, structure, weights, runway design, and economics, and has become extremely sophisticated in the last few decades.

The landing gear design process is well-documented by Conway [1] and more recently by Currey [2] and is experience-based and graphically-oriented in nature. As such, it is a key responsibility of the configuration designer during initial concept studies. However, as industry and government try to incorporate multidisciplinary design optimization (MDO) methods in the conceptual design phase, the need for a more systematic procedure has become apparent. Accordingly, NASA Ames provided Virginia Tech with a two-year research grant to develop a landing gear design methodology that can be implemented within an MDO environment, with a special emphasis on design considerations for advanced large subsonic transports. The result of this research project, known as *Landing Gear Integration in Aircraft Conceptual Design*, is the topic of this Master of Science thesis.

1.2. Overview

Several design considerations that must be addressed are briefly discussed to illustrate the complexity involved in the development of such a methodology. The list is made up of an ever-increasing, and sometimes conflicting, number of requirements, *e.g.*, component maximum strength, minimum weight, high reliability, low cost, overall aircraft

integration, airfield compatibility, *etc.*, and truly reflect the multidisciplinary nature of the task.

The location of the aircraft center of gravity (*cg*) is critical in the design and location of the landing gear. The nose and main assemblies must be located at a specific distance from the aircraft *cg*, in both the longitudinal and lateral directions, such that the aircraft is in no danger of tipping back or turning over on its side over the full range of *cg* locations. Another issue to be considered is the distribution of the aircraft weight, which is dependent on the distances between the aircraft *cg* and the nose and main assembly. Between 85 and 92 percent of the MTOW must be maintained on the main assemblies such that the brakes can provide sufficient energy to slow down the aircraft within a given runway length [3].

Airfield compatibility has become one of the primary considerations in the design of landing gears due to the high cost associated with infrastructure modification, *e.g.*, pavement reinforcement and runway and taxiway expansion [4]. Pavement bearing strength, which varies from one airport to another due to variations in subgrade materials, dictates the number and arrangement of tires needed to produce the required flotation characteristics. Flotation is defined as the capability of the runway pavement and other surfaces, *e.g.*, taxiway and apron, to support the aircraft. In addition, the disposition of the landing gear is constrained by runway and taxiway geometry as found at the airports to be served. Since the ground track is dependent on the dimensions of the wheelbase and track, an increase in these dimensions could bring the aircraft over the edge of the pavement during certain maneuvers, *e.g.*, 180-degree turn and centerline-tracing taxiing, and cause the aircraft to bog down in soft soil [5].

The soundness of a landing gear concept depends on the efficacy of overall system integration. Ground clearance, particularly between the engine nacelle and the static groundline, plays a key role in determining the length of the landing gear and the permissible takeoff rotation angle. Insufficient allowance can result in costly modifications, *e.g.*, lengthening of the strut or repositioning of the under-wing engines, that effectively

rule out future growth options. The landing gear stowage issue must also be addressed as the number of main assembly struts increases with the increase in aircraft weight [6]. Trade-off studies concerning space availability, structural integrity, and weight penalties resulting from local structural reinforcements are needed to arrive at an optimum design.

The weight of the landing gear, which typically ranges from three to six percent of the maximum aircraft takeoff weight, is also a design consideration. With advances in flight science technologies, which result in reduced structural and mission fuel weights, the landing gear may become an increasingly large weight fraction in future large aircraft. Since the landing gear has virtually no contribution toward, and in some cases even has a degrading effect on, the profitability of the aircraft, it is not surprising that the design objective is to minimize the weight of the landing gear such that additional revenue-generating payload can be carried onboard. However, a major reduction in the landing gear weight may be hard to realize because landing gears are one of the few non-redundant load-paths in an aircraft, and any reduction in reliability from current fail-safe standard is not acceptable [7].

With the financial challenges arising from the deregulation of the air-travel industry, the airlines are faced with the challenge of reducing operating costs to remain competitive. As a result, the airlines have demanded that the aircraft manufacturers produce new designs with high reliability and low maintenance requirements. Recent technologies, *e.g.*, carbon-carbon heat sinks, radial tires, and high-strength steel, are being introduced. In addition, simplified design and improved manufacturing techniques, *e.g.*, die-forging and three-dimensional machining [8], are being used to reduce the part-count associated with the landing gear system.

1.3. Objectives

The development of an MDO-capable design methodology is focused on providing the conceptual designer with tools to help automate the disciplinary analyses, *i.e.*, geometry, kinematics, flotation, and weight. Documented design procedures and analyses

as found and referenced by Curry and Torenbeek [3] were examined to determine their applicability, and to ensure compliance with current practices and regulations. Although in most cases the documented analyses were developed for a specific type of aircraft, the essential fundamentals remain unchanged for any given type of aircraft. Thus, using the latest information as obtained from industry during an initial industry survey [App. A], the analyses were in turn modified and expanded to accommodate the design criteria associated with the advanced large subsonic transports. Algorithms were then developed based on the updated analysis procedures to be incorporated into existing MDO codes.

Chapter 2 Aircraft Center of Gravity

2.1. Introduction

The precise location of the aircraft *cg* is essential in the positioning of the landing gear, as well as for other MDO applications, *e.g.*, flight mechanics, stability and control, and performance. Primarily, the aircraft *cg* location is needed to position the landing gear such that ground stability, maneuverability, and clearance requirements are met. Given the fact that none of the existing conceptual design-level *cg* estimation procedures has the degree of responsiveness and accuracy required for MDO applications, a new approach is formulated to provide a reliable range of *cg* locations that is better suited for MDO applications.

2.2. Current Capabilities

Although not expected to determine the location of the aircraft *cg*, current aircraft sizing programs, as typified by Jayaram *et al.* [9] and McCullers [10], do provide some rudimentary estimates. These codes use estimated component weights obtained from statistical weight equations, and either user-specified or default component *cg* locations to arrive at the overall aircraft *cg* location. However, as demonstrated by Chai *et al.* [11], the lack of responsiveness and accuracy have rendered current approaches inadequate for MDO application.

The lack of responsiveness is attributed to the fact that each aircraft component is assigned a specific location within the airframe. As a result, equilibrium would produce a single overall aircraft *cg* estimate as compared to a range of *cg* locations required in an MDO environment. In reality, the *cg* location is a complicated function of the configuration, loading, and fuel state, with an allowable range limited by a number of operational factors [12]. Although a range of *cg* locations can be established by varying

the configuration, equipment arrangement, and payload and fuel states individually, the process is laborious and time consuming. The accuracy limitations are attributable to the fact that the codes assume that the user has the experience and knowledge required to make the adjustments to the component weight and *cg* estimates. Unfortunately, this approach is not suitable for use in automated procedures required in MDO.

Evidently, what is needed is a new approach which is capable of establishing a maximum permissible *cg* range for a given configuration. This available *cg* range can then be compared with the desired operational *cg* range obtained from performance, control, and operational requirements. If the desired *cg* range is within the available cg range, the concept is viable and can be balanced. If not, the configuration must be changed, either by the designer or an MDO procedure if an automated process is being used.

2.3. Alternate Method

Component location uncertainty at the conceptual design phase is actively exploited as a means to improve the responsiveness and accuracy of current *cg* estimation procedures. In the proposed procedure, aircraft components are assigned a range of *cg* locations based on the geometry, as well as physical and functional considerations, associated with each component. By arranging the *cg* of the components at their fore- and aft-most limits, the maximum permissible *cg* range of a particular layout can be established. This *cg* range can then be used by an MDO procedure to determine the forward and aft aircraft *cg* limits required to meet performance and stability and control considerations. Adjusted for uncertainty, this maximum permissible *cg* range can be used as a constraint for the operational *cg* range during the optimization.

2.3.1. Establishment of Component CG Range

The assignment of component *cg* range is based on the geometry, planform, and the type of components involved. In the case of the primary components, *e.g.*, fuselage, wing, and empennage, the location of these items remains relatively unchanged once the

concept is frozen. Consequently, the *cg* range is expected to be centered near the volumetric center of the component and is unlikely to shift too much. For ease of identification, the primary components will be referred to as the *constrained* items.

As for the secondary components, *e.g.*, equipment and operational items, the location of each component varies from one aircraft concept to another, depending on the philosophy and preference of the airframe manufacturer. Note that as long as the stowage and functionality constraints are not violated, these components can be assigned to any available space throughout the aircraft due to their compactness. Consequently, the corresponding *cg* range is defined by the forward and aft boundaries of the stowage space within which the item is located. Accordingly, these components are termed the *unconstrained* items.

Although the payload and passenger amenity, *i.e.*, furnishings and services, are confined within the cargo holds and cabin, operational experience has shown that the *cg* location of these items varies according to the loading condition and cabin layout as specified by the airlines, respectively. Similarly, the *cg* location of the fuel varies as a function of time as the fuel is been consumed during the duration of the mission. Given the added freedom in terms of the loading pattern, these components are classified as unconstrained items.

2.3.2. Generic Component Layout

The proposed aircraft component *cg* ranges are listed in Table 2.1 and represented graphically in Figure 2.1. The ranges are based on the layout of existing commercial transports [13 and 14] and can be modified to accommodate any unique layout of the aircraft concept under consideration.

Table 2.1 Generic component location for conventional civil transports

Component	Type	Component *cg* range
Wing	Constrained	Between fore and aft spars along wing *mac*
Fuselage	Constrained	40 to 50 percent fuselage length
Horizontal tail	Constrained	Between fore and aft spars along horizontal tail *mac*
Vertical tail	Constrained	Between fore and aft spars along vertical tail *mac*
Engines/Nacelles	Constrained	45 to 60 percent engine length
Nose gear	Constrained	Between fore and aft wheelwell bulkheads
Main gear	Constrained	Between fore and aft wheelwell bulkheads
Fuel system	Unconstrained	Between fore and aft spars along wing *mac*
Hydraulics	Unconstrained	Between fore and aft wing spars along aircraft centerline; Between aft pressure bulkhead and tip of tailcone
Electrical system	Unconstrained	Between forward pressure bulkhead and nose wheelwell; Between fore and aft wing spars along aircraft centerline
Avionics	Unconstrained	Between forward pressure bulkhead and nose wheelwell
Instrumentation	Unconstrained	Between forward pressure bulkhead and nose wheelwell
Environmental	Unconstrained	Between fore and aft wing spars along aircraft centerline
Flight control	Unconstrained	Between aft spar and trailing-edge along surface *mac*
Auxiliary power	Unconstrained	Between aft pressure bulkhead and tip of tailcone
Furnishings	Unconstrained	45 to 60 percent cabin length
Services	Unconstrained	45 to 60 percent cabin length
Passengers	Unconstrained	45 to 60 percent cabin length
Cargo	Unconstrained	45 to 55 percent forward and aft cargo holds
Fuel	Constrained	Between fore and aft spars along wing *mac*; Between fore and aft wing spars along aircraft centerline

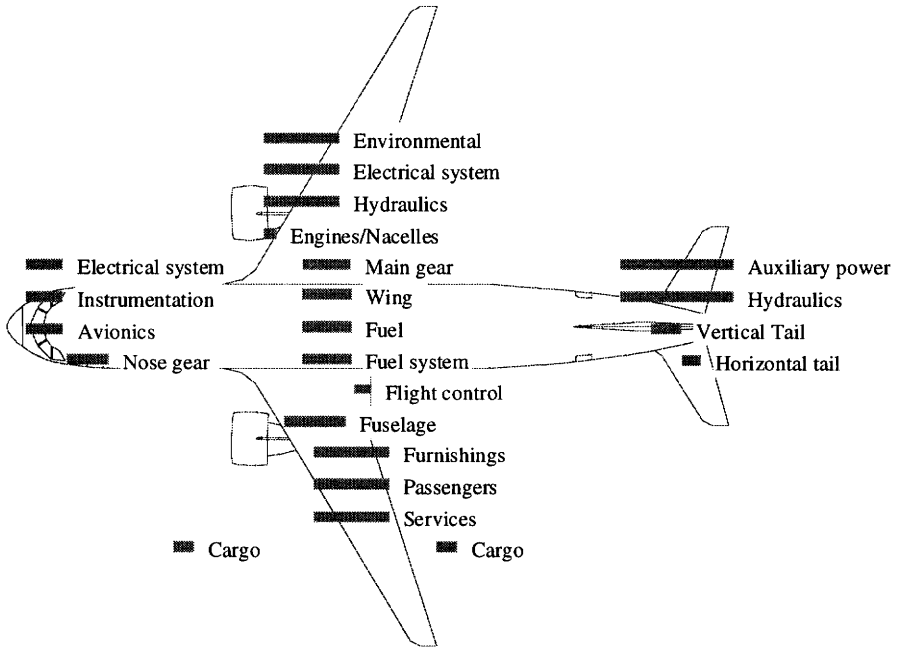

Figure 2.1 Ranges of available component *cg* locations

The locations of the front and rear spar for the wing and empennage are dictated by space required for housing the control surfaces and the associated actuation systems, where values of 15 and 65 percent chord, respectively, are typically used. As in the conventional cantilever wing and empennage construction, the majority of the structure, *i.e.*, bulkheads, ribs, and fuel tanks, are located between the front and rear spar. Thus, it can be expected that the *cg* of the wing is most likely to be located between the two, along the respective mean aerodynamic chords (*mac*). In addition, given the physical arrangement of the fuel tanks, the *cg* of the fuel and the fuel system can be expected to be located near the same vicinity.

The *cg* of the fuselage depends on the structural arrangement of the pressure bulkheads, frames, and the aft-body taper ratio. Other factors include local structural reinforcement around the landing gear wheelwells, cargo holds, and the layout of the cabin, *e.g.*, a forward upper-deck as found on the Boeing Model 747 or a double-decker as found on the proposed ultra-high-capacity transports. Taking these factors into

consideration, the proposed procedure assumes that the *cg* of the fuselage is most likely to be located between 40 and 50 percent of the fuselage length.

The *cg* of the engine group varies according to the dimensions of the engine, nacelle, and engine pylon. To account for weight-affecting factors such as compressor fan diameter, the shape of the nacelle, and pylon structure arrangement, forward and aft *cg* limit of 45 and 60 percent of the length of the engine, respectively, were assigned.

Regardless of the configuration of the landing gear, the *cg* of the landing gear will be confined between the landing gear wheelwells in flight. Thus, the forward and aft *cg* limits of the landing gear are assumed to coincide with the forward and aft stowage volume boundaries of the nose and main assembly wheelwells.

Hydraulics is divided into the wing and empennage group, with the weight proportional to the ratio of the respective control surface area to the total control surface area. The wing group is assumed to be located beneath the wing torsion box, which results in a *cg* range that is defined by the fore and aft wing spars along the aircraft centerline. On the other hand, the *cg* range of the empennage group is limited to the space behind the aft pressure bulkhead. Besides providing the stowage volume for the empennage hydraulics, the tail cone space also houses the auxiliary power unit.

Similarly, flight controls are divided into the wing and empennage group, with the weight proportional to the ratio of the local control surface area to the total control surface area. The proposed procedure assumes that the weight of the leading-edge control surfaces is negligible and that the trailing-edge control surfaces are in the retracted position. Thus, the *cg* of the flight controls are bounded by the rear spar and the trailing edge of each surface, along the respective *mac*s.

The electrical system is divided into the battery and generator groups, assuming that the weight is distributed evenly between the two. The battery group is to be located between the forward pressure bulkhead and the nose wheelwell, although it can also be located in the cavity between the nose wheelwell and the forward cargo hold. The generator group is to share the wing-body fairing cavity as being used to stow the wing

hydraulics, *i.e.*, under the wing torsion box. Due to functionality constraints, avionics and instrumentation are assumed to be located in the same compartment which houses the batteries. Similarly, environmental control packs are to share the wing-body fairing cavity with the electrical generator and wing hydraulic groups.

Given that the aircraft is fully loaded, the *cg* of the furnishings, services, and passengers is limited to between 45 and 60 percent of the cabin length. This assumption takes into account the distribution of the passengers and the corresponding arrangement of the furnishings and passenger services in different cabin layouts. To accommodate the variable nature of the cargo loading operation, which is affected by the type and weight of the baggage and bulk materials, forward and aft *cg* limits of 45 and 55 percent, respectively, of both forward and rear cargo holds were assigned.

2.3.3. Validation of Analysis

A simple spreadsheet software, where the component *cg* range data as presented in Table 2.1 are stored and a macro is defined for calculation purposes, is created to establish the forward and aft limits of the permissible aircraft *cg* range. A detailed description of the spreadsheet can be found in Chapter Nine. The Boeing Models 737, 747, 767, and McDonnell Douglas DC-10 were used to validate the proposed *cg* estimation procedure as outlined above. Estimated component weights were obtained from ACSYNT(AirCraft SYNThesis) [9] and used for all four aircraft, while component *cg* ranges were determined using the generic layout as detailed in the previous section. Essentially, the four aircraft are treated as conceptual aircraft. The objective here is to determine if the maximum permissible *cg* range as established by the new approach can enclose the actual operational *cg* range. Actual [15] and estimated aircraft *cg* ranges determined using the spreadsheet are listed in Table 2.2; both sets of data are shown in Figure 2.2 for ease of comparison.

Table 2.2 Aircraft *cg* range

Aircraft	Estimated, % *mac*	Actual, % *mac*
B737 (forward/aft)	0.0/68.0	12.0/30.0
B767 (forward/aft)	-4.0/67.0	11.0/32.0
DC10 (forward/aft)	-7.0/46.0	8.0/18.0
B747 (forward/aft)	4.0/63.0	13.0/33.0

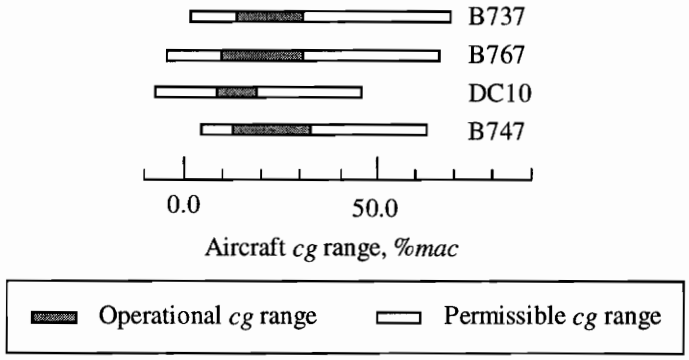

Figure 2.2 Actual and estimated aircraft *cg* range comparison

As shown in Figure 2.2, the new approach is capable of producing a permissible aircraft *cg* range that brackets in the actual operational *cg* range for all four aircraft. In addition, the estimated *cg* range offers a generous margin at either end-limit of the band representing the actual operational *cg* range. Given the fact that both the weight and location of the components are based on statistical information, the margin would ensure that the operational *cg* range remains within the obtainable range even when the uncertainty is factored in. Evidently, the proposed *cg* estimation procedure is able to meet the flexibility and reliability requirements that are essential for MDO applications.

Chapter 3 Landing Gear Concept Selection

3.1. Introduction

The design and positioning of the landing gear are determined by the unique characteristics associated with each aircraft, *i.e.*, geometry, weight, and mission requirements. Given the weight and *cg* range of the aircraft, suitable configurations are identified and reviewed to determine how well they match the airframe structure, flotation, and operational requirements. The essential features, *e.g.*, the number and size of tires and wheels, brakes, and shock absorption mechanism, must be selected in accordance with industry and federal standards discussed in the following chapters before an aircraft design progresses past the concept formulation phase, after which it is often very difficult or impossible to change the design [16].

Based on the design considerations as discussed in this chapter, algorithms were developed to establish constraint boundaries for use in positioning the landing gear, as well as to determine whether the design characteristics violate the specified requirements. The considerations include stability at takeoff/touchdown and during taxiing, braking and steering qualities, gear length, attachment scheme, and ground maneuvers.

3.2. Configuration Selection

The nose wheel tricycle undercarriage has long been the preferred configuration for passenger transports. It leads to a nearly level fuselage and consequently the cabin floor when the aircraft is on the ground. The most attractive feature of this type of undercarriages is the improved stability during braking and ground maneuvers. Under normal landing attitude, the relative location of the main assembly to the aircraft *cg* produces a nose-down pitching moment upon touchdown. This moment helps to reduce the angle of attack of the aircraft and thus the lift generated by the wing. In addition, the

braking forces, which act behind the aircraft *cg*, have a stabilizing effect and thus enable the pilot to make full use of the brakes. These factors all contribute to a shorter landing field length requirement.

The primary drawback of the nose wheel tricycle configuration is the restriction placed upon the location where the main landing gear can be attached. With the steady increase in the aircraft takeoff weight, the number of main assembly struts has grown from two to four to accommodate the number of tires required to distribute the weight over a greater area. However, stability and performance constraints as identified by Holloway *et al.* [17] and Sliwa [18] effectively eliminate all but a few locations where the main assembly can be attached. The attachment limitation phenomenon is known as the location stagnation [App. A] and can become a major concern for future large aircraft, where additional tires and struts are required to alleviate the load being applied to the pavement. Typically, a large trailing-edge extension, *i.e.*, the Yehudi, is employed to alleviate at least in part the location stagnation problem. However, a large Yehudi can result in weight and aerodynamic penalties due to local structural reinforcement and increased wetted area, respectively.

3.3. Landing Gear Disposition

The positioning of the landing gear is based primarily on stability considerations during taxiing, liftoff and touchdown, *i.e.*, the aircraft should be in no danger of turning over on its side once it is on the ground. Compliance with this requirement can be determined by examining the takeoff/landing performance characteristics and the relationships between the locations of the landing gear and the aircraft *cg*.

3.3.1. Angles of Pitch and Roll During Takeoff and Landing

The available pitch angle (θ) at liftoff and touchdown must be equal, or preferably exceed, the requirements imposed by performance or flight characteristics. A geometric limitation to the pitch angle is detrimental to the liftoff speed and hence to the takeoff field

length. Similarly, a geometric limitation to the roll angle (ϕ) could result in undesirable operational limit under cross-wind landing condition.

For a given aircraft geometry and gear height (h_g), the limit for the takeoff/landing pitch angle follows directly from Figure 3.1. The roll angle at which the tip of the wing just touches the ground is calculated using the expression [3, p. 350]

$$tan\phi = tan\Gamma + \frac{2h_g}{s-t} - tan\theta\, tan\Lambda \tag{3.1}$$

In this case, Γ is taken as the dihedral angle, s is the wing span, t is the wheel track, and Λ is the wing sweep. Similar conditions may be deduced for other parts of the aircraft, except that Γ, Λ and s in Eq. (3.1) must be replaced with appropriate values. For example, the permissible roll angle associated with nacelle-to-ground clearance is determined with the following values: Γ measured from the horizon to the bottom of the nacelle in the front view, Λ measured from the chosen landing gear location to the engine in the top view, and s the distance between the engines.

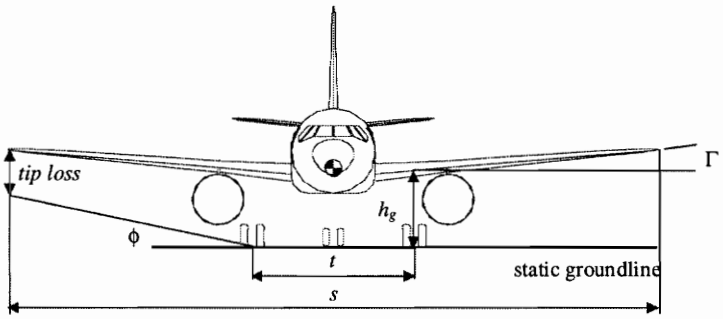

a) Front view

Figure 3.1 Geometric definitions in relation to the pitch and roll angles [3]

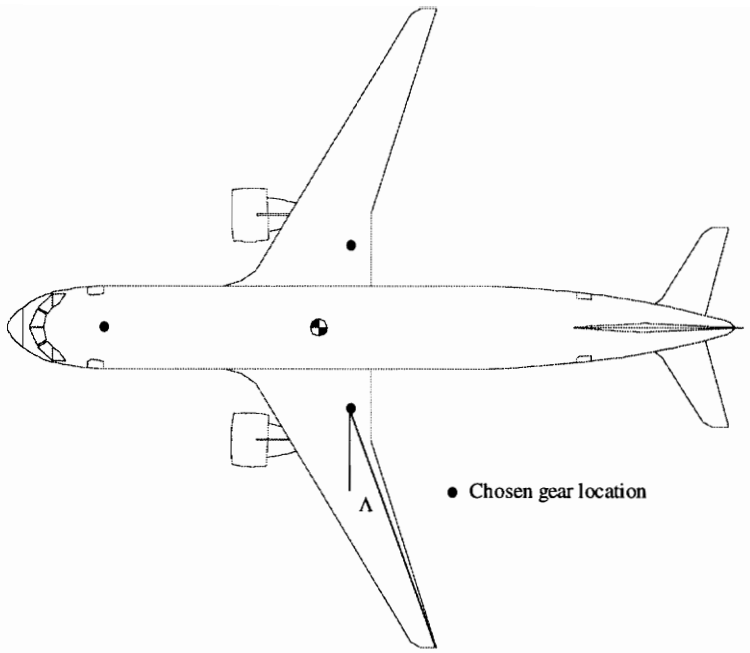

b) Top view

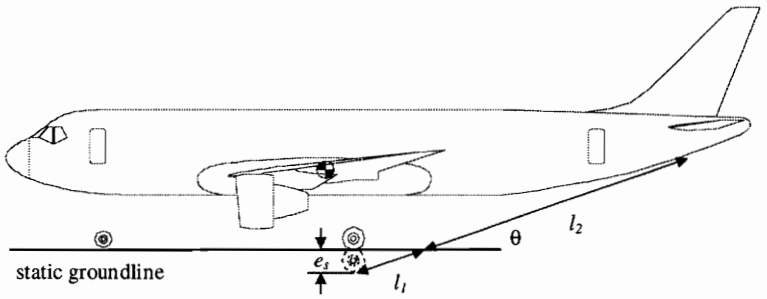

c) Side view

Figure 3.1 Geometric definitions in relation to the pitch and roll angles (cont'd)

3.3.1.1. Pitch Angle Required for Liftoff

Accurate determination of the desired values for θ and ϕ can only be carried out after the performance characteristics of the aircraft become available. The pitch angle at liftoff (θ_{LOF}) is calculated using the expression [3, p. 350]

$$\theta_{LOF} = \alpha_{LOF} + \frac{d\theta}{dt}\left(\frac{2l_1}{V_{LOF}} + \sqrt{\frac{l_2}{g}\frac{C_{L_{LOF}}}{dC_L/d\alpha}}\right) \tag{3.2}$$

where α_{LOF} is the highest angle of attack anticipated for normal operational use, V_{LOF} is the liftoff speed, g is the gravitational acceleration $C_{L,\,LOF}$ is the lift coefficient, and dC_L/d_α is the lift-curve slope. As shown in Figure 3.1, the dimension of l_1 and l_2 are defined by the line connecting the tire-ground contact point upon touchdown and the location of the tail bumper, if one is present. For large transports, the typical value for the rate of rotation ($d\theta/dt$) is taken as four degrees per second [3].

The detailed aerodynamic data required to use Eq. (3.2) is not always available at the conceptual design stage. In most aircraft the aft-body and/or tail bumper is designed such that the aircraft cannot rotate by more than a specified number of degrees at liftoff. Typically, the value is between 12 and 15 degrees [2]. In addition to the tail scrape problem, the aircraft *cg* cannot rotate over and aft of the location of the main assembly, a phenomenon known as tail tipping and is critical during landing.

3.3.1.2. Pitch and Roll Angles During Landing

With the flaps in the fully-deflected position, the critical angle of attack of the wing during landing is smaller than in takeoff. Consequently, pitch and roll angles during landing are generally less than that during takeoff. In the absence of detailed information, the pitch angle on touchdown (θ_{TD}) may be assumed equal to θ_{LOF}. As for the roll angle upon touchdown, an upper limit of between five [19] and eight [3] degrees is generally applied to large transport aircraft.

3.3.2. Stability at Touchdown and During Taxiing

Static stability of an aircraft at touchdown and during taxiing can be determined by examining the location of the applied forces and the triangle formed by connecting the attachment locations of the nose and main assemblies. Whenever the resultant of air and mass forces intersects the ground at a point outside this triangle, the ground will not be

able to exert a reaction force which prevents the aircraft from falling over. As a result, the aircraft will cant over about the side of the triangle that is closest to the resultant force/ground intersect.

Assuming first that the location of the nose assembly is fixed, the lower limit of the track of the landing gear, identified as constraint I in Figure 3.2, is defined by the line passing through the center of the nose assembly and tangential to the circle with a radius of 0.54 times the height of the aircraft *cg* (h_{cg}) from the static groundline, centered at the fore-most *cg* location [3]. The constant 0.54 is based on static and dynamic instability considerations at touchdown and during taxiing. Conversely, if the location of the main assembly is assumed to be fixed, the aft-most limit of the nose assembly mounting location, identified as constraint II in Figure 3.2, is defined as the intersection of the aircraft centerline and the line that passes through the center of the main assembly, tangential to the circle with a radius of 0.54 times of the height of aircraft *cg*.

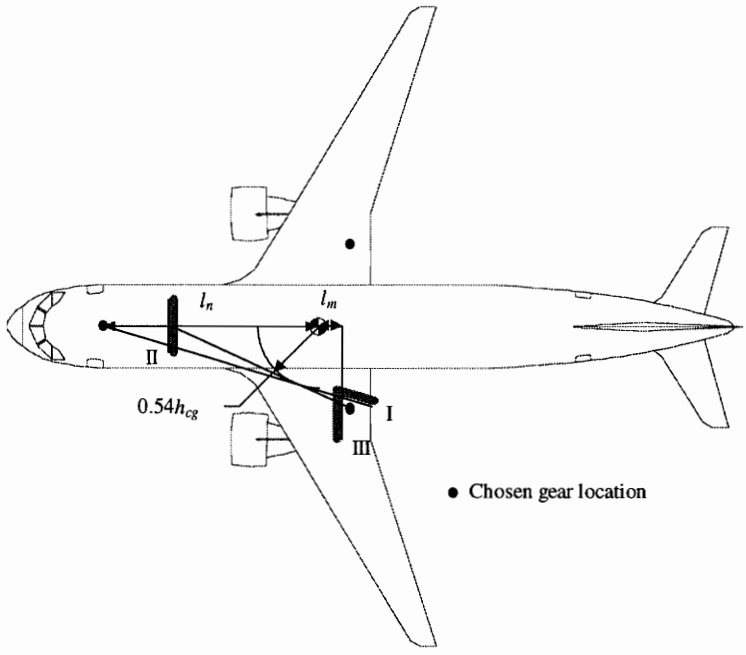

Figure 3.2 Limits for the undercarriage disposition based on stability [3]

3.3.2.1. Condition at Touchdown

The most unfavorable condition at touchdown would be a landing with the aircraft *cg* at its aft-most and highest location, which can lead to the tail scrape and tail tipping phenomenon mentioned previously. Assuming there are no retarding forces, *i.e.*, spin-up load, a vertical force acting at a distance behind the aircraft *cg* is needed to produce a moment that will pitch the nose downward. Thus, the minimum allowable offset between the aft-most *cg* and the main assembly mounting locations, identified as constraint III in Figure 3.2, is determined using the following expression [3, p. 352]

$$l_m \geq (h_{cg} + e_s) tan\theta_{TD} \tag{3.3}$$

where e_s is the total static deflection of the shock strut and tire, and θ_{TD} is the pitch angle at touchdown. Note that the offset distance is dependent on the value of the pitch angle, whose value is similar to the pitch angle at liftoff, *i.e.*, between 12 and 15 degrees. For a low-wing passenger aircraft, h_{cg} can be approximated assuming a full load of passengers and no wing fuel [2]. This generally results in a vertical *cg* position at the main passenger-deck level.

3.3.2.2. Sideways Turnover Angle

Forces acting sideways on the airplane in cross-wind landing condition or a high-speed turn during taxiing could cause the aircraft to turnover on its side. It is thus desirable to keep the turnover angle (ψ) as small as possible. The angle is determined using the expression [2, p. 38]

$$tan\psi = \frac{h_{cg}}{l_n \, sin\delta} \tag{3.4}$$

where

$$tan\delta = \frac{t}{2(l_m + l_n)} \tag{3.5}$$

and δ is defined as the angle between the aircraft centerline and the line connecting the center of the nose and main assembly. The dimensions used in the above equations are

given in Figure 3.3. For land-based aircraft, either the maximum allowable overturn angle of 63 degrees [2] or the stability considerations at takeoff/touchdown and during taxiing, whichever is the most critical, determines the lower limit for the track of the main assembly.

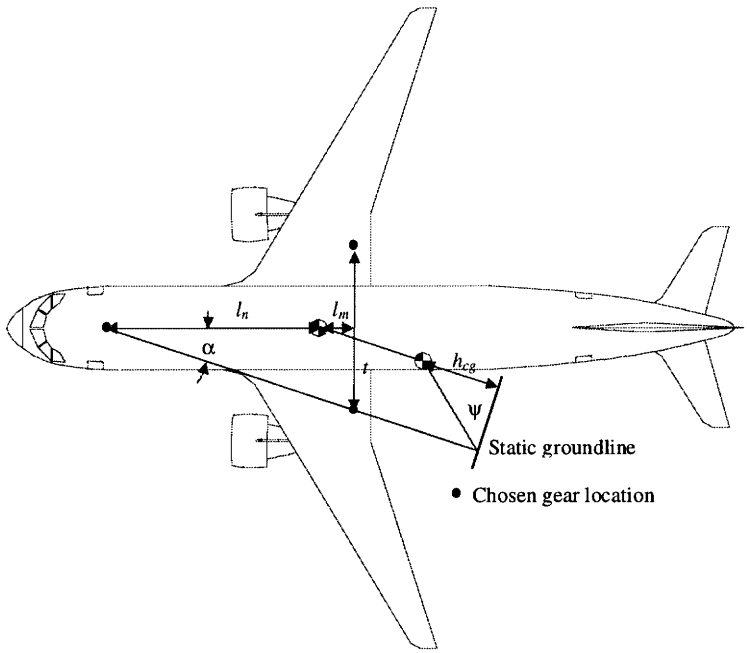

Figure 3.3 Turnover angle calculation [2]

3.3.3. Braking and Steering Qualities

The nose assembly is located as far forward as possible to maximize the flotation and stability characteristics of the aircraft. However, a proper balance in terms of load distribution between the nose and main assembly must be maintained. When the load on the nose wheel is less than about eight percent of the maximum takeoff weight (MTOW), controllability on the ground will become marginal, particularly in cross-wind conditions. On the other hand, when the static load on the nose wheel exceeds about 15 percent of the MTOW, braking quality will suffer, the dynamic braking load on the nose assembly may

become excessive, and a greater effort may be required for steering [3]. Note that these figures should be looked upon as recommendations instead of requirements.

3.3.4. Gear Length

Landing gear struts should be of sufficient length such that adequate clearance between the runway and all other parts of the aircraft, *e.g.*, the aft-body, wingtips, and engine nacelles, is maintained when the aircraft is on the ground. For a low-wing aircraft with wing-mounted engines, the above requirement proves to be one of the most challenging design issues in terms of permissible roll angle at touchdown. Although engine nacelle-to-ground clearance has not been explicitly defined, a similar requirement for propellers was specified in FAR Part 25 and can be used as an absolute minimum: a seven-inch clearance between the propellers and the ground in level takeoff or taxiing attitude, whichever is most critical. To date, the smallest offset on jet transports is found on the Boeing Model 747/GE90 testbed, where the GE90 engine nacelle clears the ground by a mere 13-inch clearance [20]. As for operational aircraft, the Boeing Model 737-300, -400, and -500 exhibit a 15-inch nacelle-to-ground clearance [21]. The length of the nose wheel strut is generally based on the requirement that the fuselage should be horizontal or tilted slightly nose-down when the aircraft is on the ground.

Besides the clearance considerations, allowance must also be considered for future stretching of the aircraft, which generally involves adding plugs forward and aft of the wing spars. Provided that the attitude of the aircraft will remain the same, the increase in the aft fuselage length would thus reduce the maximum permissible takeoff rotation angle, which can result in costly modifications and thus effectively rule out future growth options. Boeing abandoned further stretches of the Model 727 partially because of the difficulties encountered while attempting to maintain an adequate tail scrape angle, whereas Douglas was able to reduce the required tail scrape angle on the MD-11 by increasing the wing incidence by three degrees over that of its 22-foot shorter DC-10-30 forebear.

3.3.5. Landing Gear Attachment

From considerations of surrounding structure, the nose and main assembly are located such that the landing and ground loads can be transmitted most effectively, while at the same time still comply with the stability and controllability considerations. For a wing-mounted assembly, the trunnion is generally attached to the rear wing spar and the landing gear beam and the loads are transmitted directly to the primary wing-fuselage bulkheads. With the inclusion of fuselage-mounted assemblies in the multiple main-strut configurations, a secondary frame would then be added at a distance behind the rear wing-spar, where loads are transmitted forward to the primary wing-fuselage bulkhead through the keel and by shear in the fuselage skin. As for the nose assembly, structural considerations may be conclusive in deciding the mounting location, *i.e.*, at the proximity of forward cabin bulkhead to minimize weight penalty due to local structural reinforcement.

3.4. Ground Operation Characteristics

Besides ground stability and controllability considerations, the high costs associated with airside infrastructure improvements, *e.g.*, runway and taxiway extensions and pavement reinforcements, have made airfield compatibility issues one of the primary considerations in the design of the landing gear [22]. In particular, the aircraft must be able to maneuver within a pre-defined space as it taxies between the runway and passenger terminal. For large aircraft, this requirement effectively places an upper limit on the dimension of the wheelbase and track.

3.4.1. Aircraft Turning Radii

As shown in Figure 3.4, turning radii are defined as the distances between the center of rotation and various parts of the aircraft. The center of rotation is located at the intersection of the lines extending from the axes of the nose and main assemblies. For aircraft with more than two main struts, the line extending from the main assembly group

is located midway between the fore and aft gears. The turning radii are a function of nose gear steering angle (β); the greater the angle, the smaller the radii. The upper limit for this angle is determined by the methods available to provide the steering action, which generally limits the angle to ±60 degrees [2].

The turning radius corresponding to an 180-degree turn ($r_{180^\circ\, turn}$) as identified in Figure 3.4, is determined using the expression

$$r_{180^\circ turn} = b\tan(90-\beta)+\frac{t}{2} \tag{3.6}$$

where b and t are the wheelbase and track, respectively. Given the aircraft design group classification as listed in Table 3.1, the minimum turning diameter, *i.e.*, twice of the 180-degree turn radius, should be less than the corresponding runway pavement width.

Table 3.1 FAA airplane design group classification for geometric design for airports [5]

Airplane design group	Wingspan, ft	Runway width, ft
III	79.0 < s < 118.0	100.0
IV	118.0 < s < 171.0	150.0
V	171.0 < s < 197.0	150.0
VI	197.0 < s < 262.0	200.0

With the greater wheelbase and track dimensions as exhibited by large aircraft, the 180-degree turn maneuver can no longer be achieved with the conventional nose-steering scheme alone. As a result, combined nose and main assembly steering systems have been introduced on the newer large aircraft, *e.g.*, Boeing Models 747 and 777, to reduce the turning radii. Other advantages provided by this feature include reduced tire wear and scuffing of the pavement surface in a sharp turn. Note that at the conceptual design phase of an aircraft, Eq. (3.6) is sufficient in producing a first-cut estimate. The resulting turning radii, which are based on nose-steering scheme, are slightly larger than the ones corresponding to combined nose and main assembly steering scheme, and thus provide a built-in safety margin.

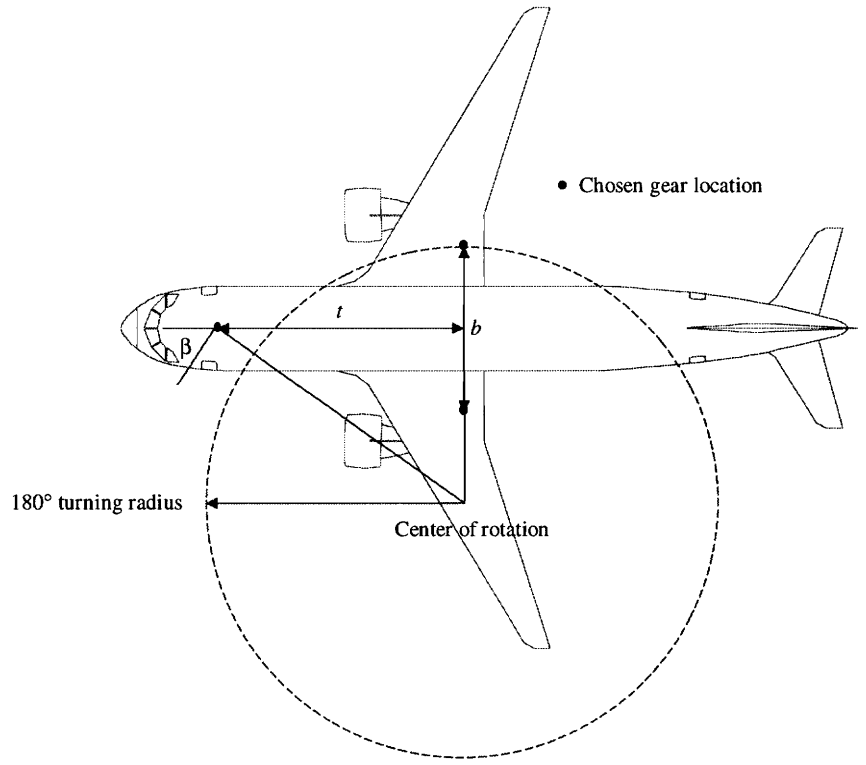

Figure 3.4 Aircraft turning radii [5]

3.4.2. Centerline-guidance Taxiing

The size of the fillets at runway and taxiway intersections depend not only on wheelbase, radius of centerline curve, width of taxiway, and total change in direction, but also on the path that the aircraft follows. There are two options in which an aircraft can be maneuvered on a turn: one is to establish the centerline of the taxiway as the path of the nose gear; the other is to assume that the nose gear follows a path offset outward of the centerline. The former is selected as the critical design case since it is the most demanding of the two in terms of piloting skill, *i.e.*, difficult to keep the nose wheel, which is below and behind the pilot's field of view, on the centerline while taxiing, and thus requires a greater area of pavement during the maneuver as safety margin.

As shown in Figure 3.5, the maximum castor angle (φ), *i.e.*, the angle formed between the tangent to the centerline and the longitudinal axis of the aircraft, will occur at

the end of the turn, where the nose wheel is at the point of tangency. The angle is approximated by [5, p. 318]

$$sin\varphi = \frac{b}{R} \tag{3.7}$$

where R is the radius of centerline curve. A re-check should be made at this point to make sure that the design castor angle is within the permissible range of the steering angle.

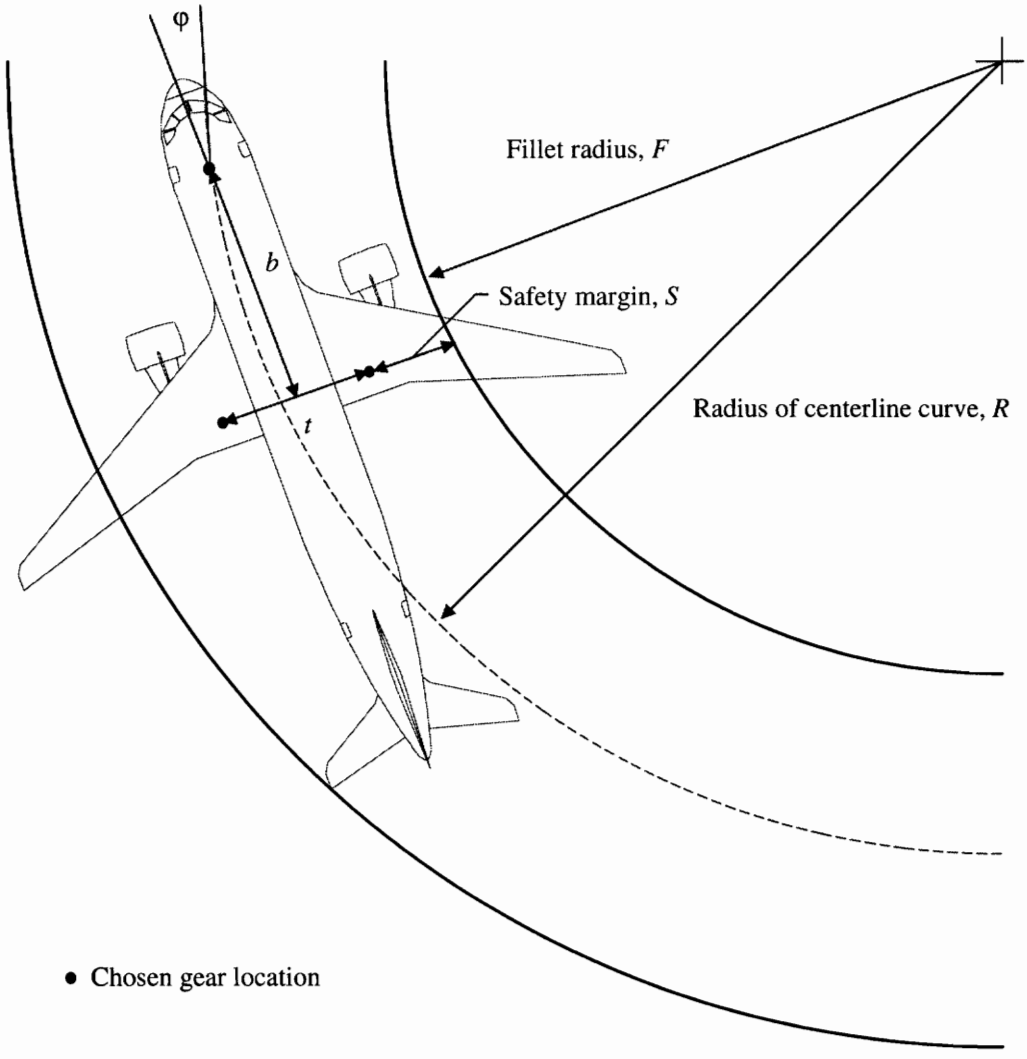

Figure 3.5 Taxiway fillet design [5]

For a given wheelbase and track dimension, the required fillet radius (F) is calculated using the expression [5, p. 318]

$$F = \sqrt{R^2 + b^2 - 2Rb\sin\varphi} - \frac{t}{2} - S \tag{3.8}$$

where S is the minimum distance required between the edge of the outboard tire and the edge of the pavement. Given the aircraft design group classification number as determined from Table 3.1 and the corresponding FAA design values as presented in Table 3.2, the upper limit for the wheelbase and track of the aircraft can be determined using Eqs (3.7) and (3.8).

Table 3.2 FAA recommended taxiway exit geometry [5]

	Group III	**Group IV**	**Group V**	**Group VI**
Centerline radius, ft	100.0	150.0	150.0	170.0
Fillet radius, ft	55.0	80.0	85	85.0
Safety margin, ft	10.0	15.0	15.0	20.0

3.5. Landing Gear Disposition Constraints

Landing gear location constraints as discussed in the above sections are superimposed on the three-view of a notional aircraft for illustrative purposes. As shown in Figure 3.6a, the main assembly must be located such that when the shock strut is at the fully-extended position, the tire-ground contact point is below constraints II and IV in the vertical direction and outboard of constraint I in the lateral direction. In the top view as shown in Figure 3.6b, the main assembly must also be located aft of constraint IV in the longitudinal direction and outboard of constraint V in the lateral direction. As for the nose assembly, it must be located between constraints I and II in the longitudinal direction. And finally, as shown in Figure 3.6c, the fully-extended tire-ground contact point is below constraint II in the vertical direction and aft of constraint II in the lateral direction.

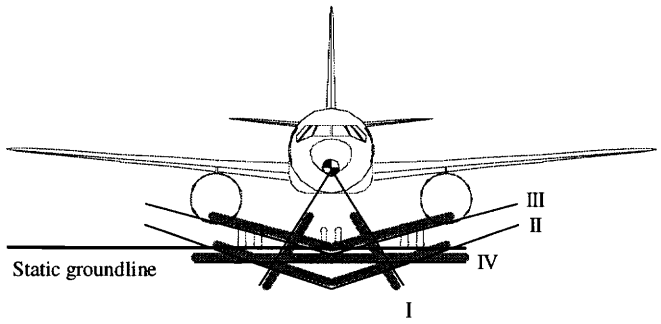

I	Sideways turnover	III	Wingtip-to-ground clearance
II	Nacelle-to-ground clearance	IV	Fuselage tail clearance at liftoff

a) Front view

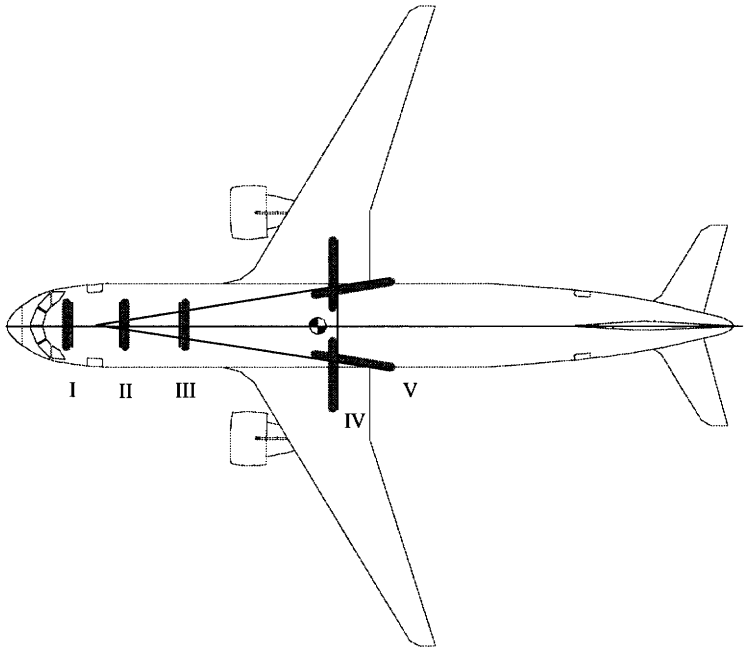

I	Nosewheel load, 8% MTOW	IV	Touchdown
II	Nosewheel load, 15% MTOW	V	Sideways turnover, fixed nosewheel location
III	Sideways turnover, fixed main wheel loaction		

b) Top view

Figure 3.6 Landing gear attachment location constraints [3]

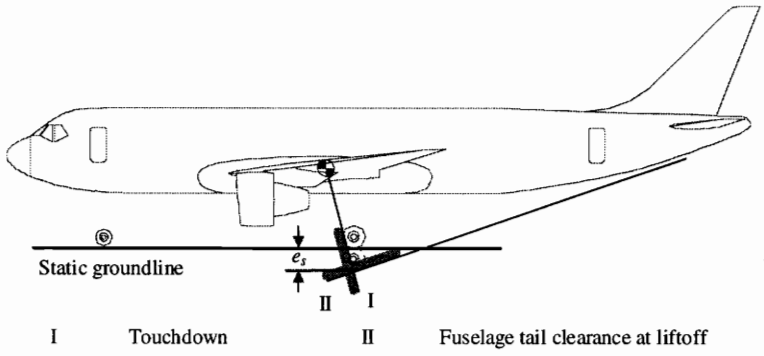

c) Side view

Figure 3.6 Landing gear attachment location constraints (cont'd)

Chapter 4 Tires, Wheels, and Brakes

4.1. Introduction

The number of tires required for a given aircraft design gross weight is largely determined by the flotation characteristics, which will be discussed in detail in Chapter Seven. Assuming that the number and distribution pattern of the tires is already known, this chapter provides guidelines to the selection of the tires, wheels, and brakes that will meet the performance and safety requirements [2 and 19].

As a part of the landing gear configuration definition process, tires, wheels, and brakes selection algorithms were developed based on the procedure as discussed in this chapter. Specified selection criterion, *e.g.*, minimum size, weight, or pressure, are used to select suitable tires and wheels from manufacturer's catalog [23] and industry standards [24], while statistical database was used to size the brakes as required to meet the braking requirements.

4.2. Type, Size and Inflation Pressure of the Tire

The tire selection process involves listing all candidate that meet the performance requirements. A list of tires and wheels used on commercial transports can be found in Appendix D. The primary consideration is the load-carrying capacity of the tire during the speed regime normally applicable for landing or takeoff cycles. In addition, the number of plys and type of construction, which determines the weight of the tire and its operational life, is important from an economic standpoint. Other considerations include the inflation pressure of the tire and the size of the wheel. The former must be chosen in accordance with the bearing capacity of the airfield from which the aircraft is designed to operate from, whereas the latter must have sufficient space to house the brake assembly.

4.2.1. Basic Tire Constructions

Radial tires have gained growing acceptance since their introduction despite a somewhat cautious approach at the beginning, which is attributed to lack of applicable standards, concerns about the *mixability* with bias tires, and *retreadability* of refurbished tires. Intermixing of radial and bias tires, or even with radial tires of different construction, is possible only if the loading is no more uneven than currently encountered with mixing of bias tires only. As for retreadability, it should be noted that multiple retreating is not necessarily a benefit to the airlines; instead, it could be an indication of low tire performance in terms of tread wear. Thus, the concern here is not as much how often the tire can be retreated, but how to extend the average total carcass life.

In radial construction, shear stresses in the rubber matrix are minimized and loads are efficiently distributed throughout the tire. Even if the same basic materials used in bias tires are used in the radials, the amount of material required for a particular application can be reduced. As a result, weight savings of up to 20 percent have been realized [25]. In addition, minimized slippage between the tire and the contact surface and the near optimal tuning of belt stiffness that comes with the radial construction all contributed to improved wear performance. In fact, some radial tires currently achieve twice as many landings per tread as conventional bias tires [25].

Operational experience has also shown that radial tires offer a greater overload bearing capacity and withstand under-inflation better. An approximately 10-percent increase in the footprint area improves the flotation characteristics and reduces hydroplaning on wet runways [25]. In addition, radial tires do not fail as suddenly as bias tires do. Warning signs such as external deformation and out-of-roundness exhibited prior to catastrophic failure provide indications of a potential blowout to maintenance personnel, and thus enhance operational safety.

4.2.2. Size of the Tire

The choice of the main wheel tires is made on the basis of the static loading case. The total main gear load (F_m) is calculated assuming that the aircraft is taxiing at low speed without braking. As shown in Figure 4.1, equilibrium gives [3, p. 356]

$$F_m = \frac{l_n}{l_m + l_n} W \tag{4.1}$$

where W is the weight of the aircraft and l_m and l_n are the distance measured from the aircraft *cg* to the main and nose gear, respectively. The design condition occurs at MTOW with the aircraft *cg* at its aft limit. For single axle configurations, the total load on the strut is divided equally over the tires, whereas in tandem configurations, the load per wheel depends on the location of the pivot point; to reduce overloading of the front wheels during braking, the pivot is usually positioned such that the distance between it and the front and rear wheel axles is about 55 and 45 percent of the truck beam, respectively [3].

The choice of the nose wheel tires is based on the nose wheel load (F_n) during braking at maximum effort, *i.e.*, the steady braked load. Using the symbols shown in Figure 4.1, the total nose gear load under constant deceleration is calculated using the expression [3, p. 358]

$$F_n = \frac{l_m}{l_m + l_n}(W - L) + \frac{h_{cg}}{l_m + l_n}\left(\frac{a_x}{g} W - D + T\right) \tag{4.2}$$

where L is the lift, D is the drag, T is the thrust, and h_{cg} is the height of aircraft *cg* from the static groundline. Typical values for a_x/g on dry concrete vary from 0.35 for a simple brake system to 0.45 for an automatic brake pressure control system [3]. As both D and L are positive, the maximum nose gear load occurs at low speed. Reverse thrust decreases the nose gear load and hence the condition $T = 0$ results in the maximum value [3, p. 359]

$$F_n = \frac{l_m + h_{cg}(a_x / g)}{l_m + l_n} W \tag{4.3}$$

The design condition occurs at MTOW with the aircraft *cg* at its forward limit.

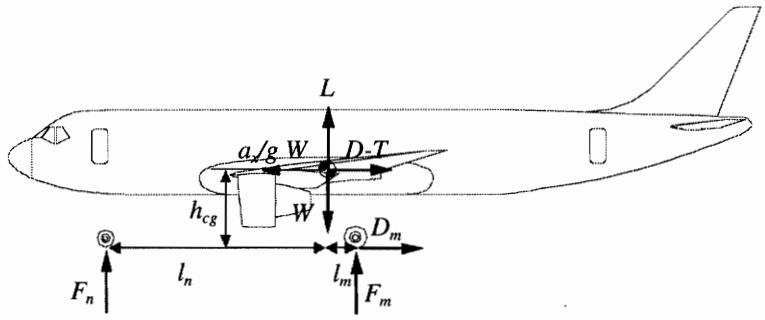

Figure 4.1 Forces acting on the aircraft during a braked roll [3]

To ensure that the rated loads will not be exceeded in the static and braking conditions, a seven percent safety factor is used in the calculation of the applied loads [2]. In addition, to avoid costly redesign as the aircraft weight fluctuates during the design phase, and to accommodate future weight increases due to anticipated aircraft growth, the calculated loads are factored upward by another 25 percent prior to tire selection [2].

4.2.3. Inflation Pressure

Provided that the wheel load and configuration of the landing gear remain unchanged, the weight and volume of the tire will decrease with an increase in inflation pressure. From the flotation standpoint, a decrease in the tire contact area will induce a higher bearing stress on the pavement, thus eliminates certain airports from the aircraft's operational bases. Braking will also become less effective due to a reduction in the frictional force between the tires and the ground. In addition, the decrease in the size of the tire, and hence the size of the wheel, could pose a problem if internal brakes are to be fitted inside the wheel rims. The arguments against higher pressure are of such a nature that commercial operators generally prefer the lower pressures in order to maximize tire life and minimize runway stress [25].

4.3. Wheel Design

The design of the aircraft wheel is influenced primarily by its requirement to accommodate the selected tire, to be large enough to house the brake, and to accomplish the above tasks with minimum weight and maximum life. As shown in Figure 4.2, two basic configurations of wheel design are currently available: A-frame and bowl-type [26]. The former is structurally the most efficient and therefore the lightest that can be achieved. However, this design has a limited space for housing the brake as compared to the bowl-type design. Consequently, as the braking energy requirement increases with aircraft weight and hence the size of the heat sink required, it might be necessary to resort to a bowl-type design even though it has a weight penalty [26].

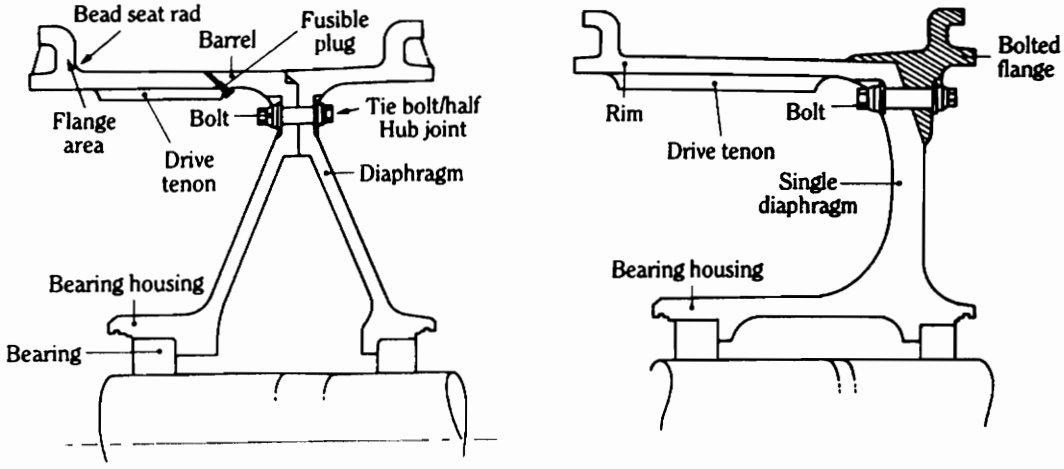

a) A-frame b) Bowl-type

Figure 4.2 Basic configuration of wheel design [26]

Continued heavy dependence on forged aluminum alloy wheels is foreseen by industry, whereas steel and magnesium alloy wheels are no longer given serious consideration due to weight and corrosion problems, respectively [27]. Although practicable, titanium wheels are still quite expensive. Most of the premium for titanium wheels results from the expense for the forging process, which could be 10 to 11 times

those of aluminum alloy [27] In addition, current titanium forging tolerances have yet to reach the precision obtainable for aluminum material, thus machining of all surfaces is required to control weight and obtain the desired form.

Based on statistical data, the wheel assembly weight is determined as a function of the rated per wheel static load (F) and average tire outer diameter (D) [2, p. 145]

$$f_w = \frac{FD}{1000} \tag{4.4}$$

Given the type of material to be used, the wheel assembly unit weight is obtained from Figure 4.3 with the weight factor (f_w) as determined from Eq. (4.4).

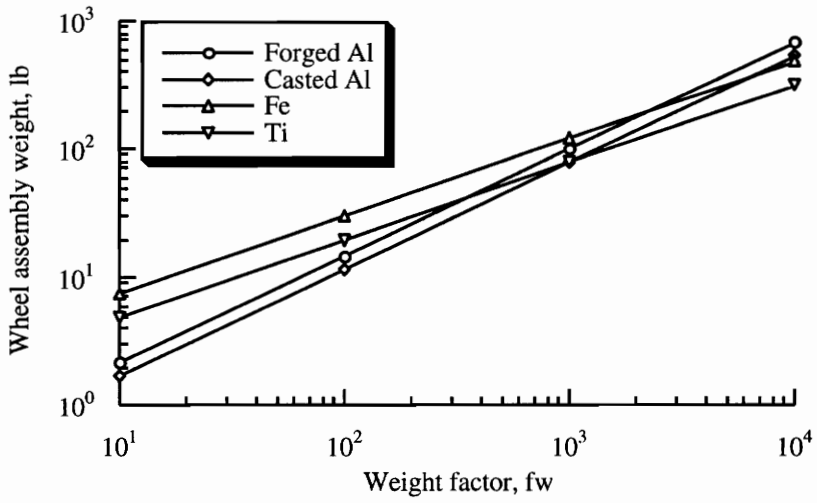

Figure 4.3 Aircraft wheel assembly weight [2]

4.4. Brake Design

Besides the primary task of stopping the aircraft, brakes are used to control speed while taxiing, to steer the aircraft through differential action, and to hold the aircraft stationery when parked and during engine run-up. Since the heat sinks account for a

significant fraction of total landing gear weight, there is a continual effort to reduce their weight through the application of advanced materials, namely, carbon [16].

4.4.1. Heat Sink Material

Material characteristics of steel and carbon are compared in Table 4.1. As shown in the table, carbon's high specific heat and thermal conductivity make it highly desirable as a heat absorber. The former ensures a reduction in brake weight, while the latter ensures that the heat transfer throughout the heat sink occurs more uniformly and at a faster rate. In addition, carbon retains much of its specific strength, which is defined as the ultimate tensile strength divided by density, at high temperature while steel loses almost all of its strength.

Table 4.1 Heat sink materials comparison [2]

Property	Steel	Carbon	Desired
Density, lb/in^3	0.283	0.061	High
Specific heat at 500°F, Btu/lb•°F	0.13	0.31	High
Thermal conductivity at 500°F, $Btu/h•ft^2•°F$	24.0	100.0	High
Thermal expansion at 500°F, 1.0E-6 in•°F/in	8.4	1.5	Low
Thermal shock resistance index, ×105	5.5	141.0	High
Temperature limit, °F	2,100	4,000	High

Long service life and low maintenance requirements for carbon brakes prove to be another plus from an economic standpoint. It was estimated that carbon would permit up to five to six times more landings as compared to steel between refurbishment and would require fewer man-hours for overhaul [26]. To illustrate the economic advantage of using carbon brakes, it was estimated that a total weight saving of 1,200 pounds could be achieved on the Concorde using carbon brakes. This is equivalent to five percent of its estimated transatlantic payload [28].

The primary drawback of carbon brakes is that a greater volume is required to absorb the same amount of energy in comparison to steel brakes. Some problems with

carbon brakes include sudden loss of strength due to oxidation of the carbon, temporary loss of braking due to moisture contamination, and high initial cost. However, these issues have largely been resolved in favor of the performance and economic aspects of carbon heat sinks [16]. In fact, advanced transports such as the Boeing Model 777 and the emerging ultra-high-capacity aircraft all feature carbon brakes.

4.4.2. Brake Sizing

The primary consideration in brake development is the size and weight of the brake required to meet the kinetic energy generated under the design landing weight, maximum landing weight, and rejected takeoff (RTO) conditions. Brake capacity requirements for these braking conditions are listed in Table 4.2.

Table 4.2 FAA commercial transport brake capacity requirements [19]

	Specifications
Design landing weight	100 stops at average of 10 ft/s^2 deceleration
Maximum landing weight	5 stops at average of 10 ft/s^2 deceleration
Rejected takeoff	1 stop at average of 6 ft/s^2 deceleration

The total kinetic energy is determined using the expression [19]

$$KE = 0.0443WV^2 \tag{4.5}$$

where V is the power-off stalling speed in knots. Assuming that the power-off stalling speed is 1.2 times of the stalling speed (V_s), it can be approximated using the expression [3, p. 577]

$$V = 1.2V_s = 1.2\sqrt{\frac{2W}{1.13\rho S C_{L,\max}}} \tag{4.6}$$

where ρ is the standard sea-level air density, S is the reference wing area, and $C_{L,max}$ is the maximum wing lift coefficient. The constant 1.13 takes into account the speed loss in the

FAA stall maneuver [3]. As illustrated above, the kinetic energy absorption requirements increase as the square of the velocity and hence the landing speed is significant.

The procedure used to size a steel brake is given here for illustrative purposes. Similar data for carbon are not available, but scaling factors of 1.28 and 0.40 can be used to relate the steel volumes and weights, respectively, to those values for carbon [29]. Kinetic energy levels expected under the normal landing weight, maximum landing weight, and RTO conditions are first calculated using Eq. (4.5) and the appropriate aircraft weights. Brake assembly weights (W_{brake}) corresponding to each kinetic energy level are obtained from Figure 4.4 and averaged to arrive at a compromise value. The required heat sink volume (V_{brake}) is then approximated using the expression

$$V_{brake} = 3.3W_{brake} - 84.2 \tag{8.7}$$

where the constant coefficients are determined using linear regression analysis on statistical database[2].

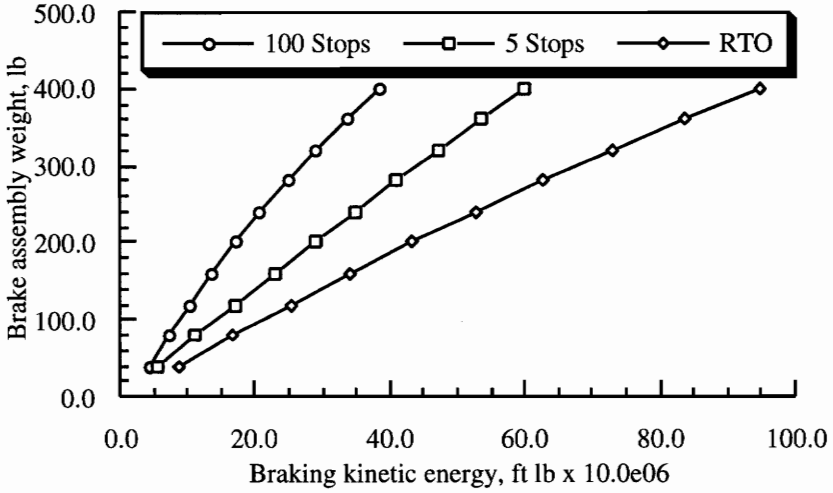

Figure 4.4 Brake assembly weight *vs.* kinetic energy level [2]

Given the tire wheel diameter as determined during the tire selection process, heat sink inner and outer diameters and the volume per inch width constant are selected from Table 4.3. Dividing the total volume by the constant then gives the necessary heat sink width. The envelope for the heat sink and torque plate carrier is established by adding 0.75 inch on the inside diameter and the end facing the wheel centerline. Finally, the piston housing envelope is approximated by adding two inches on the actuation side of the heat sink as shown in Figure 4.5 [2].

Table 4.3 Heat sink dimensions [2]

Rim dia., in	**Inner dia., in**	**Outer dia., in**	**Volume/inch width, in^2**
14.0	7.375	12.000	70.4
15.0	8.125	13.000	80.9
16.0	8.750	13.750	88.4
17.0	9.500	14.750	100.0
18.0	10.125	15.750	114.3
19.0	10.750	16.500	123.1
20.0	11.500	17.500	136.7
21.0	12.250	18.500	150.9
22.0	12.875	19.500	168.5
23.0	12.750	20.375	176.3
24.0	14.375	21.375	195.2
25.0	15.125	22.375	212.1

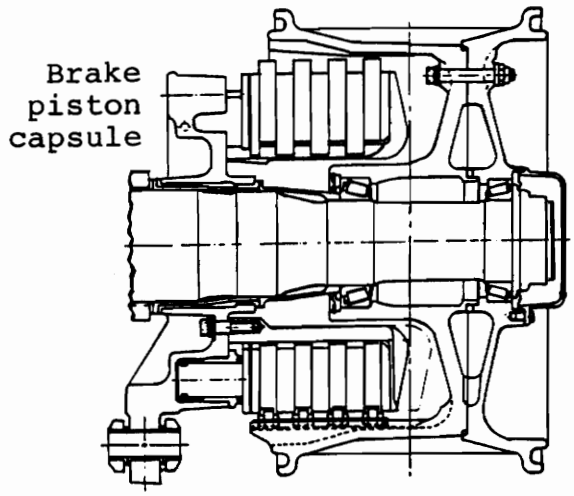

Figure 4.5 Carbon brake cross-sectional view [2]

Chapter 5 Shock Absorber Design

5.1. Introduction

The basic function of the shock absorber is to absorb and dissipate the impact kinetic energy to the extent that accelerations imposed upon the airframe are reduced to a tolerable level [2 and 19]. Existing shock absorbers can be divided into two classes based on the type of the spring being used: those using a solid spring made of steel or rubber and those using a fluid spring with gas or oil, or a mixture of the two that is generally referred to as oleo-pneumatic. The high gear and weight efficiencies associated with the oleo-pneumatic shock absorber made it the preferred design for commercial transports [2].

Based on the analysis procedure as outlined in this chapter, algorithms were developed to determine the required stroke and piston length to meet the given design conditions, as well as the energy absorption capacity of the shock absorber.

5.2. Oleo-Pneumatic Shock Strut Design

The basic weight support function of the oleo-pneumatic shock struts, which have a high efficiency under dynamic conditions both in terms of energy absorption and dissipation, is provided by a compressed cylinder of air and oil. A single-acting shock absorber, which is the most commonly used design for commercial transports, is shown in Figure 5.1. This type of shock strut absorbs energy by first forcing a chamber of oil against a chamber of dry air or nitrogen and then compressing the gas and oil. During the compression process, the oil and gas either remain separated or are mixed depending on the type of design. After the initial impact, energy is dissipated as the air pressure forces the oil back into its chamber through recoil orifices.

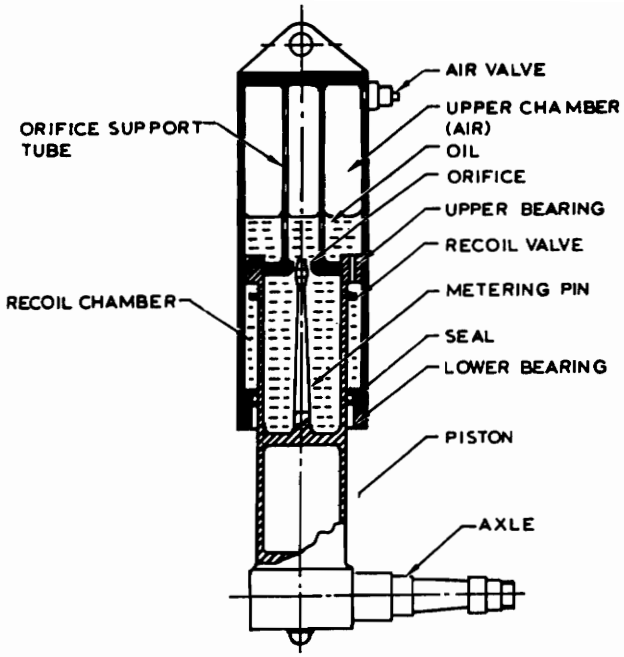

Figure 5.1 Single-acting shock absorber [7]

Although the compression orifice could be merely a hole in the orifice plate, most designs have a pin extending through it, and by varying the pin diameter the orifice area is varied. This variation is adjusted so that the strut load is fairly constant under dynamic loading. If this can be made constant, the gear efficiency would be 100 percent. In practice, this is never obtained and efficiencies of 80 to 90 percent are more usual [7]. Since only the efficiency factor is of interest in the conceptual design phase, no additional discussion on the design of the metering pin will be provided.

5.2.1. Stroke Calculation

The first step in calculating the stroke (S) is to select the design reaction factor (N), sometimes called the landing load factor. This factor should not be confused with aircraft load factor, which results from maneuvers or atmospheric disturbances. For a transport-type aircraft the landing load factor varies from 0.7 to 1.5, with 1.2 being the most widely used value [2].

Sink speed (V_s) is usually legislated by the procuring authority and/or the regulations pertaining to a particular category of aircraft. The FAA requires that a transport-type aircraft be able to withstand the shock of landing at 10 ft/s at design landing weight and 6 ft/s at maximum gross weight [19]. In practice, sink speeds of such magnitude rarely occur due to ground effects and flare-out of the aircraft prior to touchdown.

The total energy (E) of the aircraft at the instant of touchdown, which consists of kinetic and potential energy, is approximated using the expression [2, p. 35]

$$E = \frac{WV^2}{2g} + (W - L)(S + S_t) \tag{5.1}$$

where W is the aircraft weight, g is the gravitational acceleration, L is the wing lift, and S_t is the tire deflection. Given that the kinetic energy capacity of the shock absorber and tire must be equal to the total energy, Eq. (5.1) becomes [2, p. 35]

$$\eta_s SNW + \eta_t S_t NW = \frac{WV^2}{2g} + (W - L)(S + S_t) \tag{5.2}$$

where η_s and η_t are the shock absorber and tire absorber efficiency factors, respectively. The former is generally assumed to be 0.47 and the latter 0.8 for an oleo-pneumatic strut [2]. To maintain an adequate safety margin, an extra one inch of stroke is usually added to the calculated stroke.

5.2.2. Compression Ratios

Compression ratios are the ratios of the pressure under one condition divided by the pressure under another condition, *e.g.*, fully compressed to static. Two compression ratios are normally considered: static to fully extended and fully compressed to static. For transport-type aircraft, where floor height variation is important, a ratio of 4:1 for the static to extended case and 3:1 for the compressed to static case would be satisfactory [2]. Assuming a static pressure (P_2) of 1,500 psi, which enables standard compressors to be

used for servicing and provides enough margin to allow for aircraft growth, pressures at the extended (P_1) and compressed (P_3) positions are calculated using the compression ratios given above. Note that the piston area (A), and subsequently the displacement (d), are both a function of the static pressure, that is

$$A = \frac{F}{P_2} \tag{5.3}$$

and

$$d = SA \tag{5.4}$$

where F is the maximum static load per strut.

5.2.3. The Load-stroke Curve

The energy absorbed by the strut during its stroke is obtained by integrating the area beneath the load-stroke curve, which relates the magnitude of the applied ground loads to the stroke traversed. To accommodate excess energy produced in a heavy or semi-crash landing, shock absorbers are designed such that the piston is not fully bottomed even at the compressed position, *i.e.*, $V_3 \neq 0$. The reserve air volume, which is assumed to be 10 percent of the displacement [2], allows the shock strut at a predetermined load to move through extra travel, absorbing the excess energy by the work done. Hence, the air volume at the fully-extended position is approximated as [2, p. 100]

$$V_1 = V_3 + d \tag{5.5}$$

Pressures between the extended and static positions are defined by the isothermal compression curve, which is representative of normal ground handling activity [2, p. 100]

$$P_1 V_1 = P_x V_x = const \tag{5.6}$$

Given the relationships of Eqs (5.4) and (5.5), the pressure at stroke X is obtained using the expression [2, p. 100]

$$P_x = \frac{P_1 V_1}{V_x} = \frac{P_1 (V_3 + d)}{V_1 - XA} \qquad S_{extend} < X < S_{static} \tag{5.7}$$

Pressures obtained using Eq. (5.7) are then multiplied by the piston area to arrive at the design loads as shown on the load-stroke curve.

A polytropic, *i.e.*, real-gas, compression curve should be considered for pressures between the static and compressed positions. It is representative of dynamic compression cases such as landing impact and bump traversal and is based upon PV^n being constant [2], hence

$$P_x = P_2\left(\frac{V_2}{V_1 - XA}\right)^n \qquad S_{static} < X < S_{compress} \tag{5.8}$$

The constant n can either be 1.35 or 1.1; the former is used when the gas and oil are separated and the latter when they are mixed during compression. The distance from the static to the fully compressed position is largely a matter of choice. Statistical data indicate that transport-type aircraft typically have extensions of about 16 percent [2] of the total stroke, a figure which tends to give a hard ride while taxiing. However, with the static position being so far up the load-stroke curve, where a large amount of energy is absorbed with a relatively small stroke travel, aircraft weight variations do not result in substantial gear deflections. That is, the built-in margin minimizes the need of redesigning the baseline shock strut for uses on future growth versions of the aircraft. Again, the pressures obtained using Eq. (5.9) are multiplied by the piston area to arrive at the design loads. At this point the values of P_1 and P_3 should be checked to ensure that the former is greater than 60 psi to avoid sticking due to friction between the piston and the cylinder wall, while the latter is less than 6,000 psi to prevent seal leakage [2].

5.2.4. Internal Cylinder Length

As specified by MIL-L-8552, the distance between the outer ends of the bearings shall be not less than 2.75 times the internal cylinder/piston outside diameter (D). Thus the minimum piston length is given by [2, p. 111]

$$L_{pist} = S + 2.75D \tag{5.9}$$

where

$$D = \sqrt{\frac{4A}{\pi}} \tag{5.10}$$

5.2.5. Sample Calculation

The load-stroke curve of a notional single-acting shock absorber is generated for illustrative purposes. Based on the design requirements as stated in Table 5.1, Eq. (5.3) gives a piston cross-sectional area of 33.3 in^2, while Eq. (5.4) places the total displacement at 666.7 in^3. Using the 16 percent extension figure, the static position at which the gas law switches from isothermal to polytropic gas law is estimated to be 3.2 inches from the fully compressed position, *i.e.*, X at 16.8 inches. Loads corresponding to isothermal and polytropic compression were determined using Eqs (5.7) and (5.8), respectively, and presented in Table 5.2. The corresponding load-stroke curves are shown in Figure 5.2.

Table 5.1 Shock absorber sizing parameters

Parameter	**Design value**
Total stroke	20.0 in
Static position	16 percent of total stroke
Static load	50,000 lb
Static pressure	1,500 lb
Compression ratio	4:1 static to extended
	3:1 compressed to static

Table 5.2 Calculations of isothermal and polytropic compression

X, in.	V, in^3	P_{iso}, psi	P_{poly}, psi	P_{comb}, psi	F_{comb}, lb
0.0	727.3	375.0	375.0	375.0	12500.0
2.0	660.6	412.8	427.0	412.8	13760.0
4.0	593.9	459.2	493.0	459.2	15306.7
6.0	527.3	517.2	578.9	517.2	17240.0
8.0	460.6	592.1	694.8	592.1	19736.7
10.0	393.9	692.4	858.2	692.4	23080.0
12.0	327.3	833.3	1102.0	833.3	27776.7
14.0	260.6	1046.5	1498.9	1046.5	34883.3
16.0	193.9	1406.5	2234.2	1406.5	46883.3
16.8	167.3	1630.2	2726.6	1630.2	54340.0
18.0	127.3	2142.5	3943.0	2214.6	73820.0
20.0	60.6	4500.6	10740.1	5645.3	188176.7

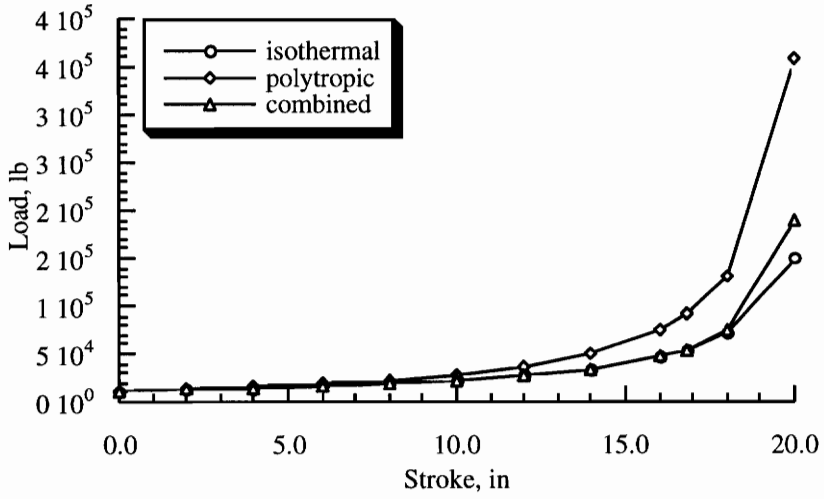

Figure 5.2 The load-stroke curve

Chapter 6 Kinematics

6.1. Introduction

Kinematics is the term applied to the design and analysis of those parts used to retract and extend the gear [2]. Particular attention is given to the determination of the geometry of the deployed and retracted positions of the landing gear, as well as the swept volume taken up during deployment/retraction. The objective is to develop a simple deployment/retraction scheme that takes up the least amount of stowage volume, while at the same time avoiding interference between the landing gear and surrounding structures. The simplicity requirement arises primarily from economic considerations. As shown from operational experience, complexity, in the forms of increased part-count and maintenance down-time, drives up the overall cost faster than weight [3]. However, interference problems may lead to a more complex system to retract and store the gear within the allocated stowage volume.

Based on the analysis as outlined in this chapter, algorithms were developed to establish the alignment of the pivot axis which permits the deployment/retraction of the landing gear to be accomplished in the most effective manner, as well as to determine the retracted position of the assemblies such that stowage boundary violations and structure interference can be identified.

6.2. Retraction Scheme

For safety reasons, a forward-retracting scheme is preferable for the fuselage-mounted assemblies. In a complete hydraulic failure situation, with the manual release of uplocks, the gravity and air drag would be utilized to deploy the assembly and thus avoid a wheels-up landing [2]. As for wing-mounted assemblies, current practice calls for an inboard-retraction scheme which stows the assembly in the space directly behind the rear

wing-spar. The bogie undercarriage may have an extra degree of freedom available in that the truck assembly can rotate about the bogie pivot point, thus requiring a minimum of space when retracted. As will be illustrated in the following section, deployed/retracted position of the landing gear, as well as possible interference between the landing gear and surrounding structures, can easily be identified using the mathematical kinematic analysis.

6.3. Mathematical Kinematic Analysis

A mathematical kinematic analysis, which is more effective and accurate than the graphical technique, was selected to determine the axis of rotation that will, in one articulation, move the landing gear assembly from a given deployed position to a given retracted position. As shown in Figure 6.1, a new coordinate system, termed the kinematic reference frame here, is defined such that the origin is located at the respective landing gear attachment locations with the axes aligned with the aircraft reference frame. The aircraft coordinate system-based origin permits constraints established in the kinematic reference frame, *e.g.*, assembly clearance envelope, retraction path, and swept volume, be translated into the aircraft reference frame and checked for interference with surrounding structures.

6.3.1. The Pivot Axis and Its Direction Cosines

In the determination of the alignment of the landing gear pivot axis, it is assumed that the axle/piston centerline intersection is brought from its deployed position to a given location within the stowage volume. For wing-mounted assemblies, the retracted position of axle/piston centerline intersection is assumed to coincide with the center of the stowage volume. In the case of fuselage-mounted assemblies with a forward-retracting scheme, the retracted position is assumed to be at the center of the cross-sectional plane located at the forward third of the stowage length.

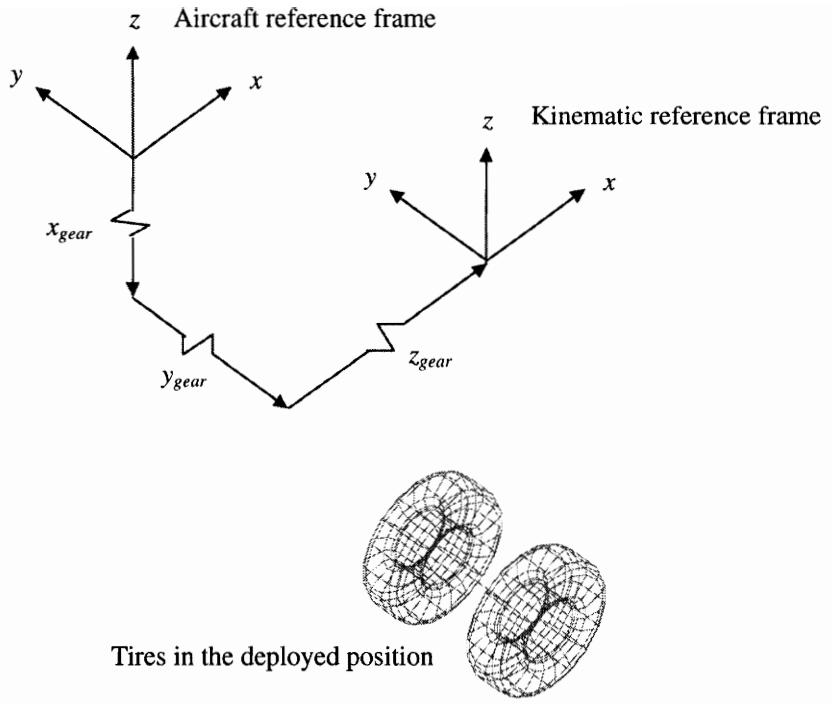

Figure 6.1 Relationships between the aircraft and kinematic reference frames

6.3.1.1. The Fuselage-mounted Assembly

For fuselage-mounted assemblies with a forward retracting-scheme, the pivot axis is defined by the cross product of the space vectors corresponding to the deployed and retracted position of a point location on the truck assembly. As shown in Figure 6.2, the cross product of two vectors ($\mathbf{V}_1$ and $\mathbf{V}_2$) representing the deployed and retracted positions of a given point location, here taken as the axle/piston centerline intersection, is orthogonal to both vectors, *i.e.*, in the direction of the pivot axis. Thus,

$$\mathbf{V} = \mathbf{V}_1 \times \mathbf{V}_2 \tag{6.1}$$

From standard vector operation, the direction cosines of the fuselage-mounted assembly is given as

$$l = \frac{X}{\sqrt{X^2 + Y^2 + Z^2}} \qquad m = \frac{Y}{\sqrt{X^2 + Y^2 + Z^2}} \qquad n = \frac{Z}{\sqrt{X^2 + Y^2 + Z^2}} \tag{6.2}$$

and the angle between the two vectors, *i.e.*, the angle of retraction (ϕ_{full}) in this case, is calculated using the expression

$$\cos\phi_{full} = l_1 l_2 + m_1 m_2 + n_1 n_2 \tag{6.3}$$

where l_i, m_i, and n_i are the respective direction cosines of the deployed and retracted space vectors.

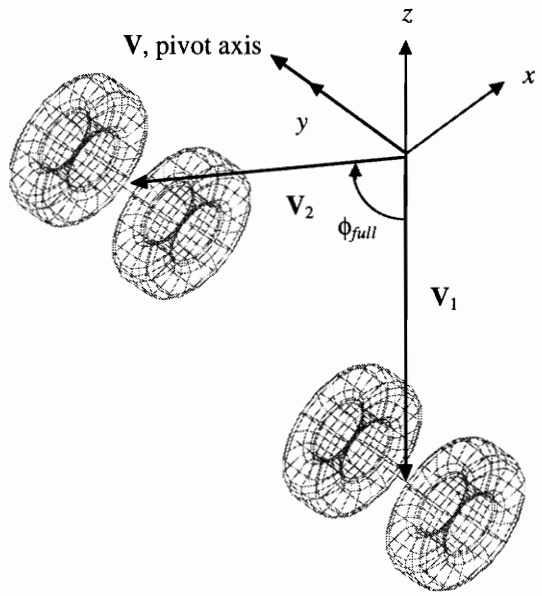

Figure 6.2 Fuselage-mounted assembly pivot axis alignment

6.3.1.2. The Wing-mounted Assembly

The determination of the wing-mounted assembly pivot axis involves the deployed and retracted positions of two points on the assembly. Essentially, the problem consists of bringing the line segment between the two points from its deployed position to its retracted position [30]. For ease of visualization, a twin-wheel configuration is used here to illustrate the procedure involved in determining the alignment of the desired pivot axis. Identical procedure is used for other configurations as well.

As shown in Figure 6.3, the axle/piston centerline intersection is selected as the first point (point A), while the second point (point B) is conveniently located at a distance

of unity along the axle, inboard from the first point location. retracted positions of the first and second points are given as point A' and B', respectively.

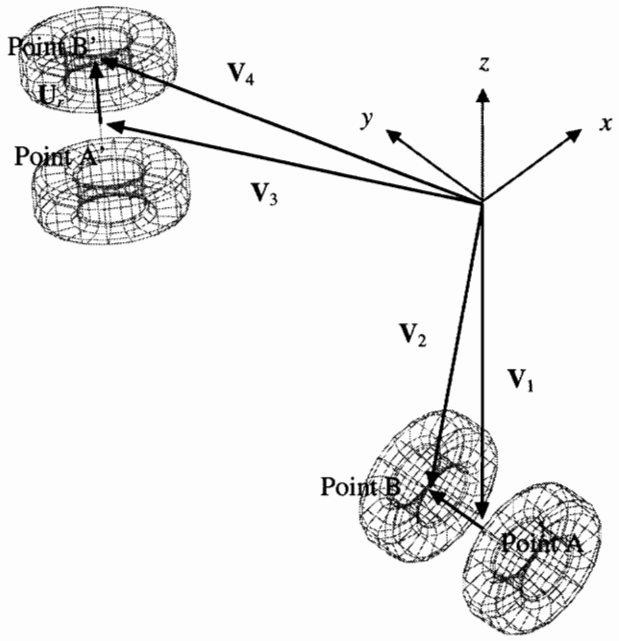

Figure 6.3 Vector representation of the wing-mounted landing gear

Of the four point positions required in the analysis, the positions of point A and A' are readily determined from the geometry of the landing gear and the stowage volume, respectively. From simple vector algebra

$$\mathbf{V}_2 = \mathbf{V}_1 + \hat{j} \tag{6.4}$$

where subscripts 1 and 2 denote the space vector corresponding to the deployed positions of points A and B, respectively. Similarly,

$$\mathbf{V}_4 = \mathbf{V}_3 + \mathbf{U}_r \tag{6.5}$$

where subscript 3 and 4 denote the retracted positions of point A and B, respectively, and $\mathbf{U}_r$ defines the orientation of the unit vector in its retracted position and is unknown.

To solve for $\mathbf{U}_r$, it is assumed that no devices are used to shorten the length of the strut during the retraction process, *i.e.*, that the magnitudes of $\mathbf{V}_2$ and $\mathbf{V}_4$ remain constant,

$$X_1^2 + (Y_1 + 1)^2 + Z_1^2 = (X_3 + X_U)^2 + (Y_3 + Y_U)^2 + (Z_3 + Z_U)^2 \tag{6.6}$$

and that the magnitude of the retracted unit vector remains at unity

$$X_U^2 + Y_U^2 + Z_U^2 = 1 \tag{6.7}$$

The angle of inclination (θ) of $\mathbf{U}_r$ in the *yz*-plane, which is one of the design variables that can be used to position the retracted truck assembly to fit into the available stowage space, is given as

$$\tan\theta = \frac{Y_U}{Z_U} \tag{6.8}$$

The vector components of $\mathbf{U}_r$, and subsequently $\mathbf{V}_4$, can then be determined by solving Eqs (6.6), (6.7), and (6.8) simultaneously.

As shown in Figure 6.4, the pivot axis that will permit the achievement of the desired motion is defined by the cross product of the space vectors between the deployed and retracted positions of the two point locations, in this case points A and B,

$$\mathbf{V} = \mathbf{V}_B \times \mathbf{V}_A \tag{6.9}$$

where

$$\mathbf{V}_A = (X_3 - X_1)\hat{i} + (Y_3 - Y_1)\hat{j} + (Z_3 - Z_1)\hat{k} \tag{6.10}$$

and

$$\mathbf{V}_B = (X_4 - X_2)\hat{i} + (Y_4 - Y_2)\hat{j} + (Z_4 - Z_2)\hat{k} \tag{6.11}$$

Thus, the direction cosines of the wing-mounted assembly and the angle of rotation can be determined using Eqs (6.2) and (6.3), respectively. Note that the subscripts in Eq. (6.3) will be 1 and 3 in this case, *i.e.*, the vectors corresponding to the deployed and retracted positions of point A, respectively.

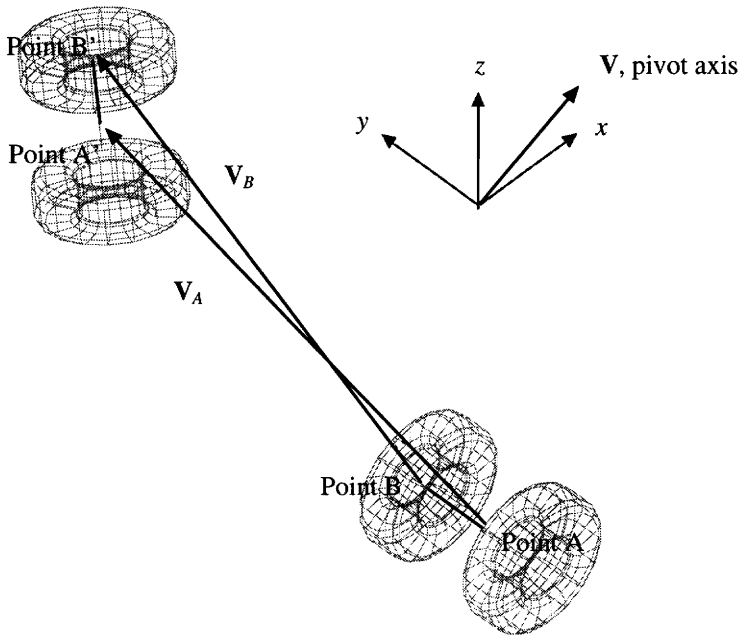

Figure 6.4 Wing-mounted assembly pivot axis alignment

6.3.2. Retracted Position of a Given Point Location

In addition to determining the required pivot axis and angle of retraction, the analytic method is used to establish the retraction path and the stowed position of the landing gear assembly. Note that the drag and side struts are excluded in the analysis since the retraction of these items involves additional articulation, *e.g.*, folding and swiveling, that cannot be modeled by the analysis.

Define point A as an arbitrary point location on the landing gear assembly. Given the angle of rotation and the direction cosines of the pivot axis as determined above, the retracted position of point A, denoted here as **A'**, can be determined by solving the following system of linear algebraic equations [2, pp. 193-194]

$$\begin{bmatrix} X_{A'} \\ Y_{A'} \\ Z_{A'} \end{bmatrix} = c_1 \begin{bmatrix} l(lX_A + mY_A + nZ_A) - X_A \\ m(lX_A + mY_A + nZ_A) - Y_A \\ n(lX_A + mY_A + nZ_A) - Z_A \end{bmatrix} + c_2 \begin{bmatrix} mZ_A - nY_A \\ nX_A - lZ_A \\ lY_A - mX_A \end{bmatrix} + \begin{bmatrix} X_A \\ Y_A \\ Z_A \end{bmatrix} \tag{6.12}$$

where

$$c_1 = 1 - \cos\phi \qquad c_2 = \sin\phi \qquad 0 < \phi < \phi_{full} \tag{6.13}$$

Similarly, the retraction path and swept volume of the assembly, as shown in Figure 6.5, can be established by calculating several intermediate transit positions at a given interval of degrees. The above information can then be used to identify possible interference between the landing gear and surrounding structures during deployment/retraction.

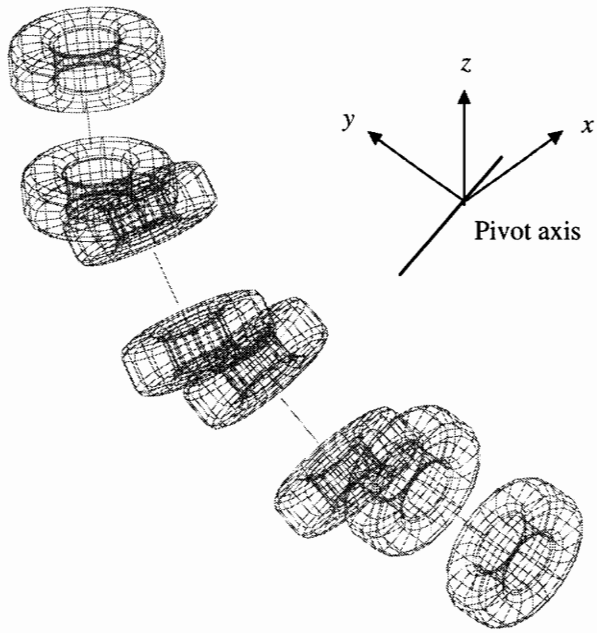

Figure 6.5 Retraction path and swept volume of the landing gear

6.4. Integration and Stowage Considerations

For future large aircraft, interference between the landing gear assembly and the surrounding structure is one of the more important considerations in the development of kinematics. With the large number of doors required to cover the stowage cavity on such aircraft, a complex deployment/retraction scheme for both the landing gear and doors is required to ensure that no interference will occur under all conditions. Additionally, the availability of stowage volume can become a major integration problem as the number of tires increases with aircraft takeoff weight. Given the conflicting objectives between

maximizing the volume that can be allocated for revenue-generating cargoes and providing adequate landing gear stowage space, a trade-off study involving crucial design parameters, *e.g.*, pivot axis alignment, angle of retraction, and bogie rotation, is needed to arrive at a satisfactory compromise with surround structures.

6.4.1. Truck Assembly Clearance Envelope

Clearances are provided to prevent unintended contact between the tire and the adjacent parts of the aircraft during operation, particularly in the case when the tire is damaged and continues to spin when stowed. As shown in Figure 6.6, the maximum grown outside diameter (D_G) and section width (W_G) are determined using the expressions [24, p. 8]

$$D_G = D + 2(1.115 - 0.074AR)H \tag{6.14}$$

and

$$W_G = 1.04W \tag{6.15}$$

where D is the specified rim diameter, H is the maximum section height, W is the maximum section width, and AR is the tire aspect ratio defined as

$$AR = \frac{H}{D} \tag{6.16}$$

The values for the radial and lateral clearance, *i.e.*, C_R and C_W, respectively, are calculated using the expressions [24, p. 9]

$$C_R = \begin{bmatrix} 0.073 \\ 0.060 \\ 0.047 \\ 0.037 \\ 0.029 \end{bmatrix} W_G + 0.4 \qquad at \quad \begin{Bmatrix} 250\,MPH \\ 225\,MPH \\ 210\,MPH \\ 190\,MPH \\ 160\,MPH \end{Bmatrix} \tag{6.17}$$

and

$$C_W = 0.019W_G + 0.23 \tag{6.18}$$

The constant coefficients found in Eqs (6.14), (6.15), and (6.16) are based on the maximum overall tire dimensions, plus growth allowance due to service and the increase in diameter due to centrifugal force.

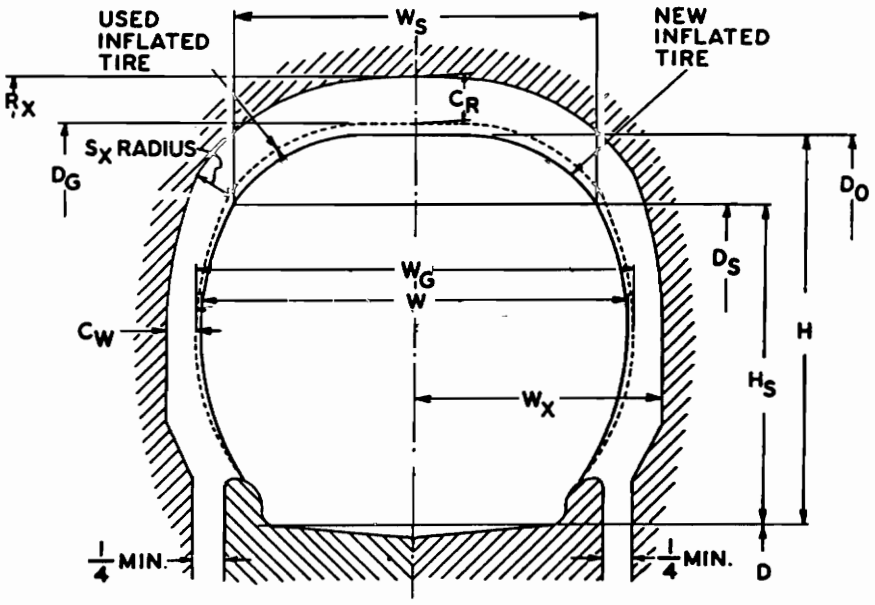

Figure 6.6 Clearance envelope for aircraft tires

Based on the clearance as determined above, the minimum radial and lateral distance between the tire and surrounding structures are calculated as follows [24, p. 9]

$$R_x = \frac{D_G}{2} + C_R \tag{6.18}$$

$$W_x = \frac{W_G}{2} + C_W \tag{6.19}$$

$$S_x = \frac{C_W + C_R}{2} \tag{6.20}$$

Given the minimum allowable distances obtained using Eqs (6.18), (6.19), and (6.20), a clearance envelope is established around the truck assembly. Then, using the kinematic analysis as outlined in the previous section, the boundary of the envelope is re-established

in the retracted position. Note that the envelope is represented in the kinematic coordinate system, while the boundaries of the landing gear wheelwell are in the aircraft coordinate system. Recall that the origin of the kinematic reference frame is defined in the aircraft coordinate system. Thus, simple algebraic manipulation would bring both sets of data under the same coordinate system, whether it be the airframe or the kinematic reference frame. Stowage boundary violations can then be identified by comparing both sets of data for discrepancies.

Chapter 7 Aircraft Flotation Analysis

7.1. Introduction

The configuration of the landing gear has a direct impact on ground flotation, a term used to describe the capability of pavement and other surfaces to support an aircraft [31]. The number and arrangement of the wheels, along with the aircraft weight and its distribution between the nose and main assemblies, dictates the required pavement thickness for a particular aircraft. In addition, the type of the pavement found at the airports to be served by the aircraft also need to be considered. As shown in Figure 7.1, existing runway and apron pavements can be grouped into two categories: flexible and rigid [5]. A flexible pavement, more commonly known as asphalt, may consist of one or more layers of bituminous materials and aggregate, *i.e.*, surface, base, and subbase courses, resting on a prepared subgrade layer. On the other hand, rigid pavement may consist of a slab of portland cement concrete placed on a layer of prepared soil. The thickness of each of the layers must be adequate to ensure that the applied loads will not damage the surface or the underlying layers.

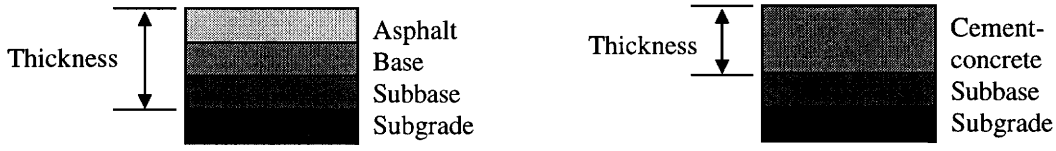

a) Flexible pavements b) Rigid pavements

Figure 7.1 Theoretical pavement cross-sections [32]

Based on the analyses as outlined in this chapter, a program was developed to determine the required flexible and rigid pavement thickness for a particular aircraft.

Results obtained from the program were validated with actual design data to ensure that a high degree of reliability can be placed upon the program itself.

7.2. Design Pavement Thickness

Various flotation analyses have been developed over time in different countries and by different government agencies and organizations. Some agencies and organizations and the corresponding design methods are listed as follows [5]: the Federal Aviation Administration (FAA), the Portland Cement Association (PCA), the Waterways Experiment Station (S-77-1), and the British Air Ministry (LCN). The majority of these methods use the California bearing ratio (CBR) method of design for flexible pavements and Westergaard stress analysis for the rigid pavements [5].

7.2.1. Flexible Pavements

For flexible pavements, CBR is the standard measurement used to classify the bearing strength of the subgrade. It is essentially the ratio of the bearing strength of a given soil sample to that of crushed limestone gravel. It is expressed as a percentage of the limestone figure, *i.e.,* a CBR of ten means that the subgrade has a bearing strength of ten percent to that of crushed aggregate. The original design method, which was developed by the California Division of Highways in 1928, evaluates the pavement thickness requirements for a given load condition and soil strength, assuming that the load is carried on a single wheel with a circular footprint area.

Until the middle of the 1950s, the analysis developed for the B-29, which features a dual wheel configuration, was extended to develop thickness design relationships for new aircraft with twin-tandem configurations. However, it appears that the analysis tends to produce slightly unconservative thickness estimates. Subsequent reevaluation of the theoretical work, which is based on Boussinesq's theory [5], and test data showed that the slopes of pavement deflection versus wheel offset for the single wheel were equal to or steeper than for dual wheels at equal depths, as shown here in Figure 7.2. A direct result

of this study is the introduction of the concept of the equivalent single-wheel load (*ESWL*), which eventually became the foundation of the S-77-1 design method [33 and 34]. *ESWL* is essentially a fictitious load on a isolated wheel, having the same inflation pressure, and causing the same stresses in the runway material as those due to a group of wheels. This fictitious wheel load accounts for the fact that a given loading, spread over a number of contact areas, causes lower stresses in the runway material than would be the case when the same load is concentrated on a single wheel.

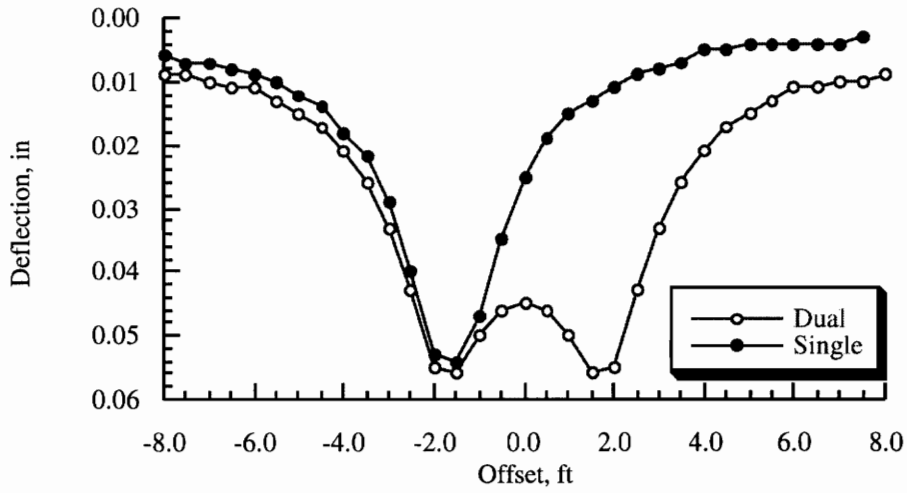

Figure 7.2 Comparison of single- and dual-deflection profiles, 1.0-foot depth [5]

Probable locations where maximum pavement bearing stress might occur, *e.g.*, directly under and between the tire contact areas, are shown in Figure 7.3. The offset distance between these points and the center of individual tire contact area, as well as the depths below the surface at which the *ESWL* is computed, which is treated as the thickness of the pavement in the analysis, are subsequently represented in terms of the radius of the footprint area (r) [5, p. 429]

$$r = \sqrt{\frac{A}{\pi}} \tag{7.1}$$

and the tire-ground contact area (A) is defined as

$$A = \frac{F}{P} \tag{7.2}$$

where F is the vertical main assembly load (per strut) and P is the tire inflation pressure.

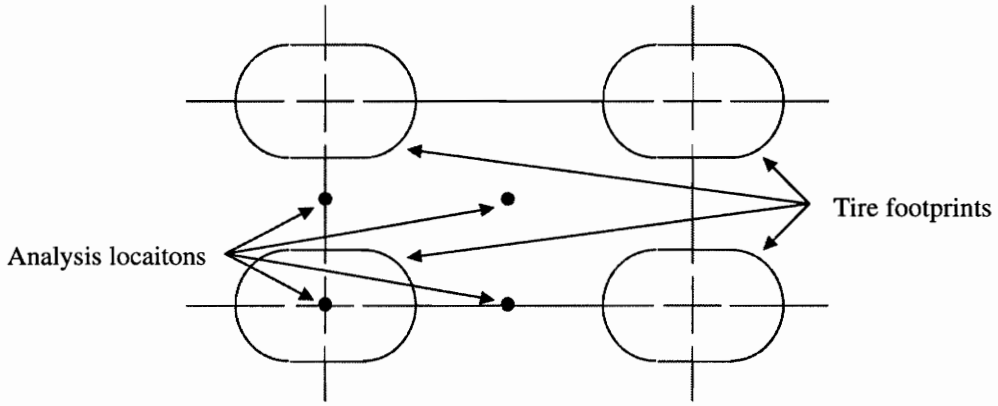

Figure 7.3 Relationship between the tire-contact areas and the analysis locations

Given the offset distances and depths, curves such as the ones shown in Figure 7.4 are used to determine the corresponding deflection factors. The principle of superposition is then used in calculating the multiple-wheel deflection factor (f), which is equal to the summation of the deflection factors produced by each tire in the multiple-wheel assembly at the point of analysis.

The ratio of load intensity of the single-wheel configuration to a single wheel of the multiple-wheel configuration is defined as the inverse of the ratio of the maximum deflection factors at a given depth, *i.e.*, the pavement thickness, [5, p. 430]

$$\frac{F_s}{F_m} = \frac{f_m}{f_s} \tag{7.3}$$

where subscripts s and m denote single- and multiple-wheel configurations, respectively. Once the ratio of load intensity is determined, the *ESWL* is calculated using the expression

$$ESWL = \frac{F_s F}{F_m N_w} \tag{7.4}$$

where N_w is the number of wheels per strut. To account for the loading effect caused by the number of annual aircraft operations, the design thickness (t) corresponding to a given CBR value is estimated using the expression [5, p. 433]

$$t = \alpha_i \sqrt{\frac{ESWL}{8.1CBR} - \frac{A}{\pi}} \tag{7.5}$$

where α_i is the load repetition factor as shown in Figure 7.5. It is categorized by the number of tires used to calculate the *ESWL* and typically value corresponding to 10,000 passes are used in the calculation [32].

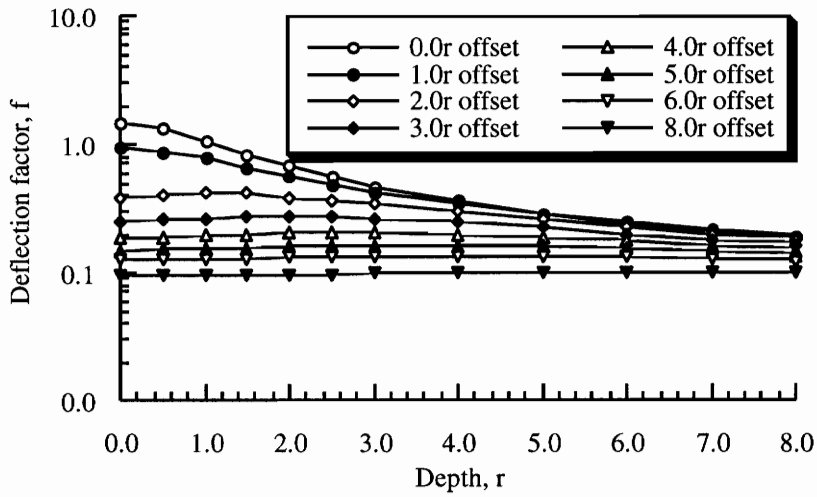

Figure 7.4 Deflection factor curves for Poisson's ratio of 0.5 [33]

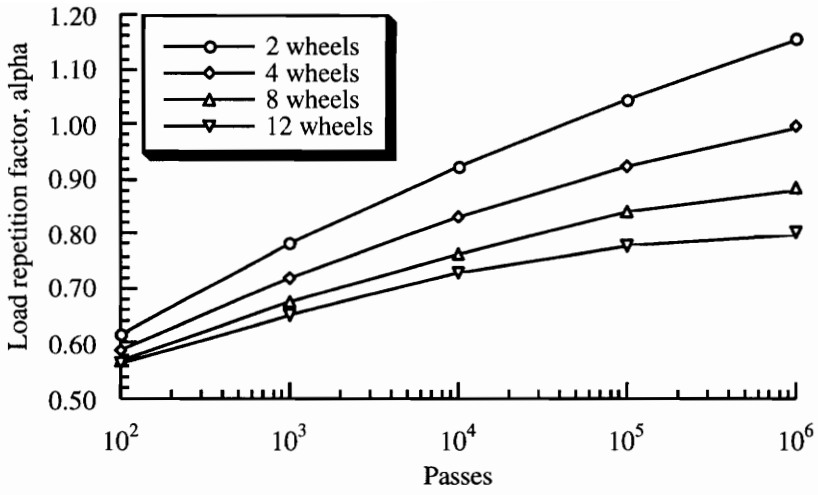

Figure 7.5 Aircraft load repetition factor [5]

7.2.2. Rigid Pavements

Stress in a concrete pavement is induced in four ways: tire loads, change of shape of slab due to differential in temperature and moisture between the top and the bottom of the slab, and the friction developed between slab and foundation when the slab expands/contracts. Since the primary consideration in the design of any pavement is the load which it is to carry, only the stresses induced by tire loads will be addressed.

The Westergaard stress analysis [35] assumes that the slab is a homogeneous, isotropic, and elastic solid in equilibrium. The reactions of the subgrade are assumed to be in the vertical direction only, and is proportional to the deflections of the slab. Additionally, the wheel load is assumed to be distributed over an elliptical footprint area. The stiffness of the slab relative to that of the subgrade is represented by the radius of relative stiffness of the concrete (l) [36, p. 56]

$$l = \sqrt[4]{\frac{Ed^3}{12\left(1-\mu^2\right)k}} \tag{7.6}$$

where E is the modulus of elasticity for the concrete, d is the thickness of the slab, μ is the Poisson's ratio for the concrete, and k is the modulus of subgrade reaction. Typically, E is taken as 4,000,000 psi and μ as 0.15 [5].

Critical bearing stresses for the interior and edge loading cases are examined. For the interior loading case, the load is applied at the interior of the slab at a considerable distance from any edge or joint. The maximum tensile stress (σ) at the bottom of the slab is given as [5, p. 441]

$$\sigma_{int} = \frac{F_s}{d^2}\left\{0.275(1+\mu)log_{10}\frac{Ed^3}{k[(a+b)/2]^4} + 0.293(1-\mu)\frac{a-b}{a+b}\right\} \tag{7.7}$$

where F_s is the single wheel load, d is the design thickness, and a and b are the semi-axes of the footprint area ellipse. Considering the edge loading case next, the load is applied adjacent to an edge that has no capacity for load transfer. The maximum tensile stress is given as [5, p. 442]

$$\sigma_{ext} = \frac{2.2(1+\mu)F_s}{(3+\mu)d^2}log_{10}\frac{Ed^3}{100k[(a+b)/2]^4} + \frac{3(1+\mu)F}{\pi(3+\mu)d^2}\left[1.84 - \frac{4}{3}\mu + (1+\mu)\frac{a-b}{a+b} + 2(1-\mu)\frac{ab}{(a+b)^2} + 1.18(1+2\mu)\frac{b}{l}\right] \tag{7.8}$$

Although the edge loading case produces a maximum stress that is the more critical of the two cases, in reality the probability of occurrence of this type of loading is relatively small, *i.e.*, the traffic tends to be channelized with the highest concentration in the vicinity of the runway and taxiway centerlines [5]. In addition, rigid pavement design charts as provided by PCA, which are used as reference data in the following section, are based on the interior loading case. Therefore, the interior loading condition is selected as the basis of the rigid pavement analysis.

7.3. Pavement Thickness Estimates

Design pavement thickness and corresponding ACNs for the Boeing Models 737, 747, 767, and McDonnell Douglas DC10 were determined for four subgrade strength categories: ultra-low, low, medium, and high [32]. Each category is assigned a CBR value for the flexible pavements and a k value for the rigid pavements; numerical values of each category are listed in Table 7.1.

Table 7.1 Subgrade strength categories [32]

Category	**CBR**	k, **lb/in^3**
Ultra-low	3.0	75.0
Low	6.0	150.0
Medium	10.0	300.0
High	15.0	550.0

For flexible pavements, *ESWL*s were computed using Eq. (7.4) from the surface down in multiples of footprint area radius. At each analysis depth, a CBR value was calculated using Eq. (7.5) and the repetition factor corresponding to 10,000 aircraft passes [32]. The result of this calculation is a set of design thickness and CBRs. Linear interpolation is then used to determine the final design thickness corresponding to the subgrade strength CBR values.

For rigid pavements, ls were computed using Eq (7.6) from the surface down in predetermined increments, *i.e.*, the design thickness, for each of four subgrade categories. At each design thickness and k value, a maximum tensile stress was calculated using Eq. (7.7). The result of this calculation is four sets of design thickness and the corresponding stresses. Linear interpolation is then used to determine the final design thickness corresponding to a concrete working stress of 400 psi [2].

Actual [5, 21, 37, and 38] and estimated pavement thickness are compared to determine the reliability of both analyses. As shown in Figure 7.6a, the S-77-1 method tends to underestimate the required pavement thickness at the lower end of the CBR range, while it tends to overestimate the required pavement thickness at the upper end of

the CBR range. Yet, the trend is consistent with the results obtained from a number of full-scale test tracks, *i.e.*, for heavy wheel loads, the theoretical thickness appeared to be too low for lower CBR values, and too high for higher CBR values. An interesting trend is observed upon closer examination of the actual pavement thickness data. As the subgrade strength increases, the required pavement thickness for aircraft with dual-twin truck assembly configurations, *i.e.*, B747, B767, and DC10, approach, if not fall below, the one required by aircraft with twin-wheel configuration, *i.e.*, B737. This can be attributed to the fact that the load on the pavement is better distributed as the number of wheels per assembly increases.

A vastly different trend, as shown in Figure 7.6b, is exhibited by the Westergaard stress analysis: it tends to underestimate the required pavement thickness by roughly 30 percent across the entire k range. The discrepancy can be attributed to the simplicity of the analysis itself. Primarily, the analysis did not consider the variations in the location and direction of maximum moment and stress in the concrete slab [36]. Essentially, the position of the maximum stress can be shifted and rotated depending on the magnitude of l and the configuration and dimension of the truck assembly. In addition, the analysis did not include detailed design parameters such as fatigue of concrete due to repeated loading and interactions between layers of materials.

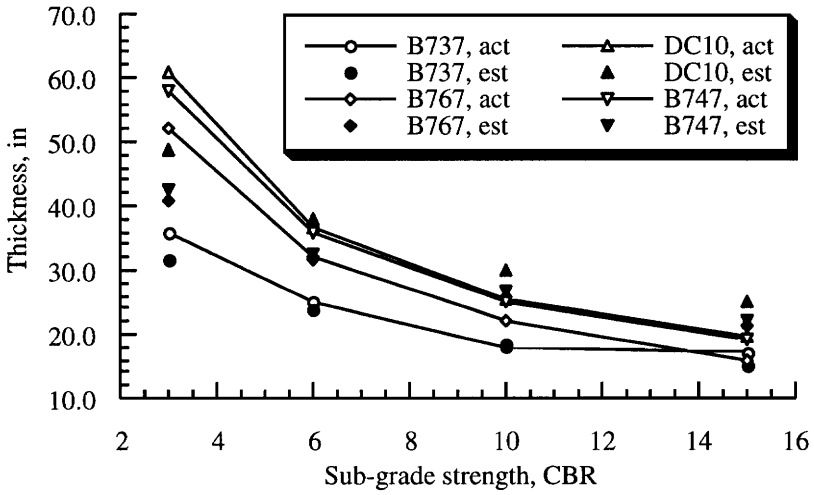

a) Flexible pavements

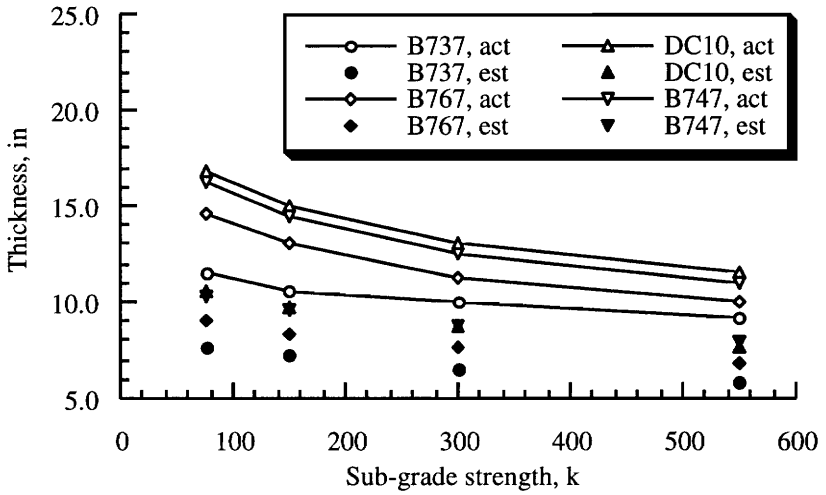

b) Rigid pavements

Figure 7.6 Actual and estimated pavement thickness comparison

Linear regression analysis was used to calibrate the estimated pavement thickness (t_{est}) against actual data. At each subgrade strength category, an aircraft weight-based correction factor is calculated using the expression

$$f_c = c_1 W + c_c \tag{7.9}$$

where c_1 and c_2 are constant coefficients as listed in Table 7.2. The estimated value and correction factor are then combined to arrive at the calibrated pavement thickness (t_{cal}), that is,

$$t_{cal} = t_{est} + f_c \tag{7.10}$$

The objective of this effort is to ensure that the discrepancy between the actual and estimated values will remain within a tolerable range. This is important when both analyses are used to examine the flotation characteristics of aircraft that are outside the existing pavement thickness database, namely, the next-generation high capacity commercial transports. As shown in Figure 7.7, the calibrated thickness compared reasonably with the actual data.

Table 7.2 Pavement thickness correction constants

	c_1	c_2
Flexible		
Ultra-low	0.000017	3.726
Low	0.000002	0.198
Medium	-0.000002	-1.630
High	-0.000007	-0.008
Rigid		
Ultra-low	0.000003	4.002
Low	0.000003	3.420
Medium	0.000001	3.407
High	0.000000	3.325

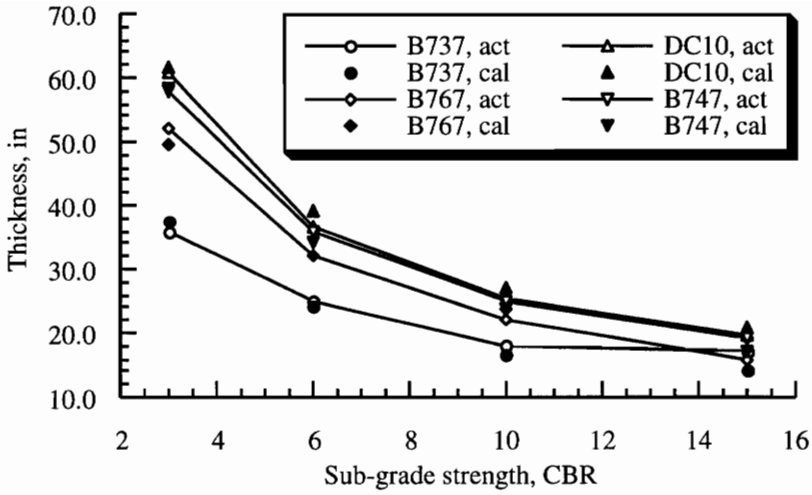

a) Flexible pavements

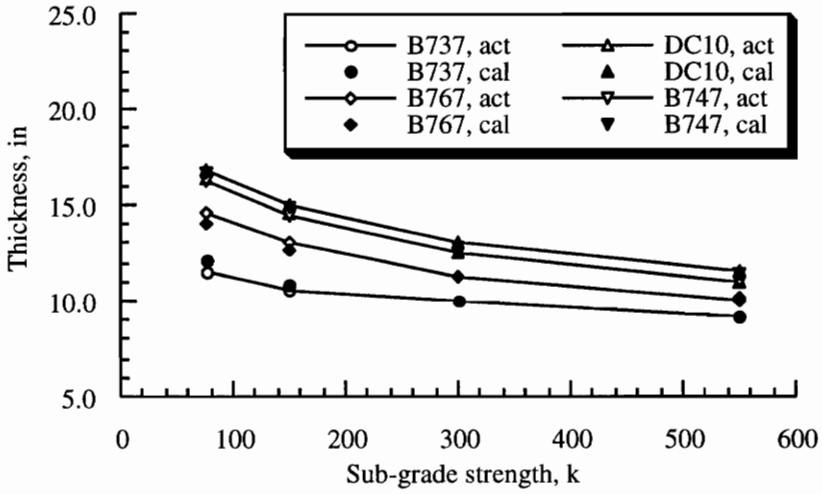

b) Rigid pavements

Figure 7.7 Actual and calibrated pavement thickness comparison

7.4. ACN-PCN Conversion

In an effort to resolve the difference among various pavement design and evaluation methods, the International Civil Aviation Organization (ICAO) recommended

universal adoption of the Aircraft-Pavement Classification Number (ACN-PCN) system [39] in 1983. The ACN-PCN system is not intended for the design or evaluation of pavements. It is, instead, a convenient and simple way of categorizing and reporting the pavement's capability to support aircraft on an unrestricted basis. The major appeal of the system is that it allows aircraft manufacturers to use any design/evaluation method of choice to determine the pavement thickness requirements of a particular aircraft. The design thickness is then converted to ACN and compared to PCNs of the airports to be served. If the ACN is equal to or less than the PCNs, the aircraft is cleared to operate out of the given airports subject to any limitation on the tire pressure.

The flexible pavement ACN is calculated using the expression [32, p. 3-11]

$$ACN = \frac{\left(t^2/1000\right)}{(0.878/CBR - 0.01249)} \tag{7.10}$$

where the design thickness t is expressed in terms of centimeters. As for the rigid pavements, ACN is obtained using the conversion chart as shown in Figure 7.8.

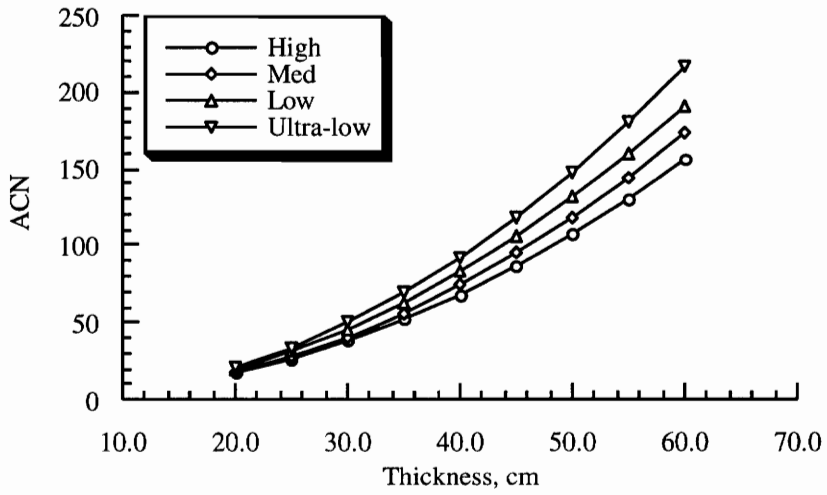

Figure 7.8 Rigid pavement ACN conversion chart [32]

7.4.1. ACN Estimates

Flexible and rigid pavement thickness requirements obtained earlier were converted to ACNs for conversion validation purposes. As shown in Figure 7.9a, the estimated flexible pavement ACNs exhibit a trend similar to that of the thickness estimates, *i.e.*, too low for lower CBR values and too high for higher CBR values. Apparently, the thickness calibration process did not eliminate the discrepancy introduced in the pavement thickness calculation entirely, and that the trend is carried over into the ACN conversion process. On the other hand, it appears that the calibration process for the rigid pavement has removed most of discrepancy that was introduced in the pavement thickness calculation. As shown in Figure 7.9b, the conversion, in fact, overestimated the ACN for all aircraft across the entire *k* range.

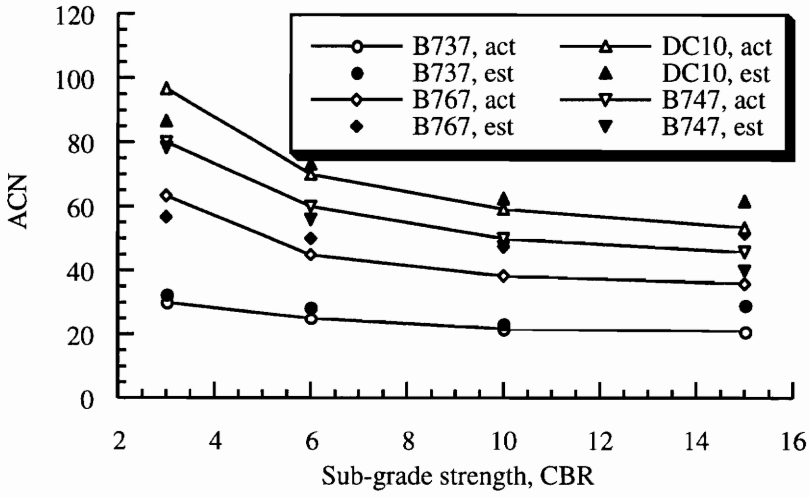

a) Flexible pavements

Figure 7.9 Actual and estimated ACN comparison

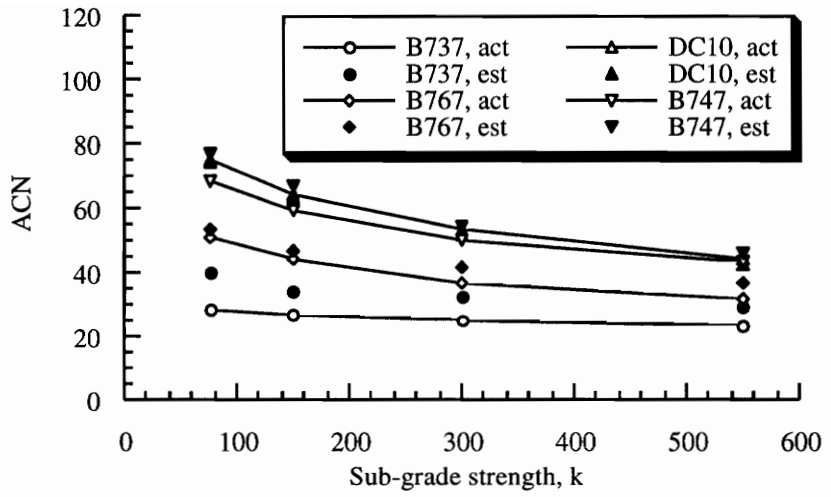

b) Rigid pavements

Figure 7.9 Actual and estimated ACN comparison (cont'd)

Linear regression analysis was again used to calibrate the estimated ACN (ACN_{est}) against actual data. At each subgrade strength category, an aircraft weight-based correction factor is calculated using Eq. (7.9), except in this case the constant coefficients are c_3 and c_4 as listed in Table 7.3. The estimated value and correction factor are then combined to arrive at the calibrated ACN (ACN_{cal}), that is,

$$ACN_{cal} = ACN_{est} + f_c \tag{7.11}$$

As shown in Figure 7.10, the calibration process has successfully brought the estimated ACNs closer to the actual data and thus improved the reliability of the flotation analysis.

Table 7.3 ACN correction constants

	c_3	c_4
Flexible		
Ultra-low	0.000008	0.5178
Low	0.000010	-6.326
Medium	0.000009	-6.769
High	0.000022	-16.182
Rigid		
Ultra-low	0.000006	-8.245
Low	0.000002	-4.940
Medium	0.000009	-7.628
High	0.000008	-6.519

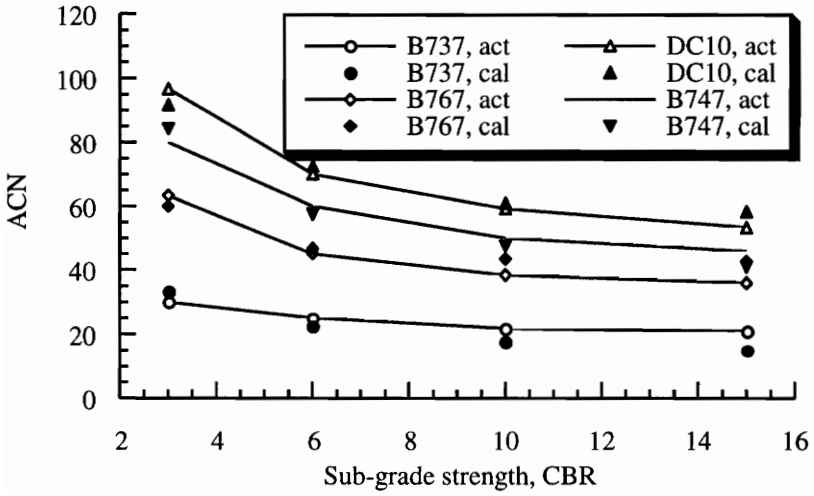

a) Flexible pavements

Figure 7.10 Actual and calibrated ACN comparison

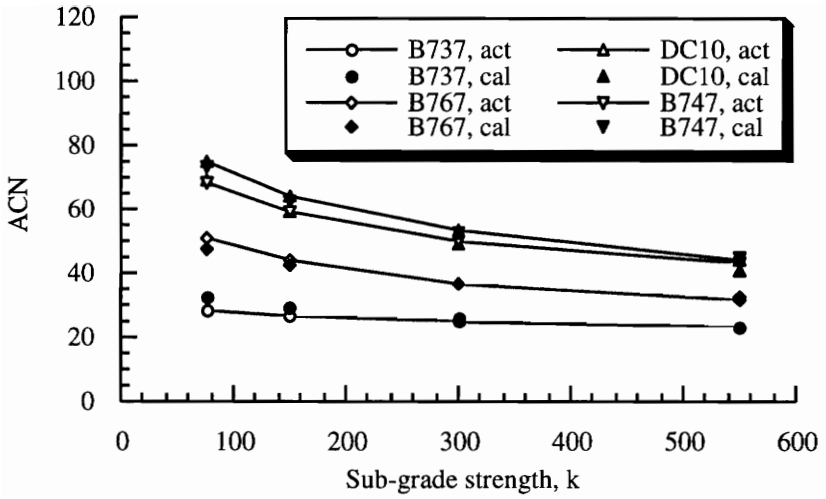

b) Rigid pavements

Figure 7.10 Actual and calibrated ACN comparison (cont'd)

Chapter 8 Weight Estimation

8.1. Introduction

Statistical weight equations, although capable of producing landing gear group weights quick and fairly accurately, do not respond to all the variations in landing gear design parameters. In addition, the equations are dependent on the database that is limited to existing aircraft. For future large aircraft, such weight data is virtually non-existent. Thus, it is desirable that an analytical weight estimation method, which is more sensitive than statistical methods to variations in the design of landing gear, should be adopted. The objectives are to allow for parametric studies involving key design considerations that drive landing gear weight, and to establish crucial weight gradients to be used in the optimization process.

Based on the procedure as outlined in this chapter, algorithms were developed to size and estimate the weight of the structural members of the landing gear. The weight of non-structure members were estimated using statistical weight equations. The two were then combined to arrive at the final group weight.

8.2. Current Capabilities

The primary shortcoming of the statistical methods lies in the fact that only a limited number of weight-affecting parameters are considered, *e.g.*, length of the strut, material ultimate strength, vertical load, and number of tires. As a result, it is extremely difficult to distinguish landing gears with different geometric arrangements using these parameters alone. Statistical weight equations are also constrained by what has been designed in the past, *i.e.*, if an unconventional design or a new class of aircraft such as the proposed ultra-high-capacity transports is involved, there might not be sufficient data to develop a statistical base for the type of landing gear required.

The majority of existing equations calculate the landing gear weight purely as a function of aircraft takeoff gross weight. It is the simplest method for use in sizing analysis, and is adopted in ACSYNT as well as by Torenbeek [3] and General Dynamics [40]. The Douglas equation used in the blended-spanload concept [41] also falls into this category. Other weight equations, *e.g.*, Raymer [42] and FLOPS (Flight Optimization System) [10], include the length of the landing gear in the calculation and thus is able to produce estimates which reflect the effect of varying design parameters to some extent.

Actual and estimated landing gear weight fractions are presented in Figure 8.1. As shown in Figure 8.1a, for an MTOW up to around 200,000 lb, the value of ACSYNT and Torenbeek are nearly equal. However, as the MTOW increases, vastly different trends are observed for the two equations: an increasing and then a decreasing landing gear weight fraction is predicted by ACSYNT, whereas a continual increasing weight fraction is predicted by Torenbeek. As for the Douglas equation, an increasing weight fraction is observed throughout the entire MTOW range. Upon closer examination of the data presented, it was found that only a small number of actual landing gear weight cases are available to establish trends for aircraft takeoff weight above 500,000 pounds. In addition, even within the range where significant previous experience is available, the data scatter between actual and estimated values is too large to draw conclusions on the accuracy of existing weight equations. Evidently a systematic procedure is needed to validate the reliability of the statistic equations, and if necessary, replace them entirely.

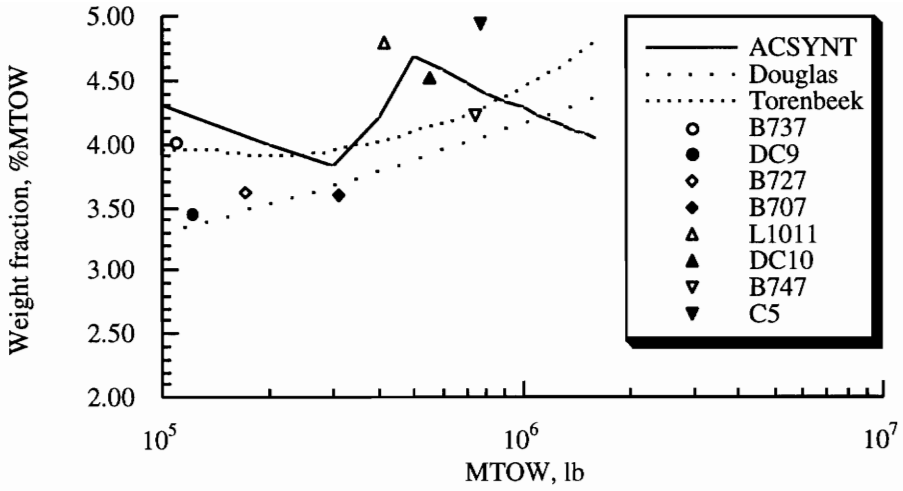

a) Pure weight fraction equations

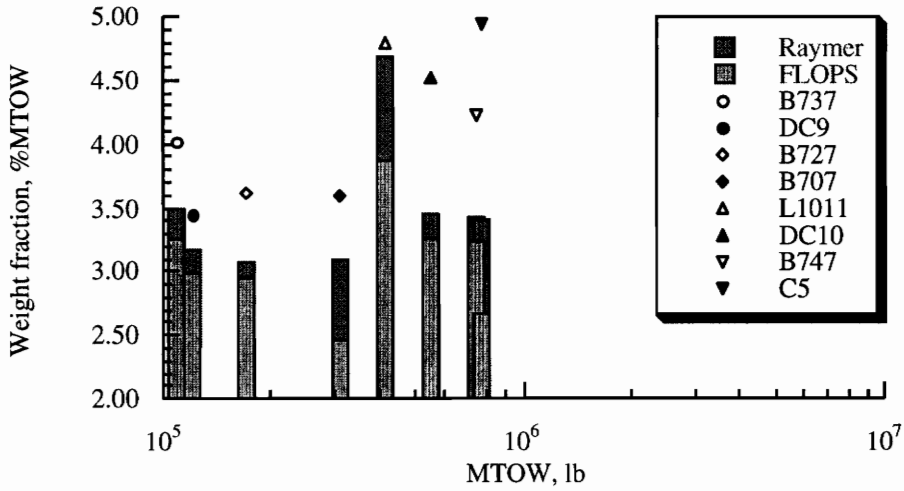

b) Weight fraction equations with landing gear length

Figure 8.1 Landing gear weights comparison

8.3. Analytical Structural Weight Estimation

Analytical weight estimation methods are capable of handling varying configurations and geometry, in addition to design parameters already covered by the

statistical methods. As typified by Kraus [43] and Wille [44], the procedure consists of five basic steps: definition of gear geometry, calculation of applied loads, resolution of the loads into each structural member, sizing of required member cross-sectional areas, and calculation of component and total structural weight. Although these studies provided an excellent guideline toward the development of an MDO-compatible analysis algorithm, detailed discussions in the area of load calculations and structure design criteria were intentionally omitted due to proprietary-nature of such information. To fill in the gap, simplified loading conditions were determined from Torenbeek and FAA [19], and structural analyses were developed as part of this work. Loading conditions are presented in Section 8.3.2., and the structural analyses are presented in Sections 8.3.3. and 8.3.4. and Appendix B.

8.3.1 Generic Landing Gear Model

A generic model consisting of axles, truck beam, piston, cylinder, drag and side struts, and trunnion is developed based on existing transport-type landing gears. Since most, if not all, of the above items can be found in both the nose and main gear, the model can easily be modified to accommodate both types of assembly without difficulty. Although the torsion links are presented for completeness, they are ignored in the analysis since their contributions to the final weight are minor.

The model shown in Figure 8.2 represents a dual-twin-tandem configuration. The model can be modified to represent a triple-dual-tandem or a dual-twin configuration with relative ease, *i.e.*, by including a center axle on the truck beam, or replacing the bogie with a single axle, respectively. The model assumes that all structural components are of circular tube construction except in the case of the drag and side struts, where an I-section can be used depending on the configuration. When used as a model for the nose gear, an additional side strut arranged symmetrically about the plane of symmetry is included.

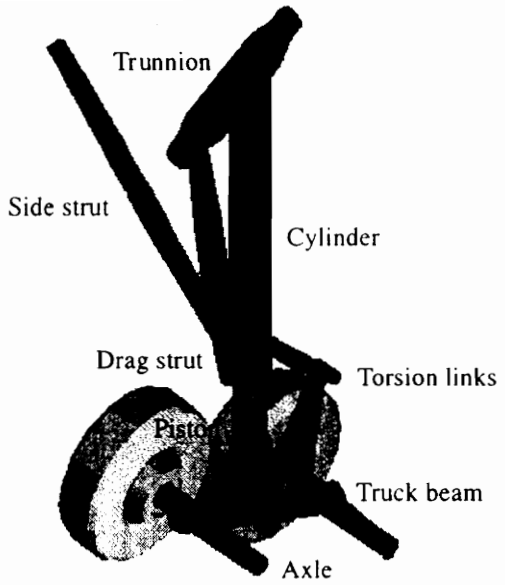

Figure 8.2 Generic landing gear model

For added flexibility in terms of modeling different structural arrangements, the landing gear geometry is represented by three-dimensional position vectors relative to the aircraft reference frame. Throughout the analysis, the *xz*-plane is chosen as the plane of symmetry with the *x*-axis directed aft and the *z*-axis upward. The locations of structural components are established by means of known length and/or point locations, and each point-to-point component is then defined as a space vector in the *x*, *y*, and *z* directions. Based on this approach, a mathematical representation of the landing gear model is created and is shown in Figure 8.3.

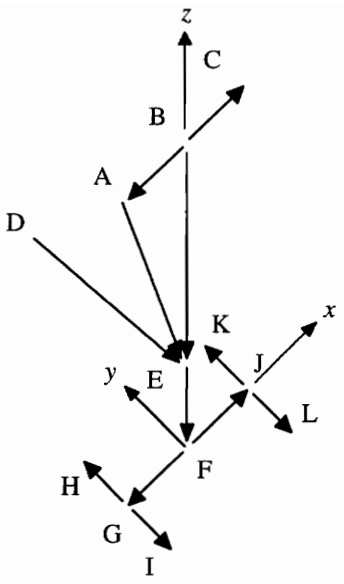

Vector	Description
BA	Forward trunnion
BC	Aft trunnion
BE	Cylinder
AE	Drag strut
DE	Side strut
EF	Piston
FG, FJ	Truck beam
GH, GI, JK, JL	Axles

Figure 8.3 Mathematical representation of the landing gear model

8.3.2. Applied Loads

External loads applied to the gear assemblies can be divided into dynamic and static loads: the former occurs under landing conditions while the latter occurs during ground operations. As listed in Table 8.1, seven basic loading conditions have been selected for analysis with the applied loads calculated as specified in FAR Part 25 [19].

Table 8.1 Basic landing gear loading conditions [19]

Dynamic	Static
Three-point level landing	Turning
One-wheel landing	Pivoting
Tail-down landing	
Lateral drift landing	
Braked roll	

The corresponding aircraft attitudes are shown in Figure 8.4, where symbols D, S and V are the drag, side and vertical forces, respectively, n is the aircraft load factor, W is aircraft maximum takeoff/landing weights, T is the forward component of inertia force,

and I is the inertial moment in pitch and roll conditions necessary for equilibrium. The subscripts m and n denote the main and nose gear, respectively.

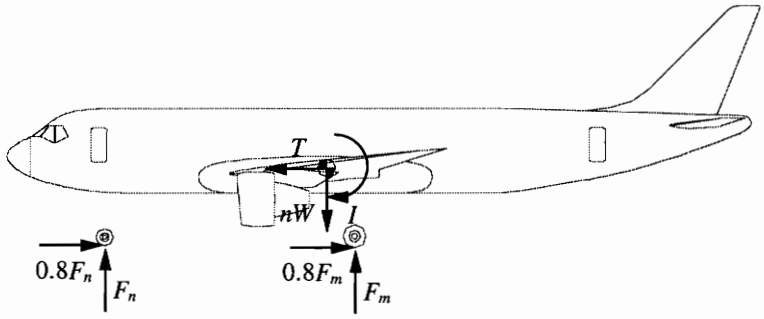

a) Three-point level landing

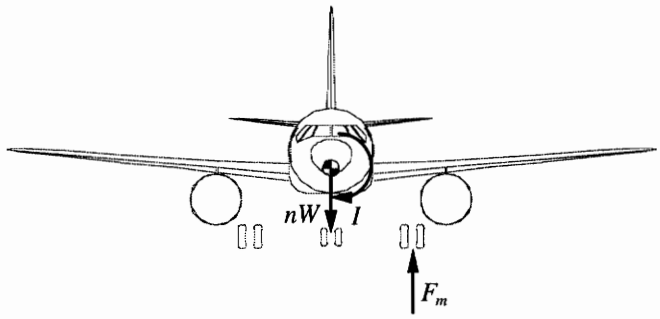

b) One-wheel landing

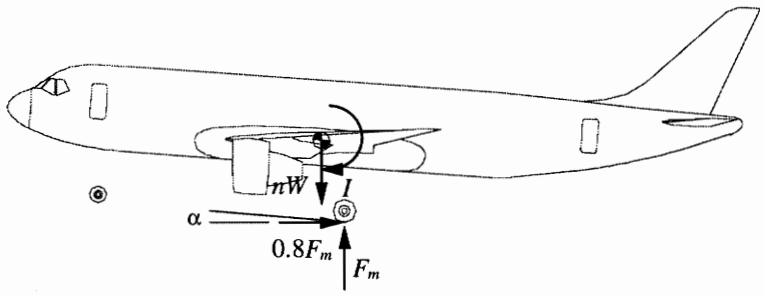

c) Tail-down landing

Figure 8.4 Aircraft attitudes under dynamic and static loading conditions [19]

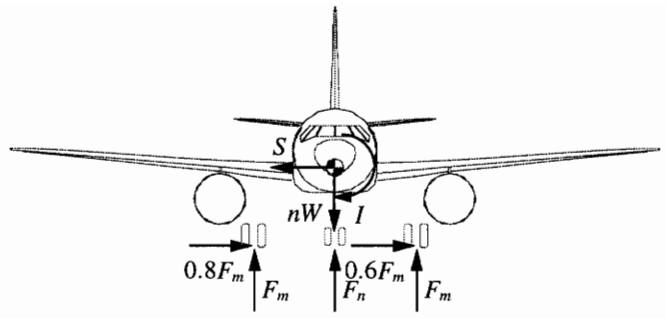

d) Lateral drift landing

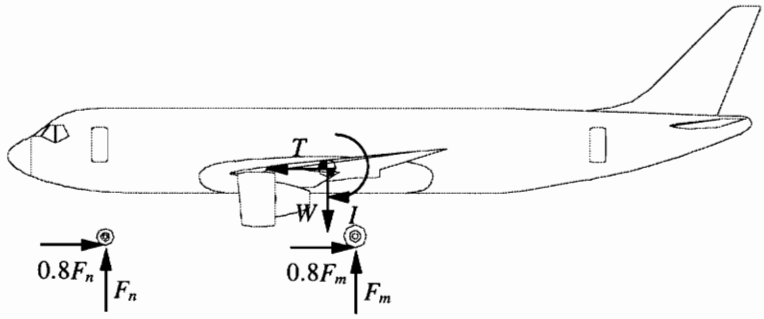

e) Braked roll

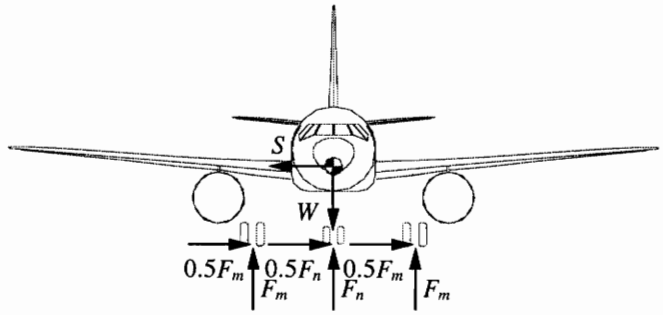

f) Turning

Figure 8.4 Aircraft attitudes under dynamic and static loading conditions [19] (cont.)

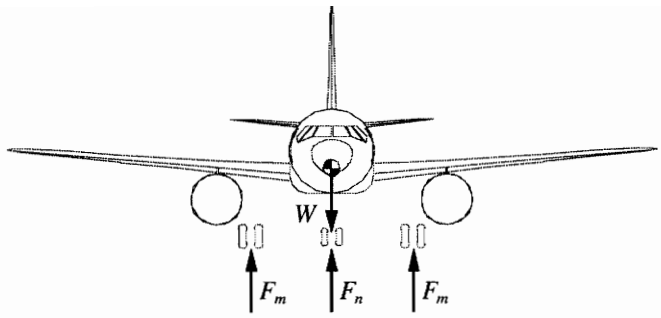

g) Pivoting

Figure 8.4 Aircraft attitudes under dynamic and static loading conditions [19] (cont'd)

For the dynamic landing conditions listed in Table 8.1, the total vertical ground reaction (F) at the main assembly is obtained from the expression [43]

$$F = \frac{cW}{\eta S \cos\alpha}\left(\frac{V_s^2}{g} + S\cos\alpha\right) \tag{8.1}$$

where c is the aircraft weight distribution factor, η is the gear efficiency factor, S is the total stroke length, α is the angle of attack at touchdown, V_s is the sink speed, and g is the gravitational acceleration. Although the vertical force generated in the gear is a direct function of the internal mechanics of the oleo, in the absence of more detailed information, however, Eq. (8.1) provides a sufficiently accurate approximation.

The maximum vertical ground reaction at the nose gear, which occurs during low-speed constant deceleration, is calculated using the expression [3, p. 359]

$$F_n = \frac{l_m + a_x / g \quad h_{cg}}{l_m + l_n} W \tag{8.2}$$

For a description of variables and the corresponding values involved in Eq. (8.2), refer to Chapter Four, Section Two.

The ground loads are initially applied to the axle-wheel centerline intersection except for the side force. As illustrated in Figure 8.5, the side force is placed at the tire-

ground contact point and replaced by a statically equivalent lateral force in the y direction and a couple whose magnitude is the side force times the tire rolling radius.

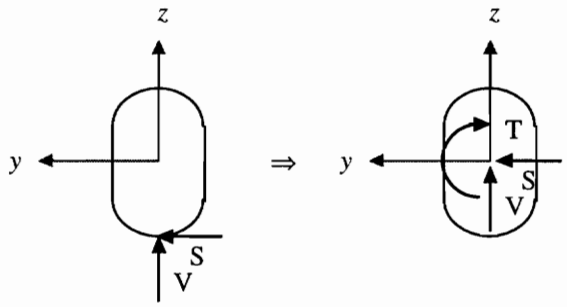

Figure 8.5 Location of the applied ground loads

To determine the forces and moments at the selected structural nodes listed in Table 8.2, the resisting force vector ($\mathbf{F}_{res}$) is set equal and opposite to the applied force vector ($\mathbf{F}_{app}$)

$$\mathbf{F}_{res} = -\mathbf{F}_{app} \tag{8.3}$$

whereas the resisting moment vector ($\mathbf{M}_{res}$) is set equal and opposite to the sum of the applied moment vector ($\mathbf{M}_{app}$) and the cross product of the space vector ($\mathbf{r}$) with $\mathbf{F}_{app}$

$$\mathbf{M}_{res} = -\left(\mathbf{M}_{app} + \mathbf{r} \times \mathbf{F}_{app}\right) \tag{8.4}$$

Table 8.2 Selected structural nodes description

Node	Description	Location (Figure 8.3)
1	Axle-beam centerline intersection	G/J
2	Beam-piston centerline intersection	F
3	Drag/side/shock strut connection	E
4	Cylinder-trunnion centerline intersection	B

8.3.3. Forces and Moment Resolution

Three-dimensional equilibrium equations are used to calculate member end reactions. Internal forces and moments are then determined from equilibrium by taking

various cross-sectional cuts normal to the longitudinal axis of the member. To ensure that the information is presented in a concise manner, the methods used in the analysis are discussed only in general terms, while detailed derivations are compiled and presented in Appendix B.

8.3.3.1. Coordinate Transformation

Given that the mathematical landing gear model and the external loads are represented in the aircraft reference frame, transformation of nodal force and moment vectors from the aircraft to body reference frames are required prior to the determination of member internal reactions and stresses. The body reference frames are defined such that the x_3-axis is aligned with the component's axial centerline, and xz-plane is a plane of symmetry if there is one. The transformation is accomplished by multiplying the force and moment vectors represented in the aircraft reference frame by the transformation matrix $\mathbf{L}_{BA}$ [45, p. 117]

$$\mathbf{F}_B = \mathbf{L}_{BA}\mathbf{F}_A \tag{8.5}$$

$$\mathbf{M}_B = \mathbf{L}_{BA}\mathbf{M}_A \tag{8.6}$$

where subscripts A and B denote the aircraft and body reference frames, respectively. By inspection of the angles in Figure 8.6, where subscripts 1, 2, and 3 denote the rotation sequence from the aircraft (x, y, and z) to the body (x_3, y_3, and z_3) reference frame, the three localized transformation matrices are [45, p. 117]

$$\mathbf{L}_1(\varphi_1) = \begin{bmatrix} 1 & 0 & 0 \\ 0 & cos\varphi_1 & sin\varphi_1 \\ 0 & -sin\varphi_1 & cos\varphi_1 \end{bmatrix} \tag{8.7a}$$

$$\mathbf{L}_2(\varphi_2) = \begin{bmatrix} cos\varphi_2 & 0 & -sin\varphi_2 \\ 0 & 1 & 0 \\ sin\varphi_2 & 0 & cos\varphi_2 \end{bmatrix} \tag{8.7b}$$

$$\mathbf{L}_3(\varphi_3) = \begin{bmatrix} cos\varphi_3 & sin\varphi_3 & 0 \\ -sin\varphi_3 & cos\varphi_3 & 0 \\ 0 & 0 & 1 \end{bmatrix} \tag{8.7c}$$

Thus, the matrix $\mathbf{L}_{BA}$ is given as [45, p. 117]

$$\mathbf{L}_{BA} = \mathbf{L}_3(\varphi_3)\mathbf{L}_2(\varphi_2)\mathbf{L}_1(\varphi_1) \tag{8.8}$$

or

$$\mathbf{L}_{BA} = \begin{bmatrix} cos\varphi_2\, cos\varphi_3 & sin\varphi_1\, sin\varphi_2\, cos\varphi_3 + cos\varphi_1\, sin\varphi_3 & -cos\varphi_1\, sin\varphi_2\, cos\varphi_3 + sin\varphi_1\, sin\varphi_3 \\ -cos\varphi_2\, sin\varphi_3 & -sin\varphi_1\, sin\varphi_2\, sin\varphi_3 + cos\varphi_1\, cos\varphi_3 & cos\varphi_1\, sin\varphi_2\, sin\varphi_3 + sin\varphi_1\, cos\varphi_3 \\ sin\varphi_2 & -sin\varphi_1\, cos\varphi_2 & cos\varphi_1\, cos\varphi_2 \end{bmatrix} \tag{8.9}$$

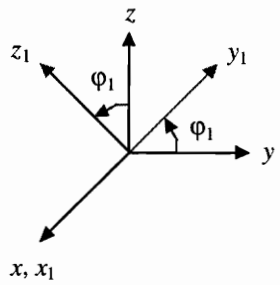

a) About the x, x_1-axis

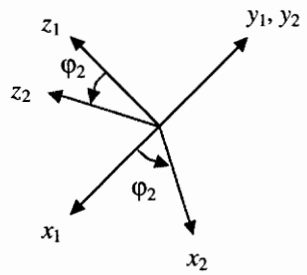

b) About the y_1, y_2-axis

Figure 8.6 Orientation of the axes and the corresponding rotation angles

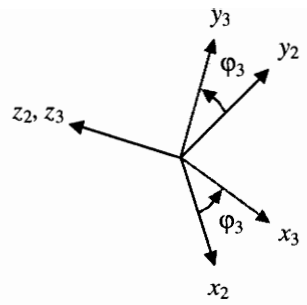

c) About the z_2, z_3-axis

Figure 8.6 Orientation of the axes and the corresponding rotation angles (cont'd)

8.3.3.2. The Main Assembly

The main assembly drag strut and side strut structure is modeled as a space truss consisting of ball-and-socket joints and two-force members. As shown in Figure 8.7, the loads applied to the cylinder consist of the side strut forces (F_{side}), drag strut force (F_{drag}), an applied force with components F_x, F_y, and F_z, and an applied couple with moment components C_x, C_y, and C_z. Internal axial actions are obtained using the method of sections. Equilibrium equations are then used to determine the magnitude of the internal axial forces in the isolated portion of the truss.

The shock strut cylinder, in addition to supporting the vertical load, also resists a moment due to asymmetric ground loads about the z-axis. This moment is transmitted from the truck beam assembly to the cylinder though the torsion links. Note that in the tandem configurations, the moment about the y-axis at the piston-beam centerline is ignored because of the pin-connection between the two. However, this moment must be considered in the dual-twin configuration, where the moment is resisted by the integrated axle/piston structure.

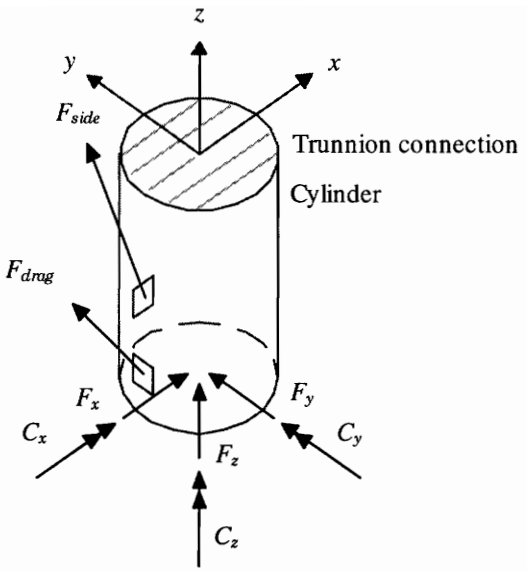

Figure 8.7 Idealized main assembly cylinder/drag/side struts arrangement

8.3.3.3. The Nose Assembly

As mentioned in the geometric definition section, an additional side strut, arranged symmetrically about the *xz*-plane, is modeled for the nose assembly. The addition of the second side strut results in a structure that is statically indeterminate to the first degree as shown in Figure 8.8. The reactions at the supports of the truss, and consequently the internal reactions, can be determined by Castigliano's theorem [46, p. 611]

$$u_j = \frac{\partial U}{\partial P_j} = \sum_{i=1}^{n} \frac{F_i l_i}{A_i E} \frac{\partial F_i}{\partial P_j} \tag{8.10}$$

where u_j is the deflection at the point of application of the load P_j, E is the modulus of elasticity, and l, F, and A are the length, internal force, and cross-sectional area of each member, respectively. The theorem gives the generalized displacement corresponding to the redundant, P_j, which is set equal to a value compatible with the support condition. This permits the solution of the redundant, and consequently all remaining internal actions, via equilibrium. As detailed in Appendix B, Section Two, the procedure is to first designate one of the reactions as redundant, and then determine a statically admissible set of internal

actions in terms of the applied loads and the redundant. By assuming a rigid support which allows no deflection, Eq. (8.10) is set to zero and solved for P_j.

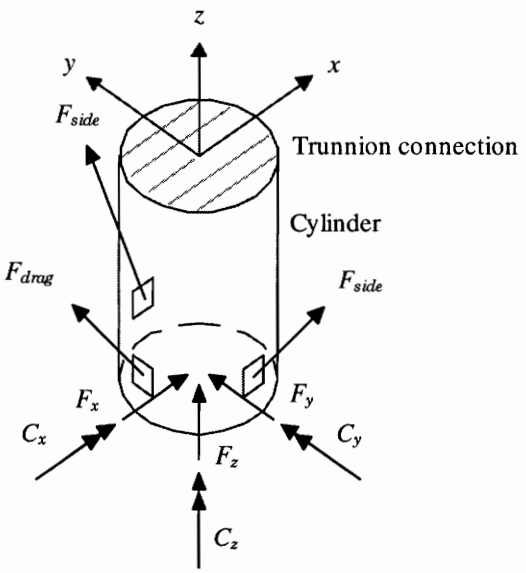

Figure 8.8 Idealized nose gear cylinder/drag/side struts arrangement

8.3.3.4. The Trunnion

When the gear is in the down-and-locked position, the trunnion is modeled as a prismatic bar of length L with clamped ends. As shown in Figure 8.9, the trunnion is subjected to a force with components F_x, F_y, and F_z, and a couple with components C_y and C_z, at axial position $x = l_1$, where $0 < l_1 < L$ and $0 \leq x \leq L$. Clamped end-conditions at $x = 0$ and $x = L$ yield ten homogeneous conditions, five at each end. At the load point $x = l_1$, there are five continuity conditions, *i.e.*, u, v, w, v', and w', and five jump conditions corresponding point-wise equilibrium of the internal actions and the external loads.

The linear elastic response of the trunnion is statically indeterminate, but can be readily solved by the superposition of an extension problem for the x-direction displacement component $u(x)$, a bending problem in the xy-plane for the y-direction displacement $v(x)$, and a bending problem in the xz-plane for the z-direction displacement

$w(x)$. Using classical bar theory, the governing ordinary differential equation (ODE) for $u(x)$ is second order, while the governing ODEs for $v(x)$ and $w(x)$ are each fourth order. The governing equations are solved in the open intervals $0 < x < l_1$ and $l_1 < x < L$, where the 20 constants of integration (c_i) resulting from integration of the ODEs with respect to x are determined using the boundary and transition conditions as given above. Details of the solution are given in Appendix B, Section Three.

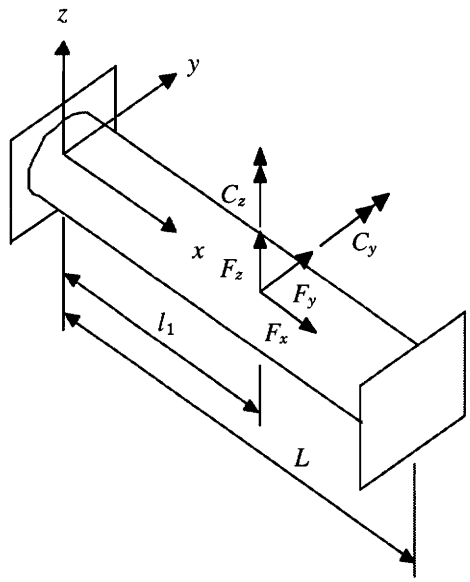

Figure 8.9 Trunnion modeled as a clamped-clamped bar

8.3.4. Member Cross-sectional Area Sizing

With the resolution of various ground loads, each structural member is subjected to a number of sets of internal actions that are due to combinations of extension, general bending, and torsion of the member. To ensure that the landing gear will not fail under the design condition, each structural member is sized such that the maximum stresses at limit loads will not exceed the allowables of the material and that no permanent deformation is permitted.

A description of selected cuts near major component joints and supports is given in Table 8.3. Normal and shear stresses acting on the cross section due to the internal actions were calculated at these locations and used in the sizing of the required member cross-sectional area.

Table 8.3 Sections description

Section	Description	Location (Figure 8.3)
1	Axle-beam centerline intersection	G/J
2	Beam-piston centerline intersection	F
3	Piston	E
4	Cylinder/struts connection	E
5	Cylinder/trunnion centerline intersection	B
6	Forward trunnion mounting	A
7	Aft trunnion mounting	C
8	Drag strut	A
9	Side strut	D

8.3.4.1. Normal and Shear Stresses In a Thin-walled Tube

The normal stresses induced on the structural members are determined by combining the effects of axial load and combined bending, while the shear stresses are determined by combining the effects of torsion and shear forces due to bending [47].

The normal stress (τ_{xx}) due to combined axial force and bending moments is given as

$$\tau_{xx} = \frac{N}{A} + \frac{M_y}{I_{yy}} z - \frac{M_z}{I_{zz}} y \tag{8.11}$$

where N is the maximum axial force, A is the cross-sectional area of the member, M_y and M_z are the internal moment components, and I_{yy} and I_{zz} are the second area moments about the y- and z-axis, respectively. As shown in Appendix B, Section Four, the extremum values of the normal stress on a circular-tube cross section under combined axial and bending actions are

$$\tau_{xx_{\substack{max \\ or \\ min}}} = \frac{N}{A} \pm \frac{1}{\pi r^2 t}\sqrt{M_y^2 + M_z^2} \tag{8.12}$$

where r is the mean radius of the tube and t is the wall thickness. In the case of drag and side struts, the last two terms in Eq. (8.11) are zero since both members are modeled as pin-ended two-force members, thus,

$$\tau_{xx} = \frac{N}{A} \tag{8.13}$$

The shear stress(τ_{xs}) due to combined transverse shear forces and torque is given as

$$\tau_{xs} = \frac{q(s)}{t} + (\tau_{xs})_{torque} \tag{8.14}$$

where q is the shear flow due to bending of a thin-walled tube, see Figure 8.10. Given that

$$tan\theta_{max} = -\frac{V_z}{V_y} \tag{8.15}$$

where θ_{max} is the polar angle where the bending shear flow attains an extremum value and V_y and V_z are the shear forces components, Eq. (8.14) then becomes

$$\tau_{xs_{\substack{max \\ or \\ min}}} = \frac{1}{\pi r t}\left(\frac{T}{2r} \pm \sqrt{V_y^2 + V_z^2}\right) \tag{8.16}$$

where T is the applied torque. Details of the solution are given in Appendix B, Section Four.

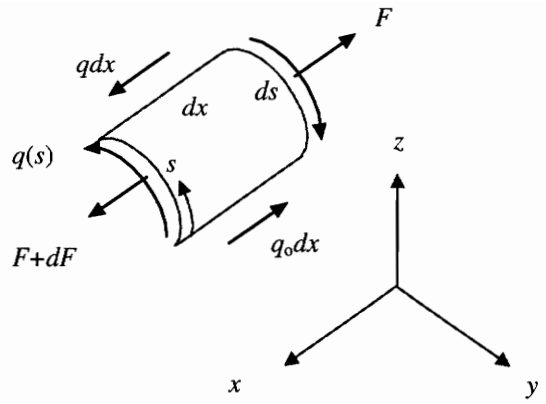

Figure 8.10 Shear flow around a tube

8.3.4.2. Design Criteria

Although aircraft structural design calls for multiple load paths be provided to give fail-safe capability, the concept cannot be applied in the design of the landing gear structures. Accordingly, the gear must be designed such that the fatigue life of the gear parts can be safely predicted or that the growth of cracks is slow enough to permit detection at normal inspection intervals [7].

Von Mises yield criterion for ductile materials combined with a factor of safety is used to determine the stress limit state. The Mises equivalent stress is given as [46, p. .368

$$\sigma_{Mises} = \sqrt{\tau_{xx}^2 + 3\tau_{xs}^2} \tag{8.17}$$

and the factor of safety is defined as the ratio of the yield stress of the material and the Mises equivalent stress, that is,

$$F.S. = \frac{\sigma_{yield}}{\sigma_{Mises}} \tag{8.18}$$

If this value is less than the specified factor of safety, the cross-sectional area of the component is increased until the desired value is attained.

In addition to material limit state, the critical loads for column buckling of the drag and side struts are considered because of the large slenderness ratio associated with these members. The slenderness ratio is defined as the length of the member (L) divided by the

minimum radius of gyration (ρ_{min}). Assuming a perfectly aligned axial load, the critical buckling load for a pin-ended two-force member can be calculated using Euler's formula [46, p. 635]

$$N_{cr} = \frac{\pi^2 EI}{L^2} \tag{8.19}$$

where E is the modulus of elasticity. In the case of a member with circular cross section, the moment of inertia I of the cross section is the same about any centroidal axis, and the member is as likely to buckle in one plane as another. For other shapes of the cross section, the critical load is computed by replacing I in Eq. (8.19) with I_{min}, the minimum second moment of the cross section (bending about the weak axis). Note that the Euler's formula only accounts for buckling in the long column mode and is valid for large slenderness ratio, *e.g.*, $L/\rho_{min} > 80$ for 6061-T6 Aluminum alloy. For slenderness ratio below this range, intermediate column buckling should be considered [48].

8.3.4.3. Sizing of the Cross-sectional Area

For thin-walled circular tubes, the cross-sectional area of the member is given as

$$A = \pi D t \tag{8.20}$$

where the mean diameter (D) and design thickness (t) are both design variables. Instead of using these two variables in the analysis directly, the machinability factor (k), which is defined as the mean diameter divided by the wall thickness, is introduced to account for tooling constraints [49]. The factor is defined as

$$k = \frac{D}{t} \tag{8.21}$$

and has an upper limit of 40. For the thin-wall approximation to be valid in the structural analysis $k > 20$. Thus, the machinability factor is limited to

$$20 \leq k \leq 40 \tag{8.22}$$

By replacing t in Eq. (8.20) with Eq. (8.21) and using D as a limiting design variable, the desired cross-sectional area can then be determined by iterating on k. Note that the lower

limit of k given in Eq. (8.21) may be violated in some instances. For structural members such as the axles, truck beam, and piston, which typically feature k values in the mid-teens, St. Venant's theory for torsion and flexure of thick-walled bars [50] should be used to calculate shear stresses. Essentially, the problem is broken down into torsion and bending problems and the shear stresses are calculated separately based on the linear theory of elasticity.

In general, the diameter of each cylindrical component is a function of either the piston or wheel dimension. In the case of shock strut, it is assumed that the internal pressure is evenly distributed across the entire cross-sectional area of the piston. That is, the piston area is a function of the internal oleo pressure (P_2) and the maximum axial force, that is,

$$A = \frac{N}{P_2} = \frac{\pi D_p^2}{4} \tag{8.23}$$

where D_p is the outer diameter of the piston. Rearrangement of Eq. (8.23) gives

$$D_p = \sqrt{\frac{4N}{\pi P_2}} \tag{8.24}$$

Assuming a perfect fit between the piston lining and the inner cylinder wall, the minimum allowable mean diameter of the cylinder is obtained by adding the wall thickness of the cylinder to the piston outer diameter. To reduce the level of complexity, the minimum allowable mean diameter of the trunnion is assumed to be identical to that of the cylinder. Similar assumptions are made concerning the axle and truck beam, except that the outer diameter of the above members is treated as a function of the diameter of the wheel hub. In the case of the axle, the maximum allowable mean diameter is obtained by subtracting the axle wall thickness from the hub diameter.

For the thin-walled I-section bar shown in Figure 8.11, the cross-sectional area and principal centroidal second area moments are

$$A = t(2b + h) \tag{8.25}$$

$$I_{yy} = t\left[\frac{h^3}{12} + 2b\left(\frac{h}{2}\right)^2\right] \tag{8.26}$$

and

$$I_{zz} = \frac{b^3 t}{6} \tag{8.27}$$

where h is the web height and b is the width of the two flanges. Assume that $I_{yy} > I_{zz}$, algebraic manipulations then result in

$$\frac{h}{b} > \sqrt{2} \tag{8.28}$$

and the z-axis is the weak axis in bending. The cross-sectional area is related to the second area moment by the minimum radius of gyration, that is,

$$A = \frac{I_{zz}}{\rho_{min}^2} \tag{8.29}$$

or for the I-section

$$\rho_{min} = \frac{b}{\sqrt{12 + 6h/b}} \tag{8.30}$$

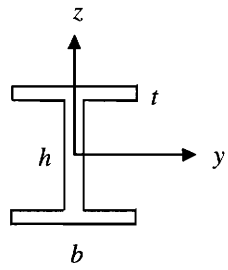

Figure 8.11 I-section truss bar

Since only the cross-sectional area is used in the weight computation, it is not necessary to determine the actual dimensions of the sectional height and width. Instead,

one of the dimensions, usually the height, is treated as a function of the piston diameter and the other is then calculated with a predetermined *h/b* ratio.

8.3.5. Structural Weight Calculation

The final step of the analytical procedure is to calculate the weight of each member based on its cross-sectional area, length, and the material density. Recall that seven different loading conditions were examined in the analysis, which results in seven sets of cross-sectional areas for each member. To ensure that the component will not fail under any of the seven loading conditions, the maximum cross-sectional area from the sets is selected as the final design value. Component weights are then calculated by multiplying each of the cross-sectional areas by the corresponding length and material density. The summation of these calculations then becomes the structural weight of the idealized analytical model.

8.3.6. Validation of the Analysis

For analysis validation purpose, the landing gear for the Boeing Models 707, 727, 737 and 747 were modeled and analyzed. The estimated structural weight, which includes the axle/truck, piston, cylinder, drag and side struts, and trunnion, accounts for roughly 75 percent of the total structural weight that can be represented in the model [43]. The remaining 25 percent of the gear structural weight is made up of the torsion links, fittings, miscellaneous hardware, and the internal oleo mechanism, *e.g.*, the metering tube, seals, oil, pins, and bearings. Note that actual and estimated structural weights presented in Tables 8.4 and 8.5 only account for the components that were modeled in the analysis.

Table 8.4 Main assembly structural weight comparison

Aircraft	Estimated, lb	Actual, lb	Est/Act
B737	784	768	1.02
B727	1396	1656	0.84
B707	2322	2538	0.91
B747	9788	11323	0.86

Table 8.5 Nose assembly structural weight comparison

Aircraft	Estimated, lb	Actual, lb	Est/Act
B737	107	145	0.74
B727	171	327	0.52
B707	159	222	0.72
B747	1010	1439	0.70

Difference between the actual and estimated structural weights can be attributed to several factors. First, the models analyzed are extremely simple, *i.e.*, structural members were represented with simple geometric shapes and no considerations have been given to fillet radii, local structural reinforcement, bearing surfaces, *etc.* As for the analysis itself, simplistic equations were used to calculate the applied static and dynamic loads, and idealized structural arrangements were used to determine the member internal reactions. However, it should be noted that the results are consistent with Kraus' original analysis; where an average of 13 percent deviation was cited [43].

8.4. Landing Gear Group Weight Estimation

Although proven to be far more responsive to variations in design parameters, it is unlikely that an analytical tool will replace statistical methods. In fact, both methods should be used as complements to one another. This is particularly true in the calculation of the landing gear group weight, where the analytical and statistical methods can be used to determine the structural and non-structural component weights, respectively.

For large transports, landing gear structural weight accounts for roughly 57 percent of the landing gear group weight. The remaining weight is made up by the rolling

stock and controls; the former accounts for roughly 34 percent of the total weight, while the latter accounts for the last nine percent. Note that the weights of the tires, wheels and brakes that made up the rolling stock have already been determined in previous chapters and no additional calculation is needed. As for the controls, *i.e.*, actuation and steering mechanisms, the items can be estimated statistically with sufficient accuracy and thus eliminates the need to resort to an analytical method [App. A]. A detailed weight breakdown is provided in Table 8.6; the values are presented in terms of percent total landing gear weight.

Table 8.6 Landing gear weight breakdown [2]

Component	Main assembly	Nose assembly
Rolling stock	**32.0**	**2.0**
Wheels	6.0	1.0
Tires	10.0	1.0
Brakes	16.0	0.0
Miscellaneous	0.0	0.0
Structure	**50.0**	**7.0**
Shock strut	32.0	4.0
Braces	12.0	1.0
Fittings	5.0	1.0
Miscellaneous	1.0	1.0
Controls	**7.0**	**2.0**
Total	**89.0**	**11.0**

Using the combined analytical and statistical approach presented here, the landing gear group weight for the Boeing Models 707, 727, 737, and 747 were calculated and compared with actual values. As presented in Table 8.7a, the analysis tends to underestimate the group weight as the aircraft takeoff weight increases. Linear regression analysis was used to calibrate the estimated group weights (W_{est}) so they agree with the actual values. Correction factors were calculated using the expression

$$f_c = 0.005W - 525 \tag{8.31}$$

where W is the aircraft weight. The correction factor is then combined with W_{es} to arrive at the calibrated landing gear group weight (W_{cal}), that is,

$$W_{cal} = W_{est} + f_c \tag{8.32}$$

The objective of this effort is to ensure that the discrepancy between the actual and estimated values will remain within a tolerable range. This is important when the analysis are used to examine the weight of landing gear for aircraft that are outside the existing pavement thickness database. The calibrated results are shown in Table 8.7b.

Table 8.7 Landing gear group weight comparison

a) Estimated group weight

Aircraft	Estimated, lb	Actual, lb	Est/Act
B737	4479	4382	1.02
B727	5976	6133	0.97
B707	9510	11216	0.85
B747	27973	31108	0.90

b) Calibrated group weight

Aircraft	Calibrated, lb	Actual, lb	Cal/Act
B737	4499	4382	1.03
B727	6301	6133	1.03
B707	10545	11216	0.94
B747	31138	31108	1.00

Chapter 9 Analysis Package

9.1. Introduction

Four FORTRAN programs and a spreadsheet based on the analyses as outlined in previous chapters were developed for eventual incorporation into existing MDO codes. Programs CONFIG, LIMIT, PAVE, and GEARWEI can be used together in an iterative fashion to study the global effects of variations in the landing gear design parameters on configuration, system integration, airfield compatibility, and weight. In addition, the programs can be used individually to analyze a particular aspect of a given concept. In both cases, aircraft configuration characteristics have to be imported either from existing aircraft sizing codes or disciplinary analyses, while landing gear-related parameters must be specified by the user or set up as defaults. Within an optimization framework, these parameters would be treated as design variables whose optimum values would be computed by the optimizer to achieve a desired objective. However, the goal here is to demonstrate the algorithms, which can be used to help automate the landing gear design process.

In addition to the four programs as mentioned above, a simple, Microsoft Excel-based spreadsheet was created to establish the maximum permissible *cg* range of a particular aircraft concept. The spreadsheet requires estimated component weights be imported from existing aircraft sizing code, while the corresponding component *cg* ranges can be specified by the user or set up as defaults.

9.2. Description of Programs

A simple spreadsheet software is used to establish the forward and aft limits of the permissible aircraft *cg* range. Given the aircraft configuration characteristics and

component weights, the spreadsheet uses the specified component *cg* range as detailed in Chapter Two to calculate the maximum permissible aircraft *cg* range.

The primary task for program CONFIG is to develop a landing gear model that can be used as the baseline configuration. Given the aircraft weight, configuration characteristics, and the number of struts and tires, the program determines the loads on the tires and the total braking energy to be absorbed by the brakes. Suitable tires, wheels, and brakes are either selected from manufacturers' catalogs or sized statistically as detailed in Chapters Four and Five. The length of the structural components, *e.g.*, axles, truck beam, piston, cylinder, and trunnion, are determined based on the attachment scheme and clearance requirements. As for the linkages, a generic attachment scheme derived from existing commercial transports is used to determine the arrangement and required length of the drag and side struts. Based on this information, the program establishes a mathematical model of the notional landing gear in three-dimensional space, which is to be used by the remaining programs for detailed analysis.

Program LIMIT is used to examine the design and kinematic characteristics of the landing gear. Given the configuration characteristics of the aircraft and the model of the notional landing gear, turnover angle, pitch and roll angles during takeoff/landing, ground clearance, and turning radii are calculated using procedures as detailed in Chapter Three. The calculated values are then compared with a list of specified requirements to identify possible constraint violations. From the dimension and arrangement of the landing gear and the allocated stowage space, pivot axis and retraction angle are determined using mathematical kinematic analysis as detailed in Chapter Six. In addition, retraction path, swept volume, and stowed position are established and compared with stowage boundaries for possible structural interference.

The flotation characteristics of the aircraft are determined by program PAVE. Flexible and rigid pavement bearing stresses associated with specified loading conditions are calculated using pavement design procedures as detailed in Chapter Seven. The

required pavement thickness is converted to the standard pavement bearing strength reporting system and tabulated for comparison purposes.

The component and group weights of the landing gear are calculated by program GEARWEI. As detailed in Chapter Eight, the structural weight of the landing gear is determined analytically from the notional landing model, while the weight of the non-structural components is determined from a statistical database. These weights are combined to arrive at the landing gear group weight.

9.3. Organization of Analyses

The programs are organized as shown in Figure 9.1 for use in an iterative fashion to study the global effects of variations in the landing gear design parameters. Aircraft weight and configuration characteristics, as well as a limited number of landing gear-related design parameters, enter the package through program CONFIG. The former set of data is obtained either from existing aircraft sizing codes or disciplinary analyses, *e.g.*, ACSYNT and FLOPS, whereas the latter is user-specified or is set up as defaults. Using this information as a starting point, program CONFIG generates a notional landing gear model, as well as data sets to be used as inputs for programs PAVE, LIMIT, and GEARWEI. The first two programs then assess flotation, operational stability, maneuverability, and stowage aspects of the aircraft/landing gear concept are examined. If all the design constraints are satisfied, landing gear weight is then estimated in program GEARWEI. Note that if any of the design constraints cannot be satisfied by the current configuration, user-specified modifications to the model or design parameters will be needed to resolve the violations through an iterative process. The execution of all the programs is essentially instantaneous.

The current state of the analysis package is a compilation of a number of separate analysis codes. The package does not have the capability to generate the required landing gear-related parameters, *e.g.*, the number of tires and struts, attachment location, and stowage space, based on imported aircraft configuration characteristics. Thus, starting

values, or "guesstimates", must be provided for these design parameters. The parameters can then easily be varied by the user, or an optimizer, for parametric study purposes and the information used to select the optimum design.

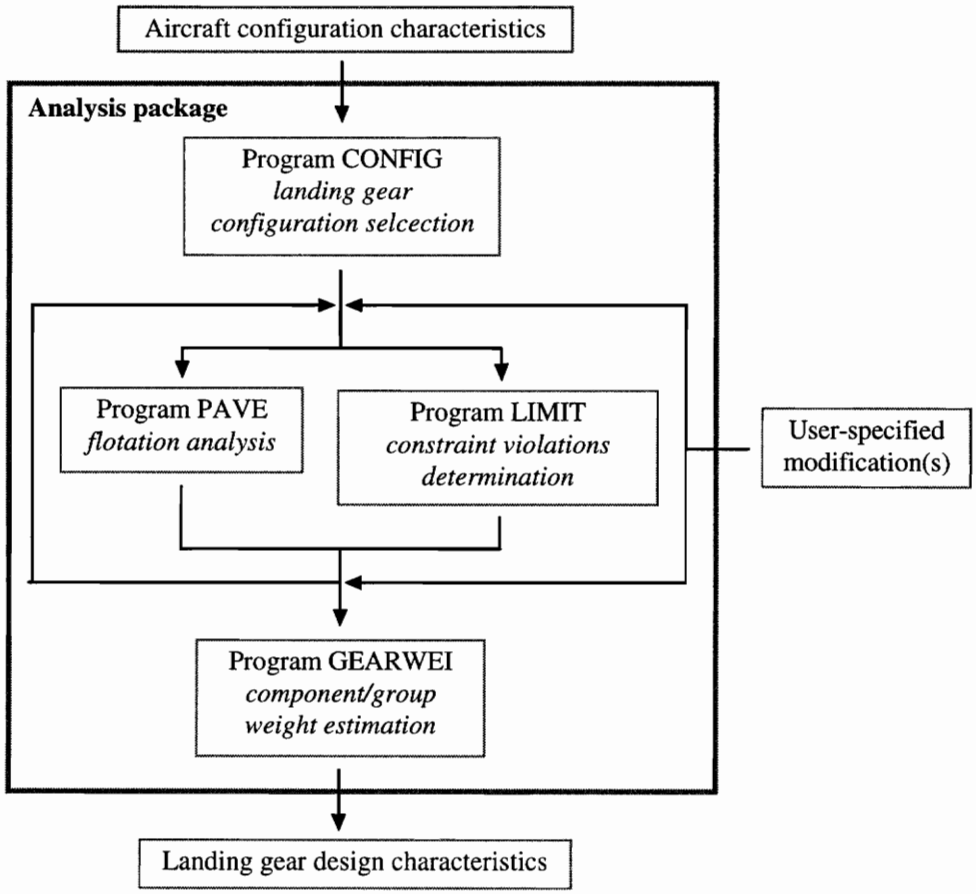

Figure 9.1 Organization of analyses

9.3.1. Input/Output Data

Data required by the analysis package are listed in Table 9.1. The majority of this information consists of geometric and weight characteristics associated with the aircraft: wing area and span, quarter chord sweep, fuselage length and width, maximum takeoff/landing weight, aircraft *cg* location, *etc*. These design parameters are readily

available from existing aircraft sizing codes and can easily be rearranged into the "card-style" inputs used by the analyses. The remaining information consists of landing-gear related parameters, and as mentioned in the previous section, must be provided by the user or selected from defaults.

Table 9.1 Required input data

Parameter	Type	Description
Wing	Imported	Geometric characteristics; location
Fuselage	Imported	Geometric characteristics
Engine/Nacelle	Imported	Geometric characteristics; location
Weight	Imported	Takeoff/landing weights; weight distribution; aircraft *cg* location
Landing gear	User-specified or default	Design/selection criteria; number of tires/struts; location; clearance; stowage space

A description of the results generated by individual analysis is given in Table 9.2. It should be pointed out that these data only represent part of information that is produced by the analyses. Intermediate results, *e.g.*, constraint boundaries, landing gear loads and induced stresses, that might be of interest or importance to a particular discipline, are currently internal to the analyses. To access this information would require modification of the output section of the program(s) to extract these data. Sample input/output files for the four programs can be found in Appendix E.

Table 9.2 Analysis-generated output data

Program	Description
CONFIG	Selected tires/wheels data; strokes; load-stroke curve; mathematical landing gear model
LIMIT	Trunnion alignment; retracted landing gear position; stability/operational characteristics; constraint violations
PAVE	*ESWL*s; concrete bearing stresses; pavement thickness; ACNs
GEARWEI	Structural member dimensions; landing gear component/group weight

9.4. Aircraft CG Estimation Spreadsheet

In addition to the four programs that made up the analysis package, a simple, Microsoft Excel-based spreadsheet was created to establish the maximum permissible aircraft *cg* range for any given aircraft concept. Aircraft component identification was provided in the first column, while estimated component weights as obtained from existing sizing codes are entered into the second column. Given the aircraft geometric characteristics, the forward and aft component *cg* limits determined based on the generic aircraft layout developed in Chapter Three are entered into column three and four, respectively. The spreadsheet calculates the moments corresponding to the forward and aft component *cg* limits, and then divides the sums of the moments by the total component weight to arrive at the maximum forward and aft aircraft *cg* limits.

Chapter 10 Parametric Studies

10.1. Introduction

The emergence of the next-generation high-capacity commercial transports [51 and 52] provides an excellent opportunity to demonstrate the capability of the landing gear analysis package as detailed in the previous chapter. Landing gear design variables were varied parametrically to show their effects on the weight, flotation, and stability characteristics. Dependencies between the variables and characteristics established from the parametric analysis, as well as the magnitude of the effect, can be used as a guideline in selecting the most effective means to alter a particular aircraft-landing gear configuration so that the desired characteristics can be obtained.

10.2. The Ultra-High-Capacity Transports

A conceptual ultra-high-capacity transport (UHCT) was established based on a study by Arcara *et al.* [53] and industry forecasts [54, 55 and 56]. Configuration characteristics of the aircraft are presented in Table 10.1. Note that the aircraft is classified as a Design Group VI aircraft according to its wingspan, which is slightly over the specified 262-foot upper limit [5]. To match the geometric model of the aircraft as found in ACSYNT, the wing is modeled as a simple trapezoid without an inboard trailing-edge extension, *i.e.*, the Yehudi. As a result, the location of the wing *mac* and hence the aircraft *cg* location and the attachment position of the main assembly are slightly forward of where they would be in the actual design.

Table 10.1 Configuration characteristics of a conceptual UHCT

	Baseline
Passenger capacity	800
Range, nmi	7,500
Fuselage length, ft	250.0
Fuselage width, ft	24.0
Wingspan, ft	264.0
Wing area, ft^2	8,324
Aspect ratio	8.4
MTOW, lb	1,230,000
Fuel, lb	550,000

Twenty-four main assembly tires arranged in a triple-dual-tandem configuration, *i.e.*, six tires per strut, is used as an initial design. Tire selection is based on the minimum weight criterion. Forged aluminum and carbon are selected as the construction materials for the wheels and brakes, respectively. For the landing gear structure, 300M high-strength steel is used. The attachment scheme calls for two main gear units mounted on the wing and two units on the fuselage: the wing-mounted units retract inboard, while the fuselage-mounted units retract forward into the fuselage. The ensuing wheelbase and track dimensions are approximately 102 and 39 feet, respectively. Given this information, the analysis package as described in Chapter Nine is used to determine the design characteristics associated with this particular aircraft-landing gear combination. As shown in Table 10.2, all design constraints are satisfied. The landing gear weighs about 56,900 pounds and accounts for roughly 17.4 percent of the aircraft structural weight, or 4.6 percent of the MTOW.

Table 10.2 Baseline aircraft design characteristics

	Calculated	Constraint
Sideways turnover angle, deg	40.7	< 63.0
Roll angle, deg	7.2	< 8.0
Available touchdown angle, deg	16.7	~ 15.0
Available takeoff rotation angle, deg	15.4	~ 15.0
Nacelle-to-ground clearance, in	10.0	> 7.0
Castor angle, deg	37.0	< 60.0
Turning radius, ft	78.4	< 100.0
Gear weight, lb	56,885	-
Weight fraction, %MTOW	4.63	-

The flotation characteristics are given in Table 10.3 along with actual data for the McDonnell Douglas DC10, which are highest among existing aircraft. As shown in Table 10.3, major runway reinforcements will be needed at airports with a combination of flexible pavements and a low bearing strength subgrade. Costs associated with such an upgrade could be in the $100 million range [4], an investment that might not be acceptable to airport authorities. Consequently, some major international airports with flexible pavements might not be able to handle the UHCT unless design changes are made to the aircraft. Results in Table 10.3 indicate that airports with rigid pavements are better suited in handling this class of aircraft. Note that as the subgrade strength approaches its upper limit, the required flexible and rigid pavement thickness for the new aircraft are actually lower than the ones required by the DC10. This is consistent with the trend observed in Chapter Seven, *i.e.*, as the number of wheels per strut increases, the required pavement thickness decreases with the increase in the subgrade strength.

Table 10.3 Baseline aircraft flotation characteristics

Subgrade strength	Thickness, in (UHCT/DC10)	ACN (UHCT/DC10)
Flexible		
Ultra-low	73.5/63.9	134/97
Low	39.1/37.8	80/70
Medium	25.5/26.9	60/59
High	16.0/20.2	47/53
Rigid		
Ultra-low	18.6/17.0	96/75
Low	16.4/15.2	79/64
Medium	13.3/13.0	62/53
High	11.5/11.8	50/44

10.3. Parametric Studies

Given the baseline aircraft-landing gear combination as characterized in the previous section, landing gear design variables were varied parametrically to show their effects on the weight, flotation, and stability characteristics. Dependencies between the various control variables and resulting aircraft characteristics established from this study, as shown here in Figure 10.1, can be used as a guideline in selecting the most effective means to alter a particular aircraft-landing gear configuration so that the desired characteristics may be obtained. Note that there are instances where flotation and stability characteristics remain unchanged despite variations in the design parameters. Thus, only the characteristics being affected will be discussed.

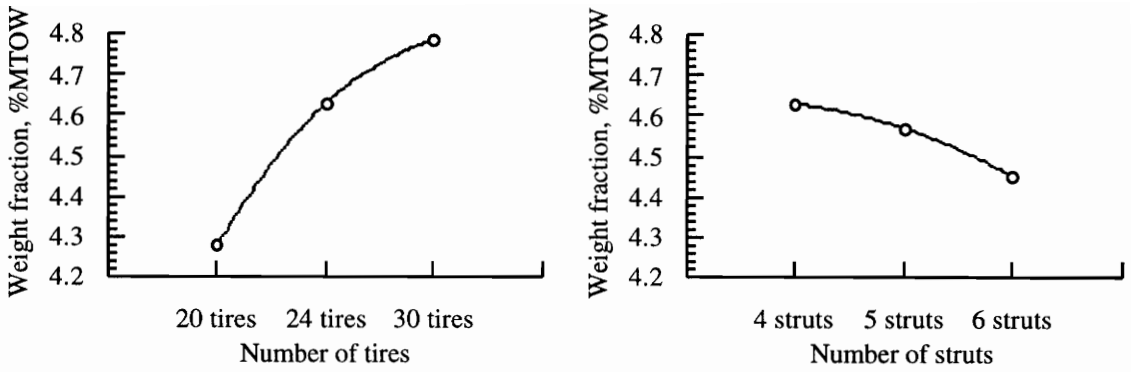

a) Number of tires, four-strut configuration

b) Number of struts, 24-tire configuration

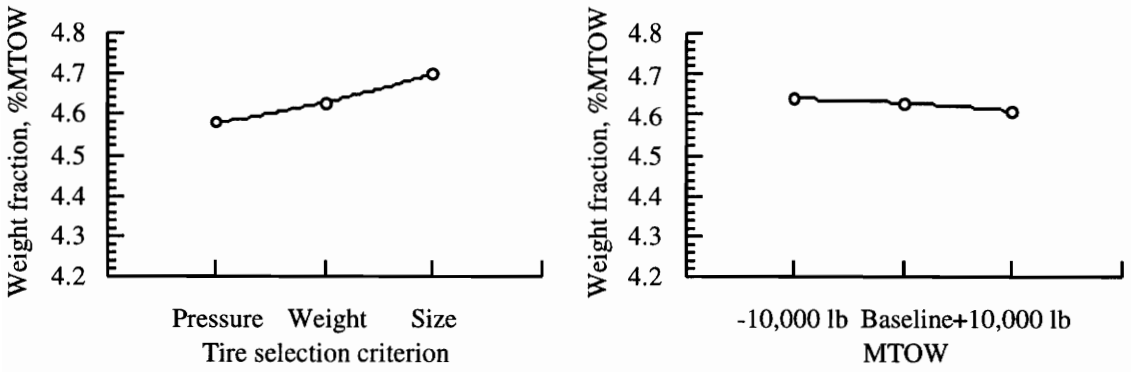

c) Tire selection criterion

d) MTOW

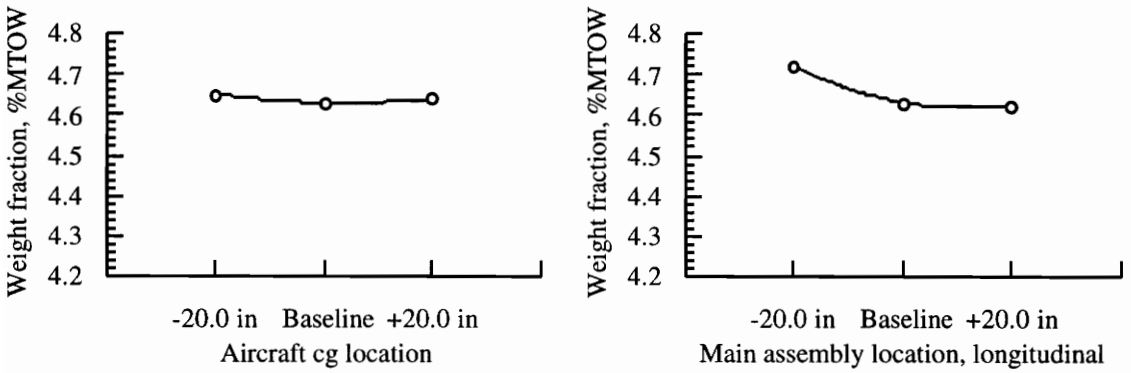

e) Aircraft *cg* location

f) Main assembly location, longitudinal

Figure 10.1 Changes in landing gear weight fraction due to design parameter variations

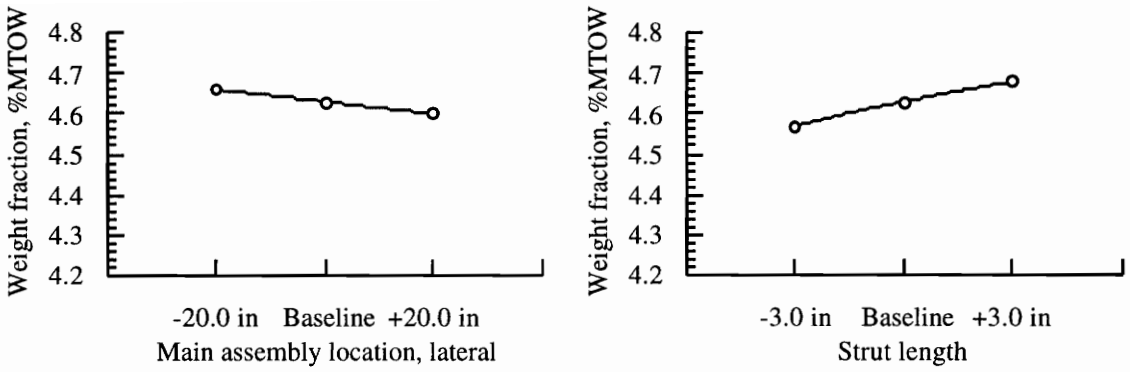

g) Main assembly location, lateral

h) Strut length

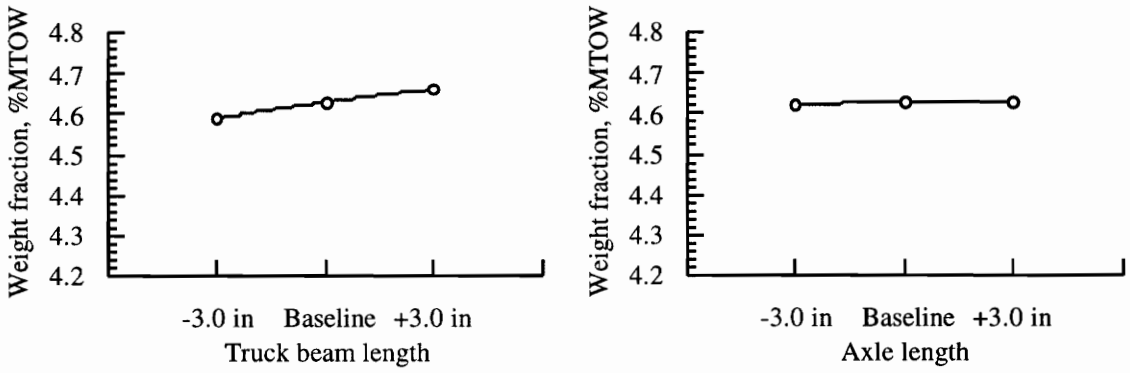

i) Truck beam length

j) Axle length

Figure 10.1 Changes in landing gear weight fraction due to design parameter variations (cont'd)

In order for the UHCT to be able to operate from current airports without extensive runway reinforcement, additional tires are required to redistribute the weight of the aircraft over a larger tire-ground contact area. Provided the number of main assembly struts remains unchanged at four, the number of tires were varied both above and below the baseline (24). As shown in Figure 10.1a, landing gear weight fraction increases with the increase in the number of tires. Evidently, weight penalties associated with increased part-count, as well as the dimension of the truck assembly, easily outstrip weight savings

obtained from lighter tire and wheel designs that come with reduced load-carrying requirements. As shown in Table 10.4, the increased tire-ground contact area leads to reductions in required pavement thickness and the corresponding ACN when compared to the baseline figures.

Table 10.4 Number of main assembly tires, four-strut configuration

Subgrade strength	Thickness, in		ACN	
	20 tires (Des./Base)	30 tires (Des./Base)	20 tires (Des./Base)	30 tires (Des./Base)
Flexible				
Ultra-low	71.1/73.5	68.5/73.5	127/134	118/134
Low	39.0/29.1	35.7/29.1	80/80	68/80
Medium	24.6/25.5	22.6/25.5	56/60	48/60
High	15.6/16.0	13.6/16.0	45/47	37/47
Rigid				
Ultra-low	19.6/18.6	17.6/18.6	106/96	86/96
Low	17.3/16.4	15.5/16.4	88/76	70/76
Medium	14.1/13.3	12.6/13.3	69/62	55/62
High	12.2/11.5	10.9/11.5	56/50	45/50

Varying the number of main assembly struts is another option to be considered in producing the desired flotation characteristics. As shown in Figure 10.1b, provided the number of tires remains unchanged at 24, a reduction in the landing gear weight fraction is realized with an increase in the number of main assembly struts. The reduction can be attributed to the decrease in the number of tires found on each strut, which effectively lowers the combined load on the structural members and therefore leads to a lighter structure. As shown in Table 10.5, a reduction in the required flexible pavement thickness is evident as the number of the struts increases. Recall that in multiple-wheel assemblies, the flexible pavement bearing stresses are directly proportional to the number of tires per strut involved in the calculation and hence the required pavement thickness. The rigid pavement thickness requirements remain unchanged since the stresses obtained from Westergaard's analysis are independent of the number of main assembly struts.

Table 10.5 Number of main struts, 24-tire configuration

Subgrade strength	Thickness, in		ACN	
	five struts (Des./Base)	six struts (Des./Base)	five struts (Des./Base)	six struts (Des./Base)
Flexible				
Ultra-low	73.5/73.5	67.4/73.5	135/134	115/134
Low	39.1/39.1	36.1/39.1	80/80	69/80
Medium	25.5/25.5	22.2/25.5	60/60	46/60
High	16.0/16.0	13.6/16.0	47/47	37/47
Rigid				
Ultra-low	18.6/18.6	18.6/18.6	96/96	96/96
Low	16.4/16.4	16.4/16.4	78/79	78/79
Medium	13.3/13.3	13.3/13.3	62/62	62/62
High	11.5/11.5	11.5/11.5	50/50	50/50

Besides increasing the number of main assembly tires and struts to bring about the desired reduction in the required pavement thickness, another option is to select a tire with a lower inflation pressure. As shown in Figure 10.1c, the minimum inflation pressure candidate offers the lowest landing gear weight fraction of the three selection criteria. A reduced inflation pressure also means an increased tire-ground contact area, hence reduced pavement loads and pavement thickness requirements as shown in Table 10.6. It should be noted that all but a select few of large tires available are capable of meeting the performance requirements imposed by the UHCT. That is, the inflation pressure, size, and weight of the candidate tires are nearly identical. As a result, the effects due to such variations might not be as apparent as they would be for other types of aircraft, where the selection is based on a larger pool of candidate tires.

Table 10.6 Tire selection criteria, 24-tire configuration

Subgrade strength	Thickness, in		ACN	
	Min. press (Des./Base)	Min. size (Des./Base)	Min. press (Des./Base)	Min. size (Des./Base)
Flexible				
Ultra-low	73.1/73.5	73.5/73.5	133/134	135/134
Low	39.4/39.1	39.1/39.1	81/80	80/80
Medium	24.3/25.5	25.5/25.5	55/60	60/60
High	15.3/16.0	16.0/16.0	44/47	47/47
Rigid				
Ultra-low	18.3/18.6	18.6/18.6	92/96	96/96
Low	16.1/16.4	16.4/16.4	75/79	78/79
Medium	12.9/13.3	13.3/13.3	58/62	62/62
High	10.9/11.5	11.5/11.5	45/50	50/20

Variations in MTOW have an obvious impact on the configuration of the landing gear and the pavement thickness. As a minimum, the structural dimensions of the landing gear and hence the structural weight would vary as the design weight of the aircraft changes between different configurations. As shown in Figure 10.1d, the landing gear weight fraction decreases even though the actual landing gear weight increases with the MTOW. This can be attributed to the fact that the landing gear weight does not increase with the MTOW in a pound-for-pound manner, and therefore a decreasing weight fraction is observed. Similarly, the landing gear weight decreases at a slower rate than the MTOW, yielding a higher weight fraction. The magnitude of the landing gear weight variation is similar to that provided by industry, where a 40-pound increase in the landing gear weight per 1,000 pounds increase in the MTOW is anticipated [App. A]. As reaffirmed in Table 10.7, an increase in the MTOW would require a thicker pavement to support the aircraft, and vice versa.

Table 10.7 MTOW variations

Subgrade strength	Thickness, in		ACN	
	-10,000 lb (Des./Base)	+ 10,000 lb (Des./Base)	-10,000 lb (Des./Base)	+ 10,000 lb (Des./Base)
Flexible				
Ultra-low	73.2/73.5	73.8/73.5	134/134	136/134
Low	39.0/39.1	39.3/39.1	80/80	81/80
Medium	25.4/25.5	25.6/25.5	59/60	60/60
High	16.0/16.0	16.0/16.0	47/47	47/47
Rigid				
Ultra-low	18.5/18.6	18.7/18.6	95/96	96/96
Low	16.3/16.4	16.5/16.4	78/79	79/79
Medium	13.3/13.3	13.3/13.3	61/62	62/62
High	11.5/11.5	11.5/11.5	50/50	50/50

Although the location of aircraft *cg* has always played a decisive role in the positioning of the landing gear, instances are possible where design considerations become conclusive in deciding the mounting location, *i.e.*, the landing gear has to be located at a specific location so that desired stability and maneuverability characteristics can be obtained. As shown in Figure 10.1e, for this particular aircraft-landing gear combination, provided that the location of the main assembly group is fixed, an optimum aircraft *cg* location exists at a short distance aft of the current position where the weight fraction of the landing gear is at its minimum. In such cases, the location of the aircraft *cg* must be maintained at a particular position during takeoff/landing conditions through a controlled loading scheme. Once airborne, the constraints can be relaxed by redistributing the fuel among various fuel tanks.

As shown in Figure 10.1f, the repositioning of the main assembly group in the aft direction results in a landing gear weight fraction that is lower than the one corresponding to a shift in the forward direction. This trend can be attributed to the reduced load that follows directly from an increased offset between the main assembly group and the location of the aircraft *cg*, *i.e.*, a longer moment arm to counteract the applied ground loads. Note that when a highly-swept, high-aspect ratio wing is considered, a rearward

movement of the main assembly group might not be feasible due to wing planform constraints, such as the size of the inboard trailing-edge extension (the Yehudi), required to provide suitable attachment location, as well as sufficient space to house the trailing-edge control surfaces and the associated actuation systems. The Yehudi also incurs drag and weight penalties that need to be considered.

The repositioning of the wing-mounted assemblies in the lateral direction affects primarily the stability and maneuverability characteristics of the aircraft. As shown in Table 10.8, an outboard movement of the wing-mounted assemblies produces a desired reduction in the sideways turnover angle; however, such a movement shifts the minimum 180-degree turn radius closer to the Class VI 100-foot upper limit [5]. As shown in Figure 10.1g, the increasing landing gear weight fraction can be associated with the outboard movement of the assemblies. This leads to an increase in the length of the side strut, as well as an increase in the drag and shock struts due to wing dihedral, and hence the structural weight of the landing gear. Conversely, an inboard movement of the assemblies exhibits a higher sideways turnover angle, a smaller turning radius, and a decreasing landing gear weight fraction.

Table 10.8 Wing-mounted assemblies location variations, lateral

Design characteristics	**20.0 in outboard**	**20.0 in inboard**
Sideways turnover angle, deg	38.4	43.2
Available touchdown angle, deg	16.9	16.5
Available takeoff rotation angle, deg	15.3	15.5
Turning radius, ft	80.1	76.7

Changes in the stability characteristics and ground clearance due to variations in landing gear strut length are of primary interest when a growth version of the aircraft is considered. Features typically associated with the growth options are a stretched fuselage obtained from the addition of plugs forward and aft of the wing, and upgraded power plants that come with a larger fan diameter. Both of the above features would require an

extension of the strut length to maintain the desired operation angles and nacelle-to-ground clearance. As shown in Table 10.9, the growth-related modifications can result in an increased sideways turnover angle and a reduced permissible pitch angle during takeoff/landing operations. As can be expected and reaffirmed in Figure 10.1h, an increase in strut length leads to an increase in structural weight, and therefore an increase in the landing gear weight fraction, as well as vice versa. The magnitude of the landing gear weight variation is again similar to the one provided by industry, where a 60-pound increase in weight per strut is anticipated for every inch increase in strut length [App. A].

Table 10.9 Strut length variations

Design characteristics	**-3.0 in**	**+3.0 in**
Sideways turnover angle, deg	40.2	41.1
Available touchdown angle, deg	16.9	16.5
Available takeoff rotation angle, deg	15.3	15.5

Changes in the size of the tires, wheels, and brakes due to varying design parameters, *e.g.*, loading conditions and braking energy requirements, can alter the dimensions of the truck beam and axles. As can expected and reaffirmed by Figures 10.1i and 10.1j, an increase in the component length leads to a higher landing gear weight fraction, and vice versa. Data presented in Tables 10.10 and 10.11 show that an increase in either truck beam or axle length will result in a thicker pavement .

Table 10.10 Truck beam length variations

Subgrade strength	Thickness, in		ACN	
	-3.0 in (Des./Base)	+3.0 in (Des./Base)	-3.0 in (Des./Base)	+3.0 in (Des./Base)
Flexible				
Ultra-low	73.1/73.5	73.7/73.5	133/134	135/134
Low	39.1/39.1	39.2/39.1	80/80	80/80
Medium	25.5/25.5	25.5/25.5	60/60	60/60
High	16.0/16.0	16.0/16.0	47/47	47/47
Rigid				
Ultra-low	18.6/18.6	18.6/18.6	96/96	96/96
Low	16.4/16.4	16.4/16.4	78/79	78/79
Medium	13.3/13.3	13.3/13.3	62/62	62/62
High	11.5/11.5	11.5/11.5	50/50	50/50

Table 10.11 Axle length variations

Subgrade strength	Thickness, in		ACN	
	-3.0 in (Des./Base)	+3.0 in (Des./Base)	-3.0 in (Des./Base)	+3.0 in (Des./Base)
Flexible				
Ultra-low	73.4/73.5	73.6/73.5	134/134	135/134
Low	38.7/39.1	39.5/39.1	79/80	82/80
Medium	25.1/25.5	25.8/25.5	58/60	61/60
High	15.7/16.0	16.3/16.0	46/47	48/47
Rigid				
Ultra-low	18.6/18.6	18.6/18.6	96/96	96/96
Low	16.4/16.4	16.4/16.4	78/79	78/79
Medium	13.3/13.3	13.3/13.3	62/62	62/62
High	11.5/11.5	11.5/11.5	50/50	50/20

10.4. Derivatives of the Baseline Aircraft

In today's highly competitive environment, flexibility in being able to meet the vastly different requirements from various airline customers, *e.g.*, a longer range and an extended payload capacity, has become one of the primary considerations in the design and marketing of a new aircraft. To ensure that a customer will have a list of options to

select from when it comes time to place an order, derivatives are considered early on in the conceptual design phase, and more than likely, pursued in parallel with the baseline aircraft.

Two derivatives were envisioned for the baseline UHCT: advanced (high aspect ratio) wing and extended range (8,000 nmi); corresponding configuration characteristics are shown in Table 10.12. Although the wing planform of the advanced wing derivative is slightly different from the baseline and the extended range version, it is assumed that the configuration of the landing gear on all three aircraft are identical, *i.e.*, 24 main assembly tires on four struts. Note that this assumption does not imply that the weights of all three landing gear are identical.

Table 10.12 Derivative configuration characteristics

	Extended range	**Advanced wing**
Passenger capacity	800	800
Range, nmi	8,000	7,500
Fuselage length, ft	250.0	250.0
Fuselage width, ft	24.0	24.0
Wing span, ft	264.0	261.0
Wing area, ft^2	8,324	7,423
Aspect ratio	8.4	9.2
MTOW, lb	1,350,000	1,140,000
Fuel, lb	640,000	460,000

As shown in Figure 10.2, the advanced wing derivative has the highest landing gear weight fraction of the three configurations, whereas the extended range derivative has the lowest of the three. For identical mission requirements between the baseline and the advanced wing derivative, the baseline aircraft will be the preferred choice if the deciding factor is based on landing gear weight fraction, its lower landing gear weight fraction implies that a greater fraction of the total aircraft weight is made up by revenue-generating payloads. However, if the deciding factor is something other than the landing gear weight faction, *e.g.*, operating cost or runway upgrade cost, the advanced wing configuration will

be the preferred choice due to its lower mission fuel requirements and lighter MTOW, respectively. As for the extended range derivative, although the landing gear weight fraction is lower than the other two aircraft, the required pavement thickness as shown in Table 10.13 can result in a prohibitive runway upgrade cost. However, the desired flotation characteristics can be obtained by replacing the conventional wing design with the one found on the advanced wing derivative. The reduction in mission fuel weight associated with higher performance due to the advanced wing design would then lower the MTOW of the extended range derivative and hence the required pavement thickness.

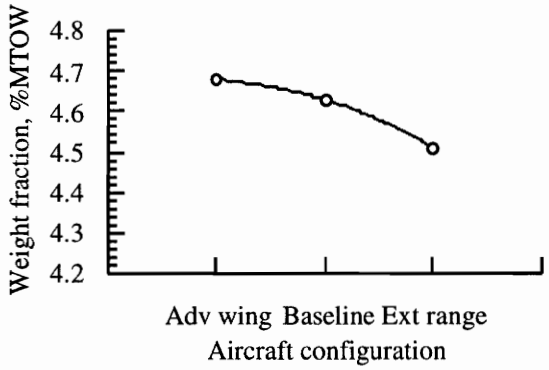

Figure 10.2 Changes in landing gear weight fraction due to aircraft configuration variations

Table 10.13 Aircraft configuration variations

Subgrade strength	Thickness, in		ACN	
	Ext. range (Des./Base)	Adv. wing (Des./Base)	Ext. range (Des./Base)	Adv. wing (Des./Base)
Flexible				
Ultra-low	77.1/73.5	70.0/73.5	148/134	90/134
Low	40.8/39.1	37.9/39.1	88/80	75/80
Medium	25.5/25.5	24.6/25.5	61/60	60/60
High	15.6/16.0	15.6/16.0	48/47	50/47
Rigid				
Ultra-low	19.3/18.6	18.2/18.6	104/96	122/96
Low	16.9/16.4	16.1/16.4	84/79	75/79
Medium	13.6/13.3	13.2/13.3	65/62	55/62
High	11.6/11.5	11.6/11.5	52/50	43/50

10.5. Landing Gear Weight Trend for Large Aircraft

The baseline aircraft along with its derivatives are used to provide some analytically-based landing gear weight estimates that can be used to help calibrate existing statistical weight equations. Although statistical weight equations are capable of producing quick and fairly accurate group weights within the range where significant previous experience is available, their reliability is questionable at best for aircraft with takeoff weight beyond one million pounds, *i.e.*, they are constrained by what has been designed in the past. The uncertainty is made evident by the two possible weight trends available: a decreasing trend as predicted by ACSYNT and an increasing trend as predicted by Douglas and Torenbeek. As shown in Figure 10.3, landing gear weight fractions corresponding to the baseline aircraft and its derivatives suggest that the weight equation used by ACSYNT is likely to produce a more accurate trend than the ones used by Douglas and Torenbeek. In addition, an increase in the number of main assembly struts from four to six did not result in a step increase in the weight fraction as expected. Again, this can be attributed to the decrease in the number of tires found on each strut, which effectively lowered the combined load on the structural members and therefore led to a

lighter structure. Note that additional aircraft within the UHCT class must be modeled to extend the database so that the weight trends as observed here may be confirmed.

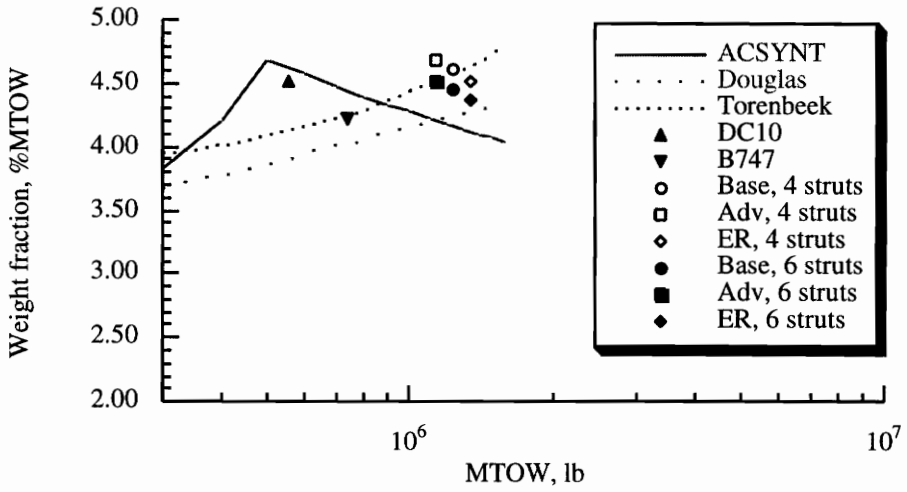

Figure 10.3 Landing gear weight fraction beyond one million pounds MTOW

Chapter 11 Costs

11.1. Introduction

The manufacturing cost of the landing gear cannot be treated simply as a function of weight or strut length. Instead, cost estimation must take into account the costs of development, certification, marketing, life-cycle, spares, *etc.* Typical program cost is roughly in the range of $10 to $12 millions based on industry survey [App. A]. However, such information is considered highly proprietary and thus is difficult to obtain from the manufacturers. Thus, the cost issue will only be discussed in qualitative terms, while actual unit cost will be provided whenever available.

11.2. Maintenance and Overhaul

The maintenance costs associated with the landing gear represent a considerable item in the total maintenance bill [3]. This is particularly hard to accept because the landing gear has virtually no contribution toward, and in some cases even has a degrading effect on, the profitability of the aircraft.

The cost of the tires, wheels and brakes will remain relatively unchanged. The limiting factor is the size of the tire that can be constructed and tested without a major new investment in manufacturing and testing facilities. Current hardware limits the maximum diameter to 56 inches for the bias-ply tire and 58 inches for the radial-ply tire [App. A]. Dimensions and costs of several tires found on existing large aircraft are listed in Table 11.1. For aluminum wheel and carbon-carbon heat sink found on the Boeing Model 747-400, the unit price is valued at $70,000.

Table 11.1 Description of selected aircraft tires [App. A]

Tire	Type	Aircraft	Application	Cost, $
H49x19.0-22, 32-ply	Bias	Boeing Model 747	Main/Nose	2,100
42x17.0-18, 28-ply	Radial	Boeing Model 777	Nose	2,100
50x20.0-22, 32-ply	Radial	Boeing Model 777	Main	2,900

The landing gear overhaul interval varies between 33,000 to 42,000 flight hours, or roughly within six years [App. A]. Generally, the parts of a landing gear are given an ultimate 'safe life' beyond which they would, if still in service, be scrapped [57]. A justification of this approach is that deterioration in service can go unseen since corrosion and other process can occur in concealed areas which are only revealed when the assembly is completely stripped down.

The preferred method is to overhaul the entire set at the same time to minimize the down-time; however, it might be necessary to overhaul the set separately due to schedule, parts and facility constraints. Components may require extensive rework in the shops and thus it is difficult to quote a total throughput time. Given a supply of serviceable components to replace those sent shop-to-shop, it is possible to turn around a B747 assembly within five weeks [57]. Due to the length of time required to rectify each constituent part of a particular assembly, a unit nearly always loses its identity as such, and the end product may contain only a few parts of the original assembly. However, it is noted that when refurbished, the assembly may be better than a new one since it embodies modifications designed to increase the subsequent overhaul life [57]. For the B747 type landing gear, the overhaul cost is estimated at $400,000 [App. A]. Replacement of the carbon heat sink occurs every 1,200 to 1,500 landings, while only 300 landings are allowed for the wheel before replacement. The overhaul cost for the wheel and heat sink is pre-negotiated with the contractors and is known as cost-per-landing. Quoting the B747 figures, the cost for the wheel, including tire, is estimated at $5 per landing, while the cost for the carbon-carbon heat sink is estimated at $10 per landing [App. A].

11.3. Cost Reduction

With the financial challenges arising from the deregulation of the air-travel industry, the airlines are faced with the challenge of reducing operating costs to remain competitive. As a result, the airlines have demanded that the aircraft manufacturers produce new designs with high reliability and low maintenance requirements. In basic design, costs associated with the landing gear may be reduced by aiming at simplicity, compactness, and minimum weight and maintenance requirements. Simplified design and improved manufacturing techniques, *e.g.*, die-forging and three-dimensional machining [8], are being used to reduce the part-count associated with the landing gear system. In addition, recent technologies, *e.g.*, carbon-carbon heat sinks, radial tires, and high-strength steel, are being introduced. Potential savings associated with the application of these technologies have already been mentioned in Chapter Four.

Chapter 12 Future Considerations

Refinement of the landing gear analysis package should include the improvement of the pavement thickness and landing gear weight predictions. A method to calculate the rigid pavement bearing stress that includes location and direction of maximum moment considerations [36] would improve the reliability of the estimated rigid pavement thickness and the corresponding ACN. The accuracy of the landing gear structural weight can be improved by extending the analysis to include intermediate column buckling analysis [48] for structural members with large slenderness ratio, *e.g.*, drag and side struts, and St. Venant's theory for torsion and flexure of thick-walled bars [50] for structural members with low machinability factor, *e.g.*, axle and truck beam.

Finally, the full potential of the analysis package would emerge if a graphical front-end and the Dynamic Integration System (DIS)-based wrapping technique [58] were incorporated. The former would enable the user to interactively prepare input for the analysis and interpret output, while the latter would provide a common interface such that coordinated execution of disciplinary analyses as found in ACSYNT can be achieved

Chapter 13 Conclusions

The design of the landing gear is one of the more fundamental aspects of aircraft design. The design and integration process encompasses numerous engineering disciplines, *e.g.*, structure, weights, runway design, and economics, and has become extremely sophisticated in the last few decades. These considerations were incorporated in an MDO procedure for use in the conceptual design of large transport aircraft. Accomplishments include:

- Aircraft *cg* estimation methods were studied and a new approach to *cg* estimation in conceptual design was demonstrated.
- An automated landing gear modeling algorithm for large transport aircraft was developed, and conformance with typical FAR requirements was assessed automatically.
- Airfield compatibility considerations associated with pavement thickness and runway and taxiway dimensions were automated.
- An analytical structural weight estimation procedure was developed to complement existing statistical landing gear weight estimation methods.
- Compilation of disciplinary analyses into a landing gear design and analysis package.
- Results obtained from the analysis package were presented, illustrating the trade-off studies and parametric results available for incorporation into a complete MDO design procedure.

References

1. Conway, H. G., *Landing Gear Design*, Chapman & Hall, London, 1958.
2. Currey, N. S., *Aircraft Landing Gear Design: Principles and Practices*, AIAA Education Series, Washington, 1988.
3. Torenbeek, E., *Synthesis of Subsonic Airplane Design*, Delft University Press, The Netherlands, 1982.
4. Fiornio, F., Comp., "Too Big For Your Britches," *Aviation Week and Space Technology*, Vol. 144, No. 21, May 20, 1996, p. 19.
5. Horonjeff, R. and McKelvey, F. X., *Planning and Design of Airports*, McGraw-Hill, New York, 1994.
6. Shifrin, C. A., "New Jumbos, SSTs Face Tough Hurdles," *Aviation Week and Space Technology*, Vol. 141, No. 21, November 21, 1994, pp. 42-43.
7. Niu, M. C. Y., *Airframe Structural Design*, Conmilit Press, Hong Kong, 1988, pp. 430-470.
8. Veaux, J., "New Design Procedures Applied to Landing Gear Development," *Journal of Aircraft*, Vol. 25, No. 10, October 1988, pp. 904-910.
9. Jayaram, S., Myklebust, A., and Gelhausen, P., "ACSYNT - A Standards-Based System for Parametric Computer Aided Conceptual Design of Aircraft," AIAA Paper 92-1268, February 1992.
10. McCullers, L. A., "Aircraft Configuration Optimization Including Optimized Flight Profiles", *Proceedings of Symposium on Recent Experiences in Multidisciplinary Analysis and Optimization,* 1984, pp. 395-412 (NASA CP-2327).
11. Chai, S., Crisafuli, P., and Mason, W. H., "Aircraft Center of Gravity Estimation in Conceptual Design," AIAA Paper 95-3882, September 1995.

12. Davis, E., "Center of Gravity Envelope Development, 747-400F, " SAWE Paper 2220, May 1994.
13. Lambert, M., Ed., *Jane's All the World's Aircraft*, Sentinel House, United Kingdom, 1994.
14. Green, W., Swanborough, G., and Mowinski, J., *Modern Commercial Aircraft*, Portland House, New York, 1978.
15. Anon., *Aircraft Type Certification Data Sheets and Specification, Vol. 3: Large Multiengine Aircraft*, Department of Transportation, Federal Aviation Administration, Washington, DC, 1985.
16. Greenbank, S. J., "Landing Gear: The Aircraft Requirement," Institution of Mechanical Engineers, Proceedings, Part G, *Journal of Aerospace Engineering*, Vol. 205, 1991, pp. 27-34.
17. Holloway, R. B., Burris, P. M. and Johannes, R. P., "Aircraft Performance Benefits from Modern Control Systems Technology," *Journal of Aircraft*, Vol. 7, No. 6, , November 1970, pp. 550-553.
18. Sliwa, S. M., "Economic Evaluation of Flying-Qualities Design Criteria for a Transport Configured With Relaxed Static Stability," NASA Technical Paper 1760, December 1980.
19. Anon., *FAR Part 25 Airworthiness Standards: Transport Category Airplanes*, Federal Aviation Administration, Washington, DC, October 1994.
20. Kandebo, S. W., and Dornheim, M. A., "Operability Verified In GE90 Flight Tests," *Aviation Week and Space Technology*, Vol. 142, No. 13, March 27, 1995, pp. 52-54.
21. Anon., *Airplane Characteristics for Airport Planning, 737-300, 737-400, 737-500*, Boeing Document D6-58325-2, Boeing Commercial Airplanes, Seattle, Washington, September 1988.
22. Mecham, M., "Airport Officials: Superjumbos Mean New Headaches," *Aviation Week and Space Technology*, Vol. 141, No. 21, November 21, 1994, pp. 76-80.
23. Anon., *Tire Data Sheets*, Goodyear, December, 1978.

24. Anon., *1994 Aircraft Yearbook*, The Tire and Rim Association, Inc., 1994.
25. Anon., "Aircraft Tires: Bias or Radials?" *Aerospace Engineering*, Vol. 11, No. 9, September 1991, pp. 13 -14.
26. Anon., "Technical Advances in Tyres, Wheels and Brakes: Dunlop Keeps Britain in the Forefront," *Aircraft Engineering*, November 1987, pp. 2-5.
27. Attri, N. S. and Amberg, R. L., "Advances in Landing Gear Systems," *Subsystem Testing and Flight Testing Instrumentation*, AGARD CP-299, October 1980
28. *Flight International*, December 30, 1971.
29. Anon., "Use of Carbon Heat Sink Brakes on Aircraft," Society of Automotive Engineers, AIR 1934, 1990.
30. Liming, R. A., "Analytic Definition of a Retractable Landing Gear Axis of Rotation," *Journal of the Aeronautical Sciences*, January 1947.
31. Anon., "Aerospace Landing Gear Systems Terminology," Society of Automotive Engineers, AIR 1489, April 1977.
32. Anon., *Aerodrome Design Manual, Part 3: Pavements*, International Civil Aviation Organization, Doc. 9157-AN/901, 1983.
33. Pereira, A. T., "Procedures for development of CBR Design Curves," Instruction Report S-77-1, US Army Corps of Engineers, Waterways Experiment Station, Vicksburg, MS, June 1977.
34. Ahlvin, R. G. "Developing a Set of CBR Design Curves," Instruction Report 4, US Army Corps of Engineers, Waterways Experiment Station, Vicksburg, MS, November 1959.
35. Westergaard, H. M., "New formulas for Stresses in Concrete Pavements of Airfields," *Transactions of American Society of Civil Engineers*, Vol. 73, May 1947.
36. Packard, R. G., *Design of Concrete Airport Pavement*, Portland Cement Association, 1973, pp. 49-59.
37. Anon., *Special Design Chart for Concrete Airport Pavement: Boeing 727*, Portland Cement Association, 1994.

38. Anon., *Airplane Characteristics for Airport Planning, 747-400*, Boeing Document D6-58326-1, Boeing Commercial Airplanes, Seattle, Washington, March 1990.
39. Anon., "Standardized Method of Reporting Airport Pavement Strength," Advisory Circular AC 150/5335-5, Department of Transportation, Federal Aviation Administration, Washington, DC, June 1983.
40. Roskam, J., *Airplane Design Part V: Component Weight Estimation*, Roskam Aviation and Engineering, Ottawa, Kansas, 1986, pp. 80-82.
41. Liebeck, R. H., Page, M. A., Rawdon, B. K., Scott, P. W., and Wright, R. A., "Concepts for Advanced Subsonic Transports," NASA CR-4624, September 1994.
42. Raymer, D. P., *Aircraft Design: A Conceptual Approach*, AIAA Education Series, Washington, 1989, pp. 391-405.
43. Kraus, P. R., "An Analytical Approach to Landing Gear Weight Estimation," SAWE Paper 829, May 1970.
44. Wille, R. H., "Analytical Weight Estimation of Unconventional Landing Gear Design," SAWE Paper 1905, May 1989.
45. Etkin, B., *Dynamics of Atmospheric Flight*, John Wiley & Sons, New York, 1972, pp. 114-117.
46. Beer, F. P. and Johnston, Jr., E. R., *Mechanics of Materials*, 2nd ed., McGraw-Hill, New York, 1992, pp. 610-616.
47. Megson, T. H. G., *Aircraft Structures*, 2nd. ed., Halsted Press, New York, 1990, pp. 225-293.
48. Chen, W. F., and Lui, E. M., *Structural Stability: Theory and Implementation*, Elsevier, New York, 1987, pp. 45-145.
49. Saelman, B., "Designing Cylinders and Struts for Maximum Strength," *Machine Design*, Vol., 25, No. 8, August 1953, pp. 133-138.
50. Timoshenko, S. P., and Goodier, J. N., *Theory of Elasticity*, McGraw-Hill, 1970, pp. 291-378.

51. Proctor, P., "Boeing Homes In on Future 747 Design," *Aviation Week and Space Technology*, Vol. 144, No. 6, February 5, 1996, pp. 32-33.
52. Sparaco, P., "No Money As Yet In Airbus Jumbo Plan," *Aviation Week and Space Technology*, Vol. 144, No. 25, June 17, 1996, pp. 27-28.
53. Arcara, Jr., P. C., Bartlett, D. W., McGraw, Jr., M. E., and Geiselhart, K. A., "Technology Benefits for Very Large Subsonic Transports," AIAA Paper 93-1178, February 1993.
54. Proctor, P., "Boeing Refines Designs for 600-seat NLA," *Aviation Week and Space Technology*, Vol. 141, No. 21, November 21, 1994, pp. 48-49.
55. Sparaco, P., "Airbus Weighs Four A3XX Versions," *Aviation Week and Space Technology*, Vol. 141, No. 21, November 21, 1994, p. 54.
56. Smith, B. A., "Douglas Awaits Chance to Revive Jumbo Plans," *Aviation Week and Space Technology*, Vol. 141, No. 21, November 21, 1994, p. 57.
57. Anon., "Landing Gear," *Aircraft Engineering*, July 1989, pp. 3-6.
58. Woyak, S. A., Malone, B., and Myklebust, A., "An Architecture for Creating Engineering Application: The Dynamic Integration System," *Proceedings of the Computers in Engineering Conference and the Engineering Database Symposium, ASME*, September 17-20, 1995, Boston, MA, pp. 1-8.

Appendix A Industry Survey

A.1. Introduction

The landing gear integration issue for advanced aircraft is being investigated under a NASA Ames research grant to Virginia Tech. The project objective is the formulation of a methodology to include landing gear consideration explicitly in the conceptual design stage. In particular, the project addresses the special design considerations associated with the next-generation high-capacity transport with a MTOW exceeding one million pounds. Landing gear design and integration related issues were defined during the initial background research with heavy reliance on N. S. Currey's *Aircraft Landing Gear Design: Principles and Practices*. Questions concerning landing gear configuration, aircraft-landing gear integration, runway compatibility, advanced technologies, weight, maintenance, and cost were compiled into a nominal questionnaire. The survey was conducted through telephone interviews, where participants from major airframers, landing gear manufacturers, government agencies, technical societies, and airlines were asked to respond to the questionnaire. The questions initiated discussions that were often broader and less focused than the questions themselves. Thus, the discussion of results presented in the following sections follows the broader areas, and does not explicitly summarize the answers to the questions.

A.2. Contacts

A list of survey participants and their telephone numbers are presented in Table A.1 for references.

Table A.1 Industry/government contact list

	Telephone
Federal Aviation Administration	
Bill Perrella	(206) 227-2116
John Rice	(202) 267-8745
Niel Schalekanp	(206) 227-2112
SAE A-5 Committee	
Richard Vandame	(412) 776-4841
The Tire & Rim Association, Inc.	
Joe Pacuit	(216) 666-8121
Boeing Commercial Airplane Group	
Edward Gervais	(206) 237-0175
Jerry Kileer	(206) 965-9775
Bob Nielson	(206) 342-1522
Dave Nielson	(206) 342-7577
John Potter	(206) 237-7745
McDonnell Douglas	
Al Kernik	(310) 593-7313
Brian Lindley	(310) 496-9129
Cleveland Pneumatic	
Gene Stuczynski	(216) 429-4213
Menasco Aerosystem	
Bill Luce	(817) 685-3538
B.F. Goodrich	
Tom Kendal	(513) 440-2205
Dave Moser	(513) 440-2206
Dean Peters	(513) 440-2209
Paul Snyder	(513) 440-2380
Michelin	
Marion DeWitt	(704) 548-2483
Ron Olds	(704) 548-2438
Northwest	
Jim Baumiller	(612) 726-3885
Steve Lydon	(612) 726-7217
United	
James Gallivan	(510) 382-8312
Ed Pozzi	(415) 634-6994
USAir	
Norman White	(412) 747-3425

A.3. Survey Questions

- What kind of information is available to the landing gear designer at the conceptual design phase of an aircraft? What are the design objectives?
- What are some current technologies that will alter the design of the landing gear? What are some advantages/disadvantages associated with these changes? What kind of weight reduction can be expected?
- What method is used to calculate the landing gear dynamic and static loads? Which specification is used?
- What method is used to determine the aircraft flotation requirements? What kind of constraint is imposed on the configuration of the landing gear?
- What will be the most likely landing gear configuration for the UHCT aircraft? The number and arrangement of the tires and struts? What are the major integration issues related to the UHCT aircraft? What kind of special design considerations are taken?
- For a MTOW outside the experience base are there some "first principles" that can be followed for landing gear weight estimation? What method is used to produce the initial landing gear weight estimation? Scaling factors?
- What method is used for initial landing gear cost estimate? What are the major cost drivers, and their effects?
- Is geometry, weight, and cost information available for uses in analysis calibration?

A.4. Preliminary Findings

Due to economic considerations, the UHCT must be able to operate out of Class V airports, *e.g.*, the Boeing Model 747 class airports, without requiring extensive runway reinforcement and modification. Flotation requirements can be obtained using the PCA methods for rigid pavement and the CBR method for flexible pavements. Effects of multiple-strut/multiple-wheel landing gear configurations on the pavement bearing strength have yet to be addressed fully by industry. However, preliminary finite element analyses suggest interaction among wheels can be neglected outside a radius of ten

footprint radii from the point where flotation analysis is performed. With current tire inflating pressure, a 20-wheel main assembly is required for a MTOW between 1 and 1.2 million pounds, while a 24-wheel main assembly is required for a MTOW between 1.3 and 1.6 million pounds to produce the desired flotation characteristics. Both numbers include a 20 percent future growth factor.

Aircraft-landing gear integration will be the primary concern for the next-generation high-capacity transports. The location dependency of the wing and the main gear assembly to the aircraft *cg* will play a major role in the integration issue. With the introduction of multiple-strut configurations, the envelope within which the landing gear has to be located to produce the ideal loading and stability characteristics may no longer be large enough to accommodate the increased number of main assembly struts. This phenomenon is known as *location stagnation* by the landing gear community. Modification in design and flotation requirements must be made, if necessary, to accommodate kinematic and stowage constrains such that the landing gear can be deployed and stowed without interference with surrounding structures. A forward-retracting scheme for the fuselage struts is preferred, which allows the gears to be deployed using the slip-stream in case of a hydraulic failure; however, stowage limitation could result in an aft-retracting scheme for the center-line strut located between the wing-mounted struts in a five-plus struts configuration.

The number of wheels imposed by the flotation requirement can be accommodated with either a four-, five- or six-strut configuration. One of the centerline strut will be located abreast of the wing-mounted struts for the five-plus main gear struts configurations. With the introduction of the centerline strut(s), a double-keel layout is required, *i.e.*, the stowage space is divided into three compartments with two identical keels placed parallel to each other. The centerline strut(s) will then be mounted and stowed between the keels. The fuselage width of the new aircraft, which will be 20 to 30 inches wider than that of the B747, should be able to accommodate the double-keel layout with relative ease. However, one of the drawbacks is that the structural weight associated

with the keels will be doubled, since both keels have to withstand the same buckling load and thus have to be similar in dimension to the one found in the single-keel layout. Another drawback is that a complex deploying/retracting scheme for the landing gear doors must be developed to prevent interference between the doors and the gear itself.

The length of the strut will be dictated by aircraft ground clearance requirements during cross-wind landing condition imposed by the large nacelle diameter of the advanced engines. , Provided that desirable flow characteristic is maintained, spacing between the nacelle and the wing, *i.e.*, the gully, will be reduced to a minimum before any extension in strut length is made. A main gear steering system will be needed to meet the ground operation requirements, with the most demanding maneuver being the 180-degree turn on existing runways. Options include the fuselage strut steering system as found on the B747 and the forward-aft wheel steering system as found on the B777. The wheel truck dimension of the dual-twin-tandem and triple-dual-tandem configurations will be similar to that of the B747 and B777, respectively. The longitudinal spacing between tires will be maintained at roughly six inches for ease of removal of the wheel plugs, while lateral spacing will be slightly wider in both configurations due to the increased brake size required for the new aircraft. Due to the limited stowage volume, the truck assembly might have to be rotated prior to retraction to minimize the required space.

The dynamic and ground loads are determined in accordance with FAR Part 25. It's unlikely that the new aircraft will be subjected to rough field operating requirements; therefore, a single-acting shock absorber will be sufficient to handle the kinetic energy experienced during landing and taxiing. Based on preliminary analysis, the new aircraft will require a shock strut with a 24-inch stroke at the minimum, a piston diameter of 15 inches, and internal oleo pressure between 1,500 and 1,800 psi.

The design of the new landing gear must be as simple as possible, since complexity drives up the cost faster than weight. Advanced technologies will play a major role in reducing the weight of the landing gears. A 14 to 35 percent weight reduction in heat sink weight can be obtained with the use of carbon instead of steel. Radial-ply tire, although

comes with a higher initial cost, offers a 20 percent weight reduction over the bias-ply tire, while at the same time allows more landing per life-cycle. Further weight reduction can be achieved by the use of a steer-by-wire concept in place of the conventional cable-and-pulley system. Electrical actuation units will be introduced as a mean to reduce weight in secondary mechanisms, but the primary actuation method will remain hydraulic. Improvements will probably be internal, *e.g.*, bearings, finishes, and rebound damping, but little difference will be seen in the configuration.

Structure weight estimation should be obtained using an analytical approach, while weight scaling taken to a 1.1 power will give a reasonable estimation for sub-components, *i.e.*, fittings and miscellaneous items. Landing gear gross weight variation of five pounds per 1,000 pounds increase in MTOW for the nose gear was suggested compare to a 40-pound variation per 1,000 pounds increase in MTOW for the main gear. Weight variation of 40 pounds per inch increase in strut length per strut was also suggested. The wheel and tire weights will be similar to that of the B747, *i.e.*, 190 pounds and 290 pounds, respectively, while the heat sink weight will be heavier, again due to the increased braking energy requirements. A step increase in the landing gear group weight will occur with each additional strut; therefore, the number of struts should be kept at a minimal. Existing data indicate that fuselage strut weight is roughly 25 to 40 percent less than that of the wing strut. Overall, total gear weight will remain at roughly five percent of the maximum take-off weight.

The manufacturing cost of the landing gear cannot be treated simply as a function of weight or strut length. Instead, cost estimation must take into account the costs of development, material and processes, certification, marketing, overhaul, refurbishment, and spares. Typical program cost is roughly in the range of $10 to $12 millions. The cost of the tire, wheel and brake will remain relatively unchanged. The limiting factor is the size of the tire that can be constructed and tested without a major new investment in the manufacturing and testing facilities. Current hardware limits the maximum diameter to 56 inches for the bias-ply tire and 58 inches for the radial-ply tire. The H49x19.0-22, a 32-

bias-ply tire found on both the nose and main gear of the B747, is valued at $2,100. Compare to the radial, the 50x20.0-22, which is found on the main gear of the B777 with a 32-ply rating, is valued at $2,900, whereas the 42x17.0-18, which is found on the nose gear of the B777 with a 28-ply rating, is valued at $2,100. Due to its light weight and the increased number of landings allowed per life-cycle, the radial tire has become the preferred choice by airlines even though it comes with a higher price tag. As for the aluminum wheel and carbon-carbon heat sink found on the B747, the unit price is valued at $70,000.

Landing gear overhaul interval varies between 33,000 to 42,000 flight hours. The preferred method is to overhaul the entire set at the same time to minimize the down-time; however, it might be necessary to overhaul the set separately due to schedule, parts and facility constrains. For the B747 type landing gear, the overhaul cost is estimated at $400,000. Replacement of the carbon heat sink occurs every 1,200 to 1,500 landings, while only 300 landings are allowed for the wheel before replacement. The overhaul cost for wheel and brake is pre-negotiated with the contractors and is known as cost-per-landing. Quoting the B747 figures, the cost for the carbon-carbon brake is estimated at $10 per landing, while the cost for the wheel, including tire, is estimated at $5 per landing.

Due to heavy competitions among the airframe and landing gear manufacturers, landing gear design procedure, weight and cost data are considered to be company-proprietary. As a result, the majority of the survey participants were only willing to address the issues in general terms. However, the survey results did provide some useful insights to the design of the landing gear, and reaffirmed design and analysis procedures as previously documented.

Appendix B Structural Analysis Derivations

B.1. Introduction

Detailed derivations of selected structure analyses as introduced in Chapter Eight are compiled and presented in the following sections. The sections outline the procedures used to determine the internal actions for the nose assembly and the trunnion, both of which involve statically-indeterminate structures, as well as stress calculation for thin-walled circular tubes. These items involve derivations of the basic equations that cannot be presented in a concise manner within the main text.

B.2. The Nose Assembly

The reactions at the supports of the truss that represents the nose gear cylinder/drag/side struts structure, and consequently the internal actions, can be determined by Castigliano's theorem [46, p. 611], that is,

$$u_j = \frac{\partial U}{\partial P_j} = \sum_{i=1}^{n} \frac{F_i l_i}{A_i E} \frac{\partial F_i}{\partial P_j} \tag{B.1}$$

where u_j is the deflection at the point of application of the load P_j, E is the modulus of elasticity, and l, F, and A are the length, internal force, and cross-sectional area of each member, respectively. The above theorem gives the generalized displacement corresponding to the redundant, P_j, which is set equal to a value compatible with the support condition. This permits the solution of the redundant, and consequently all remaining internal actions, via equilibrium.

As shown in Figure B.1, the port side strut is designated as redundant and released from its support at point K. Using Eq. (B.1) the deflection at point K can be written as

$$y_K = \frac{F_{IO} l_{IO}}{A_{IO} E} \frac{\partial F_{IO}}{\partial R_K} + \frac{F_{JO} l_{JO}}{A_{JO} E} \frac{\partial F_{JO}}{\partial R_K} + \frac{F_{KO} l_{KO}}{A_{KO} E} \frac{\partial F_{KO}}{\partial R_K} \tag{B.2}$$

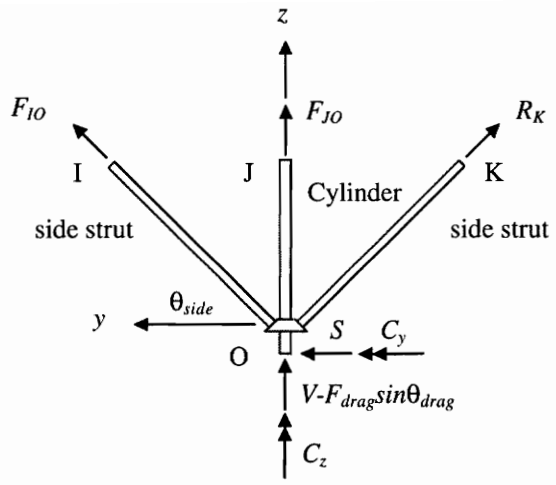

Figure B.1 Free-body diagram of the nose gear structure in the *yz*-plane

From equilibrium,

$$F_{IO} = R_K + \frac{S}{cos\theta_{side}} \tag{B.3a}$$

$$F_{JO} = V - F_{drag}\, sin\theta_{drag} - (F_{IO} + R_K)sin\theta_{side} \tag{B.3b}$$

$$F_{KO} = R_K \tag{B.3c}$$

where S and V are the applied side and vertical force, respectively, and θ_{drag} and θ_{side} are the angles between the axial centerlines of the drag and side struts and the *xy*-plane, respectively. Differentiating Eqs (B.3a, b, and c) with respect to R_K results in

$$\frac{\partial F_{IO}}{\partial R_K} = 1 \tag{B.4a}$$

$$\frac{\partial F_{JO}}{\partial R_K} = -sin\theta_{side} \tag{B.4b}$$

$$\frac{\partial F_{KO}}{\partial R_K} = 1 \tag{B.4c}$$

To determine the reaction at point K and subsequently the internal force in each structural component, substitute the relationships of Eqs (B.3a, b, and c) and (B.4a, b, and c) back into Eq. (B.2), apply the no-deflection condition and then solve for R_K.

B.3. The Trunnion

The trunnion model shown in Figure 8.9 is repeated here as Figure B.2. As shown in Figure B.2, the trunnion is subjected to a force with components F_x, F_y, and F_z, and a couple with moment components C_y and C_z, at axial position $x = l_1$, where $0 < l_1 < L$ and $0 \leq x \leq L$. Clamped end-conditions at $x = 0$ and $x = L$ yield ten homogeneous conditions, five at each end. At the load point $x = l_1$, there are five continuity conditions, *i.e.*, u, v, w, v', and w', and five jump conditions corresponding point-wise equilibrium of the internal actions and the external loads. These twenty conditions are

$$u_1(0) = u_2(L) = 0 \tag{B.5a}$$

$$v_1(0) = v_1'(0) = v_2(L) = v_2'(L) = 0 \tag{B.5b}$$

$$w_1(0) = w_1'(0) = w_2(L) = w_2'(L) = 0 \tag{B.5c}$$

$$u_1(l_1) = u_2(l_1) \tag{B.6a}$$

$$v_1(l_1) = v_2(l_1) \tag{B.6b}$$

$$w_1(l_1) = w_2(l_1) \tag{B.6c}$$

$$\frac{dv_1(l_1)}{dx} = \frac{dv_2(l_1)}{dx} \tag{B.6d}$$

$$\frac{dw_1(l_1)}{dx} = \frac{dw_2(l_1)}{dx} \tag{B.6e}$$

$$-N_{x1}(l_1) + N_{x2}(l_1) + F_x = 0 \tag{B.7a}$$

$$-V_{y1}(l_1) + V_{y2}(l_1) + F_y = 0 \tag{B.7b}$$

$$-V_{z1}(l_1) + V_{z2}(l_1) + F_z = 0 \tag{B.7c}$$

$$-M_{z1}(l_1) + M_{z2}(l_1) + C_z = 0 \tag{B.7d}$$

$$-M_{y1}(l_1) + M_{y2}(l_1) + C_y = 0 \tag{B.7e}$$

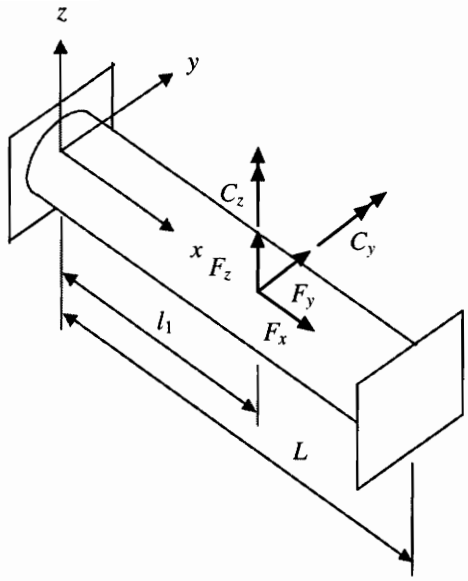

Figure B.2 Trunnion modeled as a clamped-clamped end bar

In the *xz*-plane, equilibrium gives

$$\frac{dM_y}{dx} - V_z = 0 \tag{B.8}$$

and

$$\frac{dV_z}{dx} = 0 \tag{B.9}$$

where M_y and V_z are the internal moment and shear components, respectively. Given the equation of elastic curve as

$$M_y = EI_{yy}\left(-\frac{d^2w}{dx^2}\right) \tag{B.10}$$

where E is the modulus of elasticity and I_{yy} is the second area moment about the *y*-axis, Eqs (B.8) and (B.9) become

$$V_z = EI_{yy}\left(-\frac{d^3w}{dx^3}\right) \tag{B.11}$$

and

$$EI_{yy}\left(-\frac{d^4w}{dx^4}\right)=0 \tag{B.12}$$

Integrating Eq. (B.12) four times with respect to x results in

$$w_1=\frac{c_1}{6}x^3+\frac{c_2}{2}x^2+c_3x+c_4 \qquad 0\le x\le l_1 \tag{B.13a}$$

$$w_2=\frac{c_5}{6}x^3+\frac{c_6}{2}x^2+c_7x+c_8 \qquad l_1\le x\le L \tag{B.13b}$$

To determine w_1 and w_2 at either end of the trunnion, boundary conditions as given in Eqs (B.5b and c) and (B.6b, c, d, and e) were used to solve for the eight integration constants (c_i) in Eqs (B.13a and b). Finally, substitute w_1 and w_2 back into Eqs (B.10) and (B.11) and use the static boundary conditions as given in Eqs (B.7a, b, c, and d) to obtain the internal shear force and bending moment, respectively. The same procedure is used to determine $v(x)$ and the internal actions in the xy-plane.

In the longitudinal direction, equilibrium gives

$$\frac{dN}{dx}=0 \tag{B.14}$$

where N is the axial force. In addition, the material law gives

$$N=EA\frac{du}{dx} \tag{B.15}$$

where A is the cross-sectional area. Since the axial force is spatially uniform, or piecewise constant, integrating Eq. (B.15) once with respect to x results in

$$u_1=\frac{N_1}{EA}x+c_9 \qquad 0\le x\le l_1 \tag{B.16a}$$

$$u_2=\frac{N_2}{EA}x+c_{10} \qquad l_1\le x\le L \tag{B.16b}$$

where the two integration constants c_9 and c_{10} are determined using the boundary conditions as given in Eq. (B.6a). Finally, substitute u_1 and u_2 back into Eq. (B.15) and sum the forces in the x direction at $x = l_1$ to obtain the internal axial force.

B.4. Normal and Shear Stresses In a Thin-walled Tube

The normal stresses induced on the structural members are determined by combining the effects of axial load and combined bending, while the shear stresses are determined by combining the effects of torsion and shear forces due to bending [47].

The normal stress (τ_{xx},) due to combined axial force and bending moments is given as

$$\tau_{xx} = \frac{N}{A} + \frac{M_y}{I_{yy}} z - \frac{M_z}{I_{zz}} y \tag{B.17}$$

For a thin-walled circular tube referred to polar coordinates as shown in Figure B.3, the principal centroidal second area moments about the y- and z-axes are

$$I_{yy} = I_{zz} = \oint (r \sin\theta)^2 t r d\theta = \pi r^3 t \tag{B.18}$$

where r is the mean radius and t is the wall thickness. Given the relationship of Eq. (B.18), Eq. (B.17) becomes

$$\tau_{xx} = \frac{N}{A} + \frac{1}{\pi r^2 t}\left(M_y \sin\theta - M_z \cos\theta\right) \tag{B.19}$$

Differentiate Eq. (B.19) with respect to θ to get

$$\frac{d\tau_{xx}}{d\theta} = \frac{1}{\pi r^2 t}\left(M_y \cos\theta + M_z \sin\theta\right) \tag{B.20}$$

and at the extremum, *i.e.*, $d\tau_{xx}/d\theta = 0$, so that

$$\tan\theta_{max} = -\frac{M_y}{M_z} \tag{B.21a}$$

$$\sin\theta_{max} = \frac{M_z}{\sqrt{M_y^2 + M_z^2}} \tag{B.21b}$$

$$\cos\theta_{max} = -\frac{M_y}{\sqrt{M_y^2 + M_z^2}} \tag{B.21c}$$

Given the relationships of Eqs (B.21b and c), the extremum values of the bending normal stresses are determined using the expressions

$$\tau_{xx,bending}(\theta_{max}) = -\frac{1}{\pi r^2 t}\sqrt{M_y^2 + M_z^2} \tag{B.22a}$$

and

$$\tau_{xx,bending}(\theta_{max} + \pi) = \frac{1}{\pi r^2 t}\sqrt{M_y^2 + M_z^2} \tag{B.22b}$$

Thus, the extremum values of the normal stress on a circular-tube cross section under combined axial and bending actions are

$$\tau_{xx_{\substack{max \\ or \\ min}}} = \frac{N}{A} \pm \frac{1}{\pi r^2 t}\sqrt{M_y^2 + M_z^2} \tag{B.23}$$

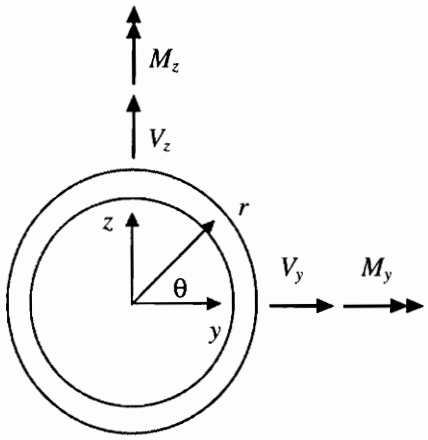

Figure B.3 Annular section showing positive shear forces and bending moments

The shear stress (τ_{xs},) due to combined transverse shear force and torque is given as

$$\tau_{xs} = \frac{q(s)}{t} + (\tau_{xs})_{torque} \tag{B.24}$$

where q is the shear flow due to bending. As indicated by in Figure B.4, the shear flow from some arbitrary origin to any point round the cross-section of a circular tube for axial equilibrium is

$$q = q_0 - \frac{dF}{dx} \tag{B.25}$$

where

$$\frac{dF}{dx} = \frac{d}{dx}\int_0^s \tau_{xx} t ds = \int_0^\theta \frac{d\tau_{xx}}{dx} t r d\theta \tag{B.26}$$

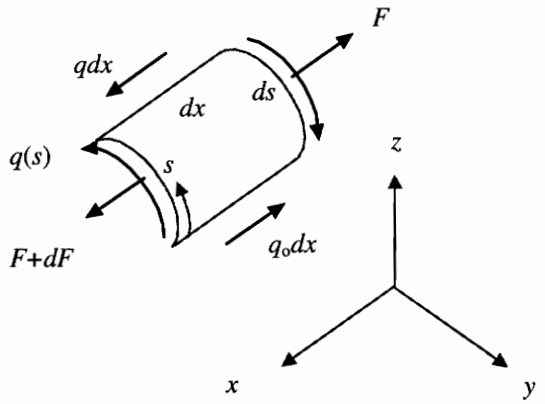

Figure B.4 Shear flow around a closed tube

Given that

$$\frac{dN}{dx} = 0 \tag{B.27}$$

$$\frac{dM_y}{dx} = V_z \tag{B.28}$$

and

$$\frac{dMz}{dx} = -V_y \tag{B.29}$$

rearrangement of Eq. (B.26) results in

$$\frac{dF}{dx} = r^2 t\left[\frac{V_z}{I_{yy}}(1-\cos\theta)+\frac{V_y}{I_{zz}}\sin\theta\right] \tag{B.30}$$

From the relationships of Eqs (B.25) and (B.30), the integral of q round the cross section is

$$\oint qrds = \oint q_0 rds - \oint \frac{dF}{dx} rds \tag{B.31}$$

Since only bending is considered in this case, the left-hand side of Eq. (B.31) is zero, that is,

$$q_0 \oint d\theta = \oint \frac{dF}{dx} d\theta \tag{B.32}$$

and the integration results in

$$q_0 = r^2 t \frac{V_z}{I_{yy}} \tag{B.33}$$

Given the relationships of Eqs (B.18), (B.30) and (B.33), the magnitude of the shear flow is determined using the expression

$$q = \frac{1}{\pi r}\left(V_z \cos\theta - V_y \sin\theta\right) \tag{B.34}$$

Differentiating Eq. (B.34) with respect to θ gives

$$\frac{dq}{d\theta} = -\frac{1}{\pi r}\left(V_y \cos\theta + V_z \sin\theta\right) \tag{B.35}$$

and at the extremum, *i.e.*, $dq/d\theta = 0$, so that

$$\tan\theta_{max} = -\frac{V_y}{V_z} \tag{B.36a}$$

$$\sin\theta_{max} = \frac{V_z}{\sqrt{V_y^2 + V_z^2}} \tag{B.36b}$$

$$\cos\theta_{max} = -\frac{V_y}{\sqrt{V_y^2 + V_z^2}} \tag{B.36c}$$

Given the relationships of Eqs (B.36b and c), the minimum and maximum values of the shear flow are determined using the expressions

$$q\left(\theta_{max}\right) = -\frac{1}{\pi r t}\sqrt{V_y^2 + V_z^2} \tag{B.37a}$$

and

$$q(\theta_{max}+\pi)=\frac{1}{\pi rt}\sqrt{V_y^2+V_z^2} \tag{B.37b}$$

The shear stress due to torque is given as

$$(\tau_{xs})_{torque}=\frac{Tr}{J} \tag{B.38}$$

where J is the polar area moment

$$J=\int r^3 td\theta = 2\pi r^3 t \tag{B.39}$$

So, for the thin-wall approximation the maximum stresses will occur on the contour of the circular tube, consistent with bending analysis. Thus, given the relationships of Eqs (B.37a and b) and (B.39), Eq. (B.24) becomes

$$\tau_{xs}=\frac{1}{\pi rt}\left(\frac{T}{2r}\pm\sqrt{V_y^2+V_z^2}\right) \tag{B.40}$$

Appendix C Bibliography

C.1. Textbooks

- Beer, F. P. and Johnston, Jr., E. R., *Mechanics of Materials*, 2nd ed., McGraw-Hill, New York, 1992.
- Chen, W. F., and Lui, E. M., *Structural Stability: Theory and Implementation*, Elsevier, New York, 1987.
- Conway, H. G., *Landing Gear Design,* Chapman and Hall, London, 1958.
- Currey, N. S., *Aircraft Landing Gear Design: Principles and Practices*, AIAA Education Series, Washington, 1988.
- Horonjeff, R. and McKelvey, F. X., *Planning and design of Airport*, McGraw-Hill, New York, 1994.
- Kirshbaum, N., *Aircraft Design Handbook: Aircraft Design Aid and Layout Guide,* VPI Aircraft Design Series, Virginia, 1993.
- Megson, T. H. G., *Aircraft Structures*, 2nd. ed., Halsted Press, New York, 1990, pp. 225-293.
- Niu, M. C. Y., *Airframe Structural Design*, Conmilit Press, Hong Kong, 1988.
- Raymer, D. P., *Aircraft Design: A Conceptual Approach*, AIAA Education Series, Washington, 1989.
- Roskan, J., *Airplane Design Part IV: Layout Design of Landing Gear and System,* Roskan Aviation and Engineering, Ottawa, Kansas, 1986.
- Roskan, J., *Airplane Design Part V: Component Weight Estimation*, Roskan Aviation and Engineering, Ottawa, Kansas, 1986.
- Torenbeek, E., *Synthesis of Subsonic Airplane Design*, Delft University Press, Delft, 1981.

C.2. Government/Industry Standards

- Anon., *FAR Part 25 Airworthiness Standards: Transport Category Airplanes*, Federal Aviation Administration, Washington, DC, October 1994.
- Anon., "Standardized Method of Reporting Airport Pavement Strength," AC 150/5335-5, Federal Aviation Administration, Washington, DC, June 1983.
- Anon., *Aerodrome Design Manual, Part 3: Pavements*, International Civil Aviation Organization, Doc. 9157-AN/901, 1983.
- Anon., *Wheels and Brakes, Supplementary Criteria for Design Endurance, Civil Transport Aircraft*, Society of Automotive Engineers, ARP 597, 1991.
- Anon., *Aircraft Landing Gear*, Society of Automotive Engineers, ARP 1311, January 1995.
- Anon., *Verification of Landing Gear Design Strength*, Society of Automotive Engineers, ARP 1494, February 1978.
- Anon., *Landing Gear System Development Plan*, Society of Automotive Engineers, ARP 1598, August 1985.
- Anon., *Aircraft Flotation Analysis Methods*, Society of Automotive Engineers, ARP 1821, May 1988.
- Anon., *Use of Carbon Heat Sink Brakes on Aircraft*, Society of Automotive Engineers, ARP 1934, April 1990.
- Anon., *Landing Area/Landing Gear Compatibility*, Society of Automotive Engineers, ARP 4243, April 1993.
- Anon., *1994 Aircraft Year Book*, The Tire and Rim Association, Inc., 1994.
- Anon., *Special Design Charts for Concrete Airport Pavement*, Portland Cement Association, 1993.
- Packard, R. G., *Design of Concrete Airport Pavement,* Portland Cement Association, 1973.

C.3. Technical Papers/Reports

- Anon., *Subsystem Testing and Flight Testing Instrumentation*, AGARD CP 299, October 1980.
- Anon., *Landing Gear Design Loads*, AGARD CP 484, October 1990.
- Anon., "Landing Gear," *Aircraft Engineering*, Vol. 58, No. 7, July 1986, pp. 3-6.
- Arcara, Jr., P. C., Bartlett, D. W., McGraw, Jr., M. E., and Geiselhart, K. A., "Technology Benefits for Very Large Subsonic Transports," AIAA Paper 93-1178, February 1993.
- Ahlvin, R. G. "Developing a Set of CBR Design Curves," Instruction Report 4, US Army Corps of Engineers, Waterways Experiment Station, Vicksburg, MS, November 1959.
- Baker, W. R. and Gonzalez, C. R., "Design Considerations for Multi-Wheel Aircraft", 22nd ASCE International Air Transportation Conference, Proceedings, June 1992.
- Cameron-Johnson, A., "The Undercarriage in Aeroplane Project Design," *Aircraft Engineering*, Vol. XLI, No. 2, February, 1969, pp. 6-11.
- Chai, S., Crisafuli, P., and Mason, W. H., "Aircraft Center of Gravity Estimation in Conceptual Design," AIAA Paper 95-3882, September 1995.
- Collins, R. L. and Black, R. J., "Tire Parameters for Landing Gear Shimmy Studies," AIAA Paper 68-311, April 1968.
- Davis, E., "Center of Gravity Envelope Development, 747-400F," SAWE Paper 2200, May 1994.
- Dawson, J. L. and Mills, R. L., "Undercarriage Effects on (a) Rigid Pavements (b) Flexible Pavements," *Aircraft Pavement Design*, Institution of Civil Engineers, Proceedings, November 1970.
- Firebaugh, J. M., "Estimation of Taxi Load Exceedances Using Power Spectral Methods," *Journal of Aircraft*, Vol. 5 No. 5, September 1968, pp. 507-509.

- Griffis, Jr., M. F. H. and Gamon, M. A., "Aircraft-Pavement Compatibility Study," Report FAA-RD-73-206, Waterways Experiment Station, US Army Corps of Engineers, Vicksburg, MS, September 1974.
- Greenbank, S. J., "Landing Gear: The Aircraft Requirement," Institution of Mechanical Engineers, Proceedings, Part G, *Journal of Aerospace Engineering*, Vol. 205, 1991, pp. 27-34.
- Holloway, R. B., Burris, P. M. and Johannes, R. P., "Aircraft Performance Benefits from Modern Control Systems Technology," *Journal of Aircraft*, Vol. 7, No. 6, November 1970, pp. 550-553.
- Jayaram, S., Myklebust, A., and Gelhausen, P., "ACSYNT - A Standards-Based System for Parametric Computer Aided Conceptual Design of Aircraft," AIAA Paper 92-1268, February 1992.
- Jenkins, S. F. N., "Landing Gear Design and Development," Institution of Mechanical Engineers, Proceedings, Part G, *Journal of Aerospace Engineering*, Vol. 203, 1989, pp. 67-73.
- Kraus, P. R., "An Analytical Approach to Landing Gear Weight Estimation," SAWE Paper No. 829, May 1970.
- Liebeck, R. H., Page, M. A., Rawdon, B. K., Scott, P. W., and Wright, R. A., "Concepts for Advanced Subsonic Transports," NASA CR-4624, September 1994.
- Liming, R. A., "Analytic Definition of a Retractable Landing Gear Axis of Rotation," *Journal of the Aeronautical Sciences*, January 1947, pp. 19-23.
- McBrearty, J. F., "A Critical Study of Aircraft Landing Gears," *Journal of the Aeronautical Sciences*, 16th IAS Annual Meeting, Proceedings, May 1948, pp. 263-280.
- McCullers, L. A., "Aircraft Configuration Optimization Including Optimized Flight Profiles", *Proceedings of Symposium on Recent Experiences in Multidisciplinary Analysis and Optimization,* 1984, pp. 395-412 (NASA CP-2327).

- Marsh, D. P., "Theory of Transport Aircraft Weight Fractions," SAWE Paper 1452, 1982.
- O'Massey, R. C., "Introduction to Landing Gear Design," ASM Paper W70-18.1, March 1970.
- Pereira, A. T., "Procedures for development of CBR Design Curves," Information Report S-77-1, Waterways Experiment Station, US Army Corps of Engineers, Vicksburg, MS, June 1977.
- Saelman, B., "Designing Cylinders and Struts for Maximum Strength," *Machine Design*, Vol. 25, No. 8, August 1953, pp. 133-138.
- Sliwa, S. M., "Economic Evaluation of Flying-Qualities Design Criteria for a Transport Configured With Relaxed Static Stability," NASA Technical Paper 1760, December 1980.
- Stanton, G., "New Design for Commercial Aircraft Wheels and Brakes," AIAA Paper 67-104, June 1967.
- Tanner, J. A. Ed., *Aircraft Landing Gear Systems*, PT-37, SAE A-5 Landing Gear Systems Committee, 1990.
- Veaux, J., "New Design Procedures Applied to Landing Gear Development," *Journal of Aircraft*, Vol. 25, No. 10, October 1988, pp. 904-910.
- Westergaard, H. M., "New formulas for Stresses in Concrete Pavements of Airfields," *Transactions of American Society of Civil Engineers*, Vol. 73, May 1947, pp. 687-701.
- Wille, R. H., "Analytical Weight Estimation of Unconventional Landing Gear Design," SAWE Paper 1905, May 1989.
- Woyak, S. A., Malone, B., and Myklebust, A., "An Architecture for Creating Engineering Application: The Dynamic Integration System," *Proceedings of the Computers in Engineering Conference and the Engineering Database Symposium, ASME*, September 17-20, 1995, Boston, MA, pp. 1-8.

C.4. Articles

- Anon., "Aircraft Tires: Bias or Radials?" *Aerospace Engineering*, Vol. 11, No. 9, September 1991, pp. 13 -14.
- Anon., "Technical Advances in Tyres, Wheels and Brakes: Dunlop Keeps Britain in the Forefront," *Aircraft Engineering*, Vol., 59, No. 11, November 1987, pp. 2-5.
- Fiornio, F., Comp., "Too Big For Your Britches," *Aviation Week and Space Technology*, Vol. 144, No. 21, May 20, 1996, p. 19.
- Kandebo, S. W., and Dornheim, M. A., "Operability Verified In GE90 Flight Tests," *Aviation Week and Space Technology*, Vol. 142, No. 13, March 27, 1995, pp. 52-54.
- Mecham, M., "Airport Officials: Superjumbos Mean New Headaches," *Aviation Week and Space Technology*, Vol. 141, No. 21, November 21, 1994, pp. 76-80.
- Mecham, M. and McKenna, J. T., "Cost, Not Size, to Drive Success of Super Jumbo," *Aviation Week & Space Technology*, Vol. 141, No. 21, November 21, 1994, pp. 45-46.
- Proctor, P., "Boeing Refines Designs for 600-Seat NLA," *Aviation Week & Space Technology*, Vol. 141, No. 21, November 21, 1994, pp. 48-53.
- Proctor, P., "Boeing Presses Need for Multinational VLCT," *Aviation Week & Space Technology*, Vol. 141, No. 21, November 21, 1994, p. 75.
- Proctor, P., "Boeing Homes In on Future 747 Design," *Aviation Week and Space Technology*, Vol. 144, No. 6, February 5, 1996, pp. 32-33.
- Shifrin, C. A., "New Jumbos, SSTs Face Tough Hurdles," *Aviation Week and Space Technology*, Vol. 141, No. 21, November 21, 1994, pp. 42-43.
- Smith, B. A., "Douglas Awaits Chance to Revive Jumbo Plans," *Aviation Week & Space Technology*, Vol. 141, No. 21, November 21, 1994, p. 57.
- Sparaco, P., "Airbus Weights Four A3XX Versions," *Aviation Week & Space Technology*, Vol. 141, No. 21, November 21, 1994, p. 54.
- Sparaco, P., "Airbus Paves Way for A3XX Megajet," *Aviation Week & Space Technology*, Vol. 142, No. 21, May 22, 1995, pp. 26-27.

- Sparaco, P., "No Money As Yet In Airbus Jumbo Plan," *Aviation Week and Space Technology*, Vol. 144, No. 25, June 17, 1996, pp. 27-28.

C.5. Aircraft Data

- Anon., *Aircraft Type Certification Data Sheets and Specification, Vol. 3: Large Multiengine Aircraft*, Federal Aviation Administration, Washington, DC, 1985.
- Anon., *Aircraft Data for Pavement Design*, American Concrete Pavement Association, 1993.
- Anon., *Special Design Chart for Concrete Airport Pavement: Boeing 727*, Portland Cement Association, 1994.
- Anon., *Airplane Characteristics for Airport Planning, 737-300, 737-400, 737-500*, Boeing Document D6-58325-2, Boeing Commercial Airplanes, Seattle, Washington, September 1988.
- Anon., *Airplane Characteristics for Airport Planning, 747-400*, Boeing Document D6-58326-1, Boeing Commercial Airplane Company, Seattle, Washington, March 1990.
- Anon., *Airplane Characteristics for Airport Planning, 777*, Boeing Document D6-58329, Boeing Commercial Airplane Company, Seattle, Washington, February 1992.
- Anon., *Boeing B737-130 Weight and Balance/Control and Loading Manual*, Boeing Commercial Airplane Company, Seattle, Washington, 1985.
- Anon., *Boeing Group Weight Statements*, Boeing Commercial Airplane Company, Seattle, Washington.
- Anon., *MD-80 Component Weight Breakdown*, McDonnell Douglas, 1987.
- Green, W., Swanborough, G., and Mowinski, J., *Modern Commercial Aircraft*, Portland House, New York, 1978.
- Lambert, M., Ed., *Jane's All The World's Aircraft*, Sentinel House, United Kingdom, 1972-1994.

Appendix D Aircraft Tire Database

Table D.1 Aircraft tire data [23]

Item	Size	Ply	Speed (mph)	Load (lb)	Infl Pres (psi)	Brake (lb)	Wei (in)	Dia (in)	Wid (in)	Rad (in)	AR
1	32x11.5-15	12.0	210.0	11200.0	120.0	16800.0	64.1	32.0	11.5	13.5	0.742
2	32x11.5-15	12.0	210.0	11200.0	120.0	16800.0	70.6	32.0	11.5	13.5	0.742
3	32x11.5-15	12.0	225.0	11200.0	120.0	16800.0	69.7	32.0	11.5	13.5	0.742
4	37x13.0-16	20.0	210.0	22200.0	165.0	33300.0	110.2	37.0	13.0	15.4	0.821
5	37x14.0-14	24.0	225.0	25000.0	160.0	37500.0	110.8	37.0	14.0	15.1	0.825
6	37x14.0-14	24.0	225.0	25000.0	160.0	37500.0	106.4	37.0	14.0	15.1	0.825
7	40x15.5-16	26.0	235.0	36300.0	180.0	54450.0	138.8	40.0	15.5	16.1	0.778
8	40x15.5-16	26.0	235.0	36300.0	180.0	54450.0	147.4	40.0	15.5	16.1	0.778
9	44.5x16.5-18	30.0	225.0	42500.0	195.0	63750.0	196.3	44.5	16.5	18.4	0.807
10	44.5x16.5-18	30.0	225.0	42500.0	195.0	63750.0	193.8	44.5	16.5	18.4	0.807
11	49x19.0-20	32.0	235.0	51900.0	195.0	77800.0	269.1	49.0	19.0	20.3	0.767
12	49x19.0-20	32.0	235.0	51900.0	195.0	77800.0	270.4	49.0	19.0	20.3	0.767
13	50x20.0-20	26.0	200.0	41800.0	150.0	62700.0	249.7	50.0	20.0	20.6	0.754
14	50x20.0-20	26.0	210.0	41800.0	150.0	62700.0	230.1	50.0	20.0	20.6	0.754
15	50x20.0-20	32.0	225.0	53800.0	190.0	80700.0	276.8	50.0	20.0	20.6	0.754
16	50x20.0-20	32.0	225.0	53800.0	190.0	80700.0	254.1	50.0	20.0	20.6	0.754
17	50x20.0-20	34.0	225.0	57000.0	205.0	85500.0	293.8	50.0	20.0	20.6	0.754
18	52x20.5-20	34.0	225.0	57800.0	185.0	86700.0	297.6	52.0	20.5	21.3	0.786
19	52x20.5-23	26.0	235.0	55000.0	165.0	82500.0	261.7	52.0	20.5	21.3	0.711
20	52x20.5-23	26.0	235.0	55000.0	165.0	82500.0	285.4	52.0	20.5	21.3	0.711
21	52x20.5-23	28.0	235.0	59500.0	180.0	98250.0	300.2	52.0	20.5	21.3	0.711
22	52x20.5-23	28.0	235.0	59500.0	180.0	89250.0	294.3	52.0	20.5	21.3	0.711
23	52x20.5-23	28.0	235.0	59500.0	180.0	89250.0	286.8	52.0	20.5	21.3	0.711
24	50x20.5-23	30.0	235.0	63700.0	195.0	95550.0	306.4	52.0	20.5	21.3	0.711
25	50x21.0-20	28.0	210.0	46700.0	150.0	70050.0	290.4	50.0	21.0	20.2	0.719
26	50x21.0-20	30.0	210.0	49000.0	160.0	73500.0	307.3	50.0	21.0	20.2	0.719

Table D.1 Aircraft tire data [23] (cont.)

Item	Size	Ply	Speed (mph)	Load (lb)	Infl Pres (psi)	Brake (lb)	Wei (in)	Dia (in)	Wid (in)	Rad (in)	AR
27	24x7.7	14.0	210.0	8200.0	135.0	12300.0	29.4	24.2	7.7	9.8	0.924
28	24x7.7	14.0	225.0	8200.0	135.0	12300.0	26.2	24.2	7.7	9.8	0.924
29	24x7.7	14.0	225.0	8200.0	135.0	12300.0	24.9	24.2	7.7	9.8	0.924
30	24x7.7	16.0	200.0	9725.0	165.0	14590.0	32.1	24.2	7.7	9.8	0.924
31	24x7.7	16.0	210.0	9725.0	165.0	14590.0	34.9	24.2	7.7	9.8	0.924
32	24x7.7	16.0	210.0	9725.0	165.0	14590.0	32.7	24.2	7.7	9.8	0.924
33	24x7.7	16.0	210.0	9700.0	165.0	14550.0	28.7	24.2	7.7	9.8	0.924
34	24x7.7	16.0	225.0	8450.0	135.0	12675.0	26.7	24.2	7.7	9.8	0.924
35	34x9.9	14.0	160.0	14000.0	150.0	21000.0	49.9	33.4	10.2	14.2	0.856
36	34x9.9	14.0	160.0	14000.0	150.0	21000.0	53.2	33.4	10.2	14.2	0.856
37	36x11	20.0	225.0	21000.0	185.0	31500.0	86.9	35.1	11.5	14.7	0.831
38	36x11	22.0	225.0	23300.0	200.0	34950.0	98.1	35.1	11.5	14.7	0.831
39	36x11	22.0	225.0	23300.0	200.0	34950.0	100.5	35.1	11.5	14.7	0.831
40	39x13	14.0	200.0	15000.0	100.0	22500.0	85.4	38.3	13.0	15.8	0.862
41	39x13	14.0	200.0	15000.0	100.0	22500.0	83.6	38.3	13.0	15.8	0.862
42	39x13	16.0	160.0	17200.0	115.0	25800.0	90.1	38.3	13.0	15.8	0.862
43	39x13	16.0	160.0	17200.0	115.0	25800.0	90.5	38.3	13.0	15.8	0.862
44	39x13	16.0	200.0	17200.0	115.0	25800.0	79.5	38.3	13.0	15.8	0.862
45	39x13	16.0	200.0	17200.0	115.0	25800.0	85.5	38.3	13.0	15.8	0.862
46	39x13	16.0	200.0	17200.0	115.0	25800.0	85.5	38.3	13.0	15.8	0.862
47	39x13	16.0	210.0	17200.0	115.0	25800.0	86.5	38.3	13.0	15.8	0.862
48	39x13	16.0	210.0	17200.0	115.0	25800.0	94.2	38.3	13.0	15.8	0.862
49	39x13	16.0	210.0	17200.0	115.0	25800.0	86.8	38.3	13.0	15.8	0.862
50	39x13	16.0	210.0	17200.0	115.0	25800.0	90.7	38.3	13.0	15.8	0.862
51	39x13	16.0	225.0	17200.0	115.0	25800.0	84.3	38.3	13.0	15.8	0.862
52	39x13	16.0	225.0	17200.0	115.0	25800.0	96.0	38.3	13.0	15.8	0.862

Table D.1 Aircraft tire data [23] (cont.)

Item	Size	Ply	Speed (mph)	Load (lb)	Infl Pres (psi)	Brake (lb)	Wei (in)	Dia (in)	Wid (in)	Rad (in)	AR
53	39x13	16.0	225.0	17200.0	115.0	25800.0	97.4	38.3	13.0	15.8	0.862
54	39x13	16.0	225.0	17200.0	115.0	25800.0	87.6	38.3	13.0	15.8	0.862
55	39x13	16.0	225.0	17200.0	115.0	25800.0	90.7	38.3	13.0	15.8	0.862
56	39x13	16.0	225.0	17200.0	115.0	25800.0	90.3	38.3	13.0	15.8	0.862
57	40x14	20.0	210.0	22300.0	135.0	33450.0	119.0	39.8	14.0	16.5	0.855
58	40x14	22.0	210.0	25000.0	155.0	37000.0	125.1	39.8	14.0	16.5	0.855
59	40x14	22.0	225.0	25000.0	155.0	37500.0	120.1	39.8	14.0	16.5	0.855
60	40x14	22.0	225.0	25000.0	155.0	37500.0	122.1	39.8	14.0	16.5	0.855
61	40x14	22.0	235.0	25000.0	155.0	37500.0	119.8	39.8	14.0	16.5	0.855
62	40x14	22.0	235.0	25000.0	155.0	37500.0	122.1	39.8	14.0	16.5	0.855
63	40x14	24.0	210.0	27700.0	170.0	41550.0	138.2	39.8	14.0	16.5	0.855
64	40x14	24.0	210.0	27700.0	170.0	41550.0	124.2	39.8	14.0	16.5	0.855
65	40x14	24.0	210.0	27700.0	170.0	41550.0	143.3	39.8	14.0	16.5	0.855
66	40x14	24.0	210.0	27700.0	170.0	41550.0	136.2	39.8	14.0	16.5	0.855
67	40x14	24.0	210.0	27700.0	170.0	41550.0	137.3	39.8	14.0	16.5	0.855
68	40x14	24.0	225.0	27700.0	170.0	41550.0	137.1	39.8	14.0	16.5	0.855
69	40x14	24.0	225.0	27700.0	170.0	41550.0	138.3	39.8	14.0	16.5	0.855
70	40x14	24.0	225.0	27700.0	170.0	41550.0	136.5	39.8	14.0	16.5	0.855
71	40x14	24.0	225.0	27700.0	170.0	41550.0	137.1	39.8	14.0	16.5	0.855
72	40x14	24.0	225.0	27700.0	170.0	41550.0	117.7	39.8	14.0	16.5	0.855
73	46x16	24.0	210.0	35700.0	170.0	53550.0	164.6	45.3	16.0	19.0	0.797
74	46x16	26.0	225.0	38300.0	185.0	57450.0	201.1	45.3	16.0	19.0	0.797
75	46x16	26.0	225.0	38300.0	185.0	57450.0	198.1	45.3	16.0	19.0	0.797
76	46x16	28.0	210.0	41800.0	210.0	62700.0	185.8	45.3	16.0	19.0	0.797
77	46x16	28.0	210.0	41800.0	210.0	62700.0	203.1	45.3	16.0	19.0	0.797
78	46x16	28.0	210.0	41800.0	210.0	62700.0	202.4	45.3	16.0	19.0	0.797

Table D.1 Aircraft tire data [23] (cont'd)

Item	Size	Ply	Speed (mph)	Load (lb)	Infl Pres (psi)	Brake (lb)	Wei (in)	Dia (in)	Wid (in)	Rad (in)	AR
79	46x16	28.0	225.0	41800.0	210.0	62700.0	191.9	45.3	16.0	19.0	0.797
80	46x16	28.0	225.0	41800.0	210.0	62700.0	203.1	45.3	16.0	19.0	0.797
81	46x16	28.0	225.0	41800.0	210.0	62700.0	192.6	45.3	16.0	19.0	0.797
82	46x16	28.0	225.0	41800.0	210.0	62700.0	186.2	45.3	16.0	19.0	0.797
83	46x16	28.0	235.0	41800.0	210.0	62700.0	203.1	45.3	16.0	19.0	0.797
84	46x16	30.0	210.0	44800.0	225.0	67200.0	213.1	45.3	16.0	19.0	0.797
85	46x16	30.0	225.0	44800.0	225.0	67200.0	193.9	45.3	16.0	19.0	0.797
86	46x16	30.0	225.0	44800.0	225.0	67200.0	219.5	45.3	16.0	19.0	0.797
87	49x17	28.0	210.0	43200.0	180.0	64800.0	217.5	48.8	17.3	20.2	0.838
88	49x17	28.0	210.0	43200.0	180.0	64800.0	225.1	48.8	17.3	20.2	0.838
89	49x17	28.0	210.0	43200.0	180.0	64800.0	209.6	48.8	17.3	20.2	0.838
90	49x17	28.0	210.0	43200.0	180.0	64800.0	228.2	48.8	17.3	20.2	0.838
91	49x17	30.0	210.0	46700.0	195.0	70050.0	225.2	48.8	17.3	20.2	0.838
92	49x17	30.0	210.0	46700.0	195.0	70050.0	259.5	48.8	17.3	20.2	0.838
93	49x17	30.0	210.0	46700.0	195.0	70050.0	219.3	48.8	17.3	20.2	0.838
94	49x17	30.0	225.0	46700.0	195.0	70050.0	219.3	48.8	17.3	20.2	0.838
95	49x17	30.0	225.0	46700.0	195.0	70050.0	238.3	48.8	17.3	20.2	0.838
96	49x17	30.0	225.0	46700.0	195.0	70050.0	212.3	48.8	17.3	20.2	0.838
97	49x17	30.0	225.0	46700.0	195.0	70050.0	227.2	48.8	17.3	20.2	0.838
98	49x17	32.0	225.0	50400.0	210.0	75600.0	243.5	48.8	17.3	20.2	0.838
99	49x17	32.0	235.0	50400.0	210.0	75600.0	243.3	48.8	17.3	20.2	0.838
100	50x18	26.0	225.0	41770.0	155.0	62660.0	197.7	49.5	17.5	20.4	0.848

Table D.2 Aircraft wheel data [23]

Item	Size	Wid (in)	Dia (in)	Item	Size	Wid (in)	Dia (in)
1	32x11.5-15	9.0	15.0	27	24x7.7	5.5	10.0
2	32x11.5-15	9.0	15.0	28	24x7.7	5.5	10.0
3	32x11.5-15	9.0	15.0	29	24x7.7	5.5	10.0
4	36x11	9.0	16.0	30	24x7.7	5.5	10.0
5	37x14.0-14	11.0	14.0	31	24x7.7	5.5	10.0
6	37x14.0-14	11.0	14.0	32	24x7.7	5.5	10.0
7	40x15.5-16	10.0	16.0	33	24x7.7	5.5	10.0
8	40x15.5-16	10.0	16.0	34	24x7.7	5.5	10.0
9	44x16	13.3	18.0	35	34x9.9	8.0	16.0
10	44x16	13.3	18.0	36	34x9.9	8.0	16.0
11	49x17	13.3	20.0	37	36x11	9.0	16.0
12	49x17	13.3	20.0	38	36x11	9.0	16.0
13	50x20.0-20	16.3	20.0	39	36x11	9.0	16.0
14	50x20.0-20	16.3	20.0	40	39x13	10.0	16.0
15	50x20.0-20	16.3	20.0	41	39x13	10.0	16.0
16	50x20.0-20	16.3	20.0	42	39x13	10.0	16.0
17	50x20.0-20	16.3	20.0	43	39x13	10.0	16.0
18	50x20.0-20	16.3	20.0	44	39x13	10.0	16.0
19	50x20.5-23	13.0	23.0	45	39x13	10.0	16.0
20	50x20.5-23	13.0	23.0	46	39x13	10.0	16.0
21	50x20.5-23	13.0	23.0	47	39x13	10.0	16.0
22	50x20.5-23	13.0	23.0	48	39x13	10.0	16.0
23	50x20.5-23	13.0	23.0	49	39x13	10.0	16.0
24	50x20.5-23	13.0	23.0	50	39x13	10.0	16.0
25	49x17	13.3	20.0	51	39x13	10.0	16.0
26	49x17	13.3	20.0	52	39x13	10.0	16.0

Table D.2 Aircraft wheel data [23] (cont'd)

Item	Size	Wid (in)	Dia (in)	Item	Size	Wid (in)	Dia (in)
53	39x13	10.0	16.0	77	46x16	13.3	20.0
54	39x13	10.0	16.0	78	46x16	13.3	20.0
55	39x13	10.0	16.0	79	46x16	13.3	20.0
56	39x13	10.0	16.0	80	46x16	13.3	20.0
57	40x14	11.0	16.0	81	46x16	13.3	20.0
58	40x14	11.0	16.0	82	46x16	13.3	20.0
59	40x14	11.0	16.0	83	46x16	13.3	20.0
60	40x14	11.0	16.0	84	46x16	13.3	20.0
61	40x14	11.0	16.0	85	46x16	13.3	20.0
62	40x14	11.0	16.0	86	46x16	13.3	20.0
63	40x14	11.0	16.0	87	49x17	13.3	20.0
64	40x14	11.0	16.0	88	49x17	13.3	20.0
65	40x14	11.0	16.0	89	49x17	13.3	20.0
66	40x14	11.0	16.0	90	49x17	13.3	20.0
67	40x14	11.0	16.0	91	49x17	13.3	20.0
68	40x14	11.0	16.0	92	49x17	13.3	20.0
69	40x14	11.0	16.0	93	49x17	13.3	20.0
70	40x14	11.0	16.0	94	49x17	13.3	20.0
71	40x14	11.0	16.0	95	49x17	13.3	20.0
72	40x14	11.0	16.0	96	49x17	13.3	20.0
73	46x16	13.3	20.0	97	49x17	13.3	20.0
74	46x16	13.3	20.0	98	49x17	13.3	20.0
75	46x16	13.3	20.0	99	49x17	13.3	20.0
76	46x16	13.3	20.0	100	50x18	14.3	20.0

Appendix E Analysis Package User's Manual

E.1. Introduction

The analysis package was developed by S. Chai for his Master's Thesis, an examination of the design and integration of the landing gear in aircraft conceptual design, with W. H. Mason as his committee chairman. The package is intended to provide aircraft conceptual designers with tools to help automate the landing gear design process.

E.2. Package Organization

The package consists of four executable files, *config.for*, *limit.for*, *pave.for*, and *gearwei.for*. An input file with extension "*.inp*" is required for each program. Program *config.for* currently acts as the front-end of the package and accepts all the data that is input, even though some of the data may not be used by the program itself. Program *config.for* then creates input files for the other three programs. Data files *tire.dat* and *pavevoef.dat* are required to provide database for programs *config.for* and *pave.for*, respectively.

It is suggested that the sample input files be used as templates. Typically, the character data is read in as alphanumeric format, the integer data is read in as 3(10x, i10), and real data is read in as 3(10x, f10.2). The fields that are skipped are intended for variable labels. Note that if the given aircraft does not exhibit a fuselage-mounted landing gear, zeros should be entered in place of those input variables that are related to the fuselage-mounted gear.

E.3. Input Variables

aircraft	Aircraft identification
brake	Brake material

	1	steel
	2	carbon
wheel	Wheel material	
	1	forged aluminum
	2	cast aluminum
	3	titanium
	4	steel
objec	Wheel selection criterion	
	1	minimum pressure
	2	minimum weight
	3	minimum size
metal	Landing gear structure material	
mtow	MTOW, lb	
mldw	Maximum landing weight, lb	
fuel	Fuel weight, lb	
cmax	Maximum main assembly load, percent MTOW	
cmin	Minimum main assembly load, percent MTOW	
warea	Wing area, ft^2	
wspan	Wing span, in	
qswep	Quarter chord sweep, deg	
dihed	Dihedral, deg	
croot	Root chord, in	
taper	Tapering ratio	
clmax	Clmax, landing	
nms	Number of main struts	
nmw	Number of main wheels	
nnw	Number of nose wheels	
wpsm	Number of wheels per strut, main assembly	

wpsn	Number of wheels per strut, nose assembly
dyna	Landing gear load factor
alpha	Angle of attack, touchdown, deg
wbeta	Truck beam rotation angle, wing-mounted assembly, deg
fbeta	Truck beam rotation angle, fuselage-mounted assembly, deg
incl	Axle incline from the vertical, deg
scrap	Tail scrape angle, deg
dnace	Nacelle diameter, in
clear	Nacelle-to-ground clearance, in
_cg	Aircraft *cg* location, aircraft reference frame, in
_wing	Wing root leading edge location, aircraft reference frame, in
_engi	Inboard engine location, aircraft reference frame, in
_tcon	Tail bumper location, aircraft reference frame, in
_main, _nose, _body	Landing gear assembly location, aircraft reference frame, in
_m_, _n_, _b_	Landing gear stowage volume, aircraft reference frame, in The number at the end of the variable denotes the corners of the rectangular-shaped stowage volume: 1 upper starboard corner, forward 2 upper port corner, forward 3 lower starboard corner, forward 4 upper port corner, forward 5 upper starboard corner, aft 6 upper port corner, aft 7 lower starboard corner, aft 8 upper port corner, aft

E.4. Sample Input Files

747conf.inp

```
c landing gear layout/configuration input file
  aircraft: b747
  brake =          1, wheel =          1, objec =          2
  metal =          1
  mtow =   738000.00, mldw =   564000.00, fuel =   316307.00
  cmax =        0.96, cmin =        0.88, warea =    5500.00
  wspan =    2348.00, qswep =      37.70, dihed =       7.00
  croot =     642.00, taper =       0.25, clmax =       2.55
  nms =         4.00, nmw =        16.00, nnw =         2.00
  wpsm =        4.00, wpsn =        2.00, dyna =        1.20
  alpha =       4.00, wbeta =      60.00, fbeta =       0.00
  incl =       10.00, scrap =      12.00, dnace =     110.00
  clear =      12.00
c component location
  xcg =      1260.00, ycg =         0.00, zcg =       -24.00
  xwing =     870.00, ywing =       0.00, zwing =      -88.00
  xengi =    1050.00, yengi =    -465.00, zengi =      -95.00
  xtcon =    2375.00, ytcon =       0.00, ztcon =       0.00
  xmain =    1254.00, ymain =    -216.00, zmain =      -62.00
  xnose =     290.00, ynose =       0.00, znose =    -106.00
  xbody =    1375.00, ybody =     -75.00, zbody =    -118.00
c wing-mounted main assembly stowage
  xm1 =      1164.00, ym1 =       -17.00, zm1 =       -38.00
  xm2 =      1164.00, ym2 =      -115.00, zm2 =       -38.00
  xm3 =      1164.00, ym3 =      -115.00, zm3 =      -136.00
  xm4 =      1164.00, ym4 =       -17.00, zm4 =      -136.00
  xm5 =      1260.00, ym5 =       -17.00, zm5 =       -38.00
  xm6 =      1260.00, ym6 =      -115.00, zm6 =       -38.00
  xm7 =      1260.00, ym7 =      -115.00, zm7 =      -136.00
  xm8 =      1260.00, ym8 =       -17.00, zm8 =      -136.00
c nose assembly stowage
  xn1 =       150.00, yn1 =        32.00, zn1 =       -38.00
  xn2 =       150.00, yn2 =       -32.00, zn2 =       -38.00
  xn3 =       150.00, yn3 =       -32.00, zn3 =       -88.00
  xn4 =       150.00, yn4 =        32.00, zn4 =       -88.00
  xn5 =       290.00, yn5 =        32.00, zn5 =       -38.00
  xn6 =       290.00, yn6 =       -32.00, zn6 =       -38.00
  xn7 =       290.00, yn7 =       -32.00, zn7 =      -112.00
  xn8 =       290.00, yn8 =        32.00, zn8 =      -112.00
c fuselage-mounted main assembly stowage
  xb1 =      1260.00, yb1 =        -8.00, zb1 =       -38.00
  xb2 =      1260.00, yb2 =      -115.00, zb2 =       -38.00
  xb3 =      1200.00, yb3 =      -115.00, zb3 =      -136.00
  xb4 =      1200.00, yb4 =        -8.00, zb4 =      -136.00
  xb5 =      1390.00, yb5 =        -8.00, zb5 =       -38.00
  xb6 =      1390.00, yb6 =      -115.00, zb6 =       -38.00
  xb7 =      1390.00, yb7 =      -115.00, zb7 =      -136.00
  xb8 =      1390.00, yb8 =        -8.00, zb8 =      -136.00
```

747limi.inp

```
c landing gear layout/stowage constraints input file
  aircraft: b747
  cmax =        0.96, cmin =        0.88, hcg =       181.00
  wspan =    2348.00, qswep =      37.70, dihed =       7.00
  croot =     642.00, taper =       0.25
  nms =         4.00, wpsm =        4.00, wpsn =        2.00
  scrap =      12.00, dnace =     110.00, clear =      12.00
  wbeta =      60.00, fbeta =       0.00, incl =        6.00
  smain =      27.65, snose =      27.97, sfuse =      27.65
c component location
  xcg =      1260.00, ycg =         0.00, zcg =       -24.00
  xwing =     870.00, ywing =       0.00, zwing =     -88.00
  xengi =    1050.00, yengi =    -465.00, zengi =     -95.00
  xtcon =    2375.00, ytcon =       0.00, ztcon =       0.00
  xmain =    1253.50, ymain =    -215.00, zmain =     -64.00
  xnose =     290.00, ynose =       0.00, znose =    -106.00
  xfuse =    1375.00, yfuse =     -75.00, zfuse =    -118.00
c wing-mounted main assembly stowage
  xm1 =      1164.00, ym1 =       -17.00, zm1 =       -38.00
  xm2 =      1164.00, ym2 =      -132.00, zm2 =       -38.00
  xm3 =      1164.00, ym3 =      -132.00, zm3 =      -136.00
  xm4 =      1164.00, ym4 =       -17.00, zm4 =      -136.00
  xm5 =      1260.00, ym5 =       -17.00, zm5 =       -38.00
  xm6 =      1260.00, ym6 =      -132.00, zm6 =       -38.00
  xm7 =      1260.00, ym7 =      -132.00, zm7 =      -136.00
  xm8 =      1260.00, ym8 =       -17.00, zm8 =      -136.00
c nose assembly stowage
  xn1 =       150.00, yn1 =        32.00, zn1 =       -38.00
  xn2 =       150.00, yn2 =       -32.00, zn2 =       -38.00
  xn3 =       150.00, yn3 =       -32.00, zn3 =       -88.00
  xn4 =       150.00, yn4 =        32.00, zn4 =       -88.00
  xn5 =       290.00, yn5 =        32.00, zn5 =       -38.00
  xn6 =       290.00, yn6 =       -32.00, zn6 =       -38.00
  xn7 =       290.00, yn7 =       -32.00, zn7 =      -112.00
  xn8 =       290.00, yn8 =        32.00, zn8 =      -112.00
c fuselage-mounted main assembly stowage
  xf1 =      1260.00, yf1 =       -17.00, zf1 =       -30.00
  xf2 =      1260.00, yf2 =      -115.00, zf2 =       -30.00
  xf3 =      1200.00, yf3 =      -115.00, zf3 =      -136.00
  xf4 =      1200.00, yf4 =       -17.00, zf4 =      -136.00
  xf5 =      1390.00, yf5 =       -17.00, zf5 =       -30.00
  xf6 =      1390.00, yf6 =      -115.00, zf6 =       -30.00
  xf7 =      1390.00, yf7 =      -115.00, zf7 =      -136.00
  xf8 =      1390.00, yf8 =       -17.00, zf8 =      -136.00


c selected tire data
  criterion: minimum weight
    type            size  ply speed    load  infl   brake   wei  dia
wid
                                (mph)    (lb) (psi)    (lb)  (lb) (in)
(in)
```

wing	49x17	32.0	235.0	50400.0	210.0	75600.0	243.3	48.8
17.3								
nose	46x16	28.0	210.0	41800.0	210.0	62700.0	185.8	45.3
16.0								
fuselage	49x17	32.0	235.0	50400.0	210.0	75600.0	243.3	48.8
17.3								

c selected wheel data

material: aluminum, forging

type	size	dia (in)	wid (in)	hub (in)	wei (lb)
wing	49x17	13.3	20.0	10.0	86.2
nose	46x16	13.3	20.0	10.0	105.3
fuselage	49x17	13.3	20.0	10.0	86.2

c mathmatical model

wing

component	x0 (in)	y0 (in)	z0 (in)	x1 (in)	y1 (in)	z1 (in)
tire	0.00	0.00	0.00	0.00	13.25	-20.20
axle	0.00	22.00	0.00	0.00	-22.00	0.00
truck beam	-29.00	0.00	0.00	29.00	0.00	0.00
piston	0.00	0.00	0.00	0.00	0.00	-50.00
cylinder	0.00	0.00	0.00	0.00	0.00	-112.00
drag strut	0.00	0.00	0.00	-42.00	-4.00	-101.00
side strut	0.00	0.00	0.00	0.00	-84.00	-88.00
forward trunnion	0.00	0.00	0.00	36.00	12.00	0.00
aft trunnion	0.00	0.00	0.00	12.00	12.00	0.00

nose

component	x0 (in)	y0 (in)	z0 (in)	x1 (in)	y1 (in)	z1 (in)
tire	0.00	0.00	0.00	0.00	13.25	-20.20
axle	0.00	18.00	0.00	0.00	-18.00	0.00
truck beam	0.00	0.00	0.00	0.00	0.00	0.00
piston	0.00	0.00	0.00	0.00	0.00	-34.00
cylinder	0.00	0.00	0.00	0.00	0.00	-75.60
drag strut	0.00	0.00	0.00	-32.40	0.00	-88.00
side strut	0.00	0.00	0.00	0.00	18.00	-32.40
forward trunnion	0.00	0.00	0.00	0.00	-18.00	0.00
aft trunnion	0.00	0.00	0.00	0.00	18.00	0.00

fuselage

component	x0 (in)	y0 (in)	z0 (in)	x1 (in)	y1 (in)	z1 (in)
tire	0.00	0.00	0.00	0.00	13.25	-20.20
axle	0.00	22.00	0.00	0.00	-22.00	0.00
truck beam	-29.00	0.00	0.00	29.00	0.00	0.00
piston	0.00	0.00	0.00	0.00	0.00	-50.00
cylinder	0.00	0.00	0.00	0.00	0.00	-60.00
drag strut	0.00	0.00	0.00	92.00	-56.00	-40.00
side strut	0.00	0.00	0.00	0.00	-48.00	-36.00
forward trunnion	0.00	0.00	0.00	0.00	56.00	0.00
aft trunnion	0.00	0.00	0.00	0.00	-8.00	0.00

747pave.inp

```
c aircraft flotation input file
  aircraft: b747
  mtow =   738000.00, mldw =   564000.00
  cmax =        0.96
  nmw =        16.00, wpsm =        4.00


c selected tire data
  criterion: minimum weight
    type            size  ply speed    load  infl   brake   wei  dia
wid
                              (mph)    (lb) (psi)    (lb)  (lb) (in)
(in)
  wing            49x17 32.0 235.0 50400.0 210.0 75600.0 243.3 48.8
17.3
  nose            46x16 28.0 210.0 41800.0 210.0 62700.0 185.8 45.3
16.0
  fuselage        49x17 32.0 235.0 50400.0 210.0 75600.0 243.3 48.8
17.3


c selected wheel data
  material: aluminum, forging
    type            size  dia  wid  hub   wei
                        (in) (in) (in)  (lb)
  wing            49x17 13.3 20.0 10.0  86.2
  nose            46x16 13.3 20.0 10.0 105.3
  fuselage        49x17 13.3 20.0 10.0  86.2


c mathmatical model
  wing
  component                 x0      y0      z0      x1      y1      z1
                          (in)    (in)    (in)    (in)    (in)    (in)
  tire                    0.00    0.00    0.00    0.00   13.25  -20.20
  axle                    0.00   22.00    0.00    0.00  -22.00    0.00
  truck beam            -29.00    0.00    0.00   29.00    0.00    0.00
  piston                  0.00    0.00    0.00    0.00    0.00  -50.00
  cylinder                0.00    0.00    0.00    0.00    0.00 -112.00
  drag strut              0.00    0.00    0.00   42.00    4.00 -101.00
  side strut              0.00    0.00    0.00    0.00  -84.00  -88.00
  forward trunnion        0.00    0.00    0.00   16.00    4.00    0.00
  aft trunnion           16.00    4.00    0.00   56.00   18.00    0.00

  nose
  component                 x0      y0      z0      x1      y1      z1
                          (in)    (in)    (in)    (in)    (in)    (in)
  tire                    0.00    0.00    0.00    0.00   13.25  -20.20
  axle                    0.00   17.00    0.00    0.00  -17.00    0.00
  truck beam              0.00    0.00    0.00    0.00    0.00    0.00
  piston                  0.00    0.00    0.00    0.00    0.00  -34.00
  cylinder                0.00    0.00    0.00    0.00    0.00  -78.00
  drag strut              0.00    0.00    0.00   41.00    0.00  -82.00
```

side strut	0.00	0.00	0.00	0.00	19.00	38.00
forward trunnion	0.00	24.00	0.00	0.00	0.00	0.00
aft trunnion	0.00	0.00	0.00	0.00	-24.00	0.00

fuselage component	x0 (in)	y0 (in)	z0 (in)	x1 (in)	y1 (in)	z1 (in)
tire	0.00	0.00	0.00	0.00	13.25	-20.20
axle	0.00	22.00	0.00	0.00	-22.00	0.00
truck beam	-29.00	0.00	0.00	29.00	0.00	0.00
piston	0.00	0.00	0.00	0.00	0.00	-50.00
cylinder	0.00	0.00	0.00	0.00	0.00	-64.00
drag strut	0.00	0.00	0.00	84.00	-56.00	-40.00
side strut	0.00	0.00	0.00	0.00	-48.00	-36.00
forward trunnion	0.00	0.00	0.00	0.00	-62.00	0.00
aft trunnion	0.00	-62.00	0.00	0.00	-72.00	0.00

747weig.inp

```
c landing gear weight estimation input file
  aircraft: b747
  metal =          1
  mtow =   738000.00, mldw =   564000.00
  cmax =        0.96, cmin =        0.88, hcg =       181.00
  nms =         4.00, nmw =        16.00, nnw =         2.00
  wpsm =        4.00, wpsn =        2.00, alpha =       4.00
  dyna =        1.20, inpr =     1500.00, bwei =      262.11
  smain =      26.65, snose =      26.97, sfuse =      26.65
c component location
  xmain =    1254.00, ymain =    -216.00, zmain =     -62.00
  xnose =     290.00, ynose =       0.00, znose =    -106.00
  xfuse =    1375.00, yfuse =     -75.00, zfuse =    -118.00


c selected tire data
  criterion: minimum weight
    type            size  ply speed    load  infl   brake   wei  dia
wid
                              (mph)    (lb) (psi)    (lb)  (lb) (in)
(in)
  wing            49x17 32.0 235.0 50400.0 210.0 75600.0 243.3 48.8
17.3
  nose            46x16 28.0 210.0 41800.0 210.0 62700.0 185.8 45.3
16.0
  fuselage        49x17 32.0 235.0 50400.0 210.0 75600.0 243.3 48.8
17.3


c selected wheel data
  material: aluminum, forging
    type            size  dia  wid  hub   wei
                        (in) (in) (in)  (lb)
  wing            49x17 13.3 20.0 10.0  86.2
  nose            46x16 13.3 20.0 10.0 105.3
  fuselage        49x17 13.3 20.0 10.0  86.2


c mathmatical model
  wing
  component                x0      y0      z0      x1      y1      z1
                         (in)    (in)    (in)    (in)    (in)    (in)
  tire                   0.00    0.00    0.00    0.00   13.25  -20.20
  axle                   0.00   22.00    0.00    0.00  -22.00    0.00
  truck beam           -29.00    0.00    0.00   29.00    0.00    0.00
  piston                 0.00    0.00    0.00    0.00    0.00  -50.00
  cylinder               0.00    0.00    0.00    0.00    0.00 -112.00
  drag strut             0.00    0.00    0.00   42.00    4.00 -101.00
  side strut             0.00    0.00    0.00    0.00  -84.00  -88.00
  forward trunnion       0.00    0.00    0.00   16.00    4.00    0.00
  aft trunnion          16.00    4.00    0.00   56.00   18.00    0.00

  nose
```

component	x0 (in)	y0 (in)	z0 (in)	x1 (in)	y1 (in)	z1 (in)
tire	0.00	0.00	0.00	0.00	13.25	-20.20
axle	0.00	17.00	0.00	0.00	-17.00	0.00
truck beam	0.00	0.00	0.00	0.00	0.00	0.00
piston	0.00	0.00	0.00	0.00	0.00	-34.00
cylinder	0.00	0.00	0.00	0.00	0.00	-78.00
drag strut	0.00	0.00	0.00	41.00	0.00	-82.00
side strut	0.00	0.00	0.00	0.00	19.00	38.00
forward trunnion	0.00	24.00	0.00	0.00	0.00	0.00
aft trunnion	0.00	0.00	0.00	0.00	-24.00	0.00

fuselage

component	x0 (in)	y0 (in)	z0 (in)	x1 (in)	y1 (in)	z1 (in)
tire	0.00	0.00	0.00	0.00	13.25	-20.20
axle	0.00	22.00	0.00	0.00	-22.00	0.00
truck beam	-29.00	0.00	0.00	29.00	0.00	0.00
piston	0.00	0.00	0.00	0.00	0.00	-50.00
cylinder	0.00	0.00	0.00	0.00	0.00	-64.00
drag strut	0.00	0.00	0.00	84.00	-56.00	-40.00
side strut	0.00	0.00	0.00	0.00	-48.00	-36.00
forward trunnion	0.00	0.00	0.00	0.00	-62.00	0.00
aft trunnion	0.00	-62.00	0.00	0.00	-72.00	0.00

Vita

The author was born in Taipei, Taiwan to Frank and Amy Chai on 4 February, 1972. After immigrating to the United States in 1984 and residing in Virginia for six years, he began his higher education at Virginia Polytechnic Institute and State University in 1990. He completed his Bachelor of Science degree in Aerospace Engineering in 1994 and furthered his education through graduate studies at Virginia Tech. He completed the Masters of Science degree in Aerospace Engineering in 1996.